

JSCSEN 79(5)517–626(2014)

ISSN 1820-7421(Online)

Journal of the Serbian Chemical Society

ersion
lectronic

VOLUME 79

No 5

BELGRADE 2014

Available on line at



www.shd.org.rs/JSCS/

The full search of JSCS
is available through

DOAJ DIRECTORY OF
OPEN ACCESS
JOURNALS

www.doaj.org



CONTENTS

Organic Chemistry

- M. G. Chochkova, A. P. Georgieva, G. I. Ivanova, N. Nikolova, L. Mukova, L. Nikolaeva-Glomb and T. S. Milkova:* Synthesis and biological activity of hydroxycinnamoyl-containing antiviral drugs 517
- D. Sharma and J. K. Makrandi:* Iodine-mediated one-pot synthesis of 3-cyanocoumarins and 3-cyano-4-methylcoumarins (Short communication)..... 527

Biochemistry and Biotechnology

- D. Ž. Ivetić, V. V. Srdić and M. G. Antov:* Immobilization of β -glucosidase onto a mesoporous silica support: physical adsorption and covalent binding of the enzyme..... 533

Inorganic Chemistry

- M. Mirković, N. Nikolić, D. Mijin, M. Avramov Ivić, A. Kapor and Z. D. Tomić:* Synthesis, characterization and crystal structure of Cu(II) complex with a diimine-dioxime ligand, $[\text{Cu}_2(\text{LH})_2](\text{ClO}_4)_2$. Influence of the weak Cu...O(perchlorate) interaction on the structure of the $\text{Cu}_2\text{N}_2\text{O}_2$ metallocycle..... 545

Theoretical Chemistry

- I. Gutman, L. Zhong and K. Xu:* Relating the ABC and harmonic indices..... 557

Physical Chemistry

- R. Biswas, D. Brahman and B. Sinha:* Thermodynamics of the complexation between salicylaldehyde thiosemicarbazone with Cu(II) ions in methanol–1,4-dioxane binary solutions 565

Analytical Chemistry

- D. Stirbet, S.-C. Litescu and G.-L. Radu:* Chromatographic analysis of immobilized cefotaxime (Short communication)..... 579

Polymers

- Z. Chen, J. He, F. Zhao, Y. Liu, Y. Liu and H. Yuan:* Effect of polar additives on melt electrospinning of non-polar polypropylene 587

Environmental

- S. Štrbac, G. Gajica, A. Šajnović, N. Vasić, K. Stojanović and B. Jovančićević:* The use of biological markers in the determination of the origin and type of organic matter in the sediments of the Tisza River 597
- K. Thirugnanasambandham, V. Sivakumar and J. Prakash Maran:* Optimization of electrocoagulation process to treat biologically pretreated bagasse effluent 613

Published by the Serbian Chemical Society
Karnegijeva 4/III, P. O. Box 36, 11120 Belgrade 35, Serbia
Printed by the Faculty of Technology and Metallurgy
Karnegijeva 4, P. O. Box 35-03, 11120 Belgrade, Serbia



J. Serb. Chem. Soc. 79 (5) 517–526 (2014)
JSCS–4603

Synthesis and biological activity of hydroxycinnamoyl-containing antiviral drugs

MAYA G. CHOCHKOVA^{1*}, ASSYA P. GEORGIEVA¹, GALYA I. IVANOVA²,
NADYA NIKOLOVA³, LUCHIA MUKOVA³, LUBOMIRA NIKOLAEVA-GLOMB³
and TSENKA S. MILKOVA¹

¹South-West University “Neofit Rilski”, Blagoevgrad, Bulgaria, ²Departamento de Química, Faculdade de Ciências, Universidade do Porto, Porto, Portugal and ³The Stephan Angeloff Institute of Microbiology, Bulgarian Academy of Sciences, Sofia, Bulgaria

(Received 22 February, revised 24 June, accepted 1 October 2013)

Abstract: Seven *N*-hydroxycinnamoyl amides were synthesized by 1-[3-(dimethylamino)propyl]-3-ethylcarbodiimide/1-hydroxybenzotriazole (EDC/HOBt) coupling of the corresponding substituted cinnamic acids (*p*-coumaric-, ferulic-, sinapic- and caffeic acids) with influenza antivirals (amantadine, rimantadine and oseltamivir). The DPPH (1,1-diphenyl-2-picrylhydrazyl) scavenging abilities and the inhibitory effect on mushroom tyrosinase activity (using L-tyrosine as the substrate) were investigated *in vitro*. Amongst the synthesized compounds, *N*-[(*E*)-3-(3,4-dihydroxyphenyl)-2-propenoyl]oseltamivir (**1**) and *N*-[(*E*)-3-(3,4-dihydroxyphenyl)-2-propenoyl]rimantadine (**4**), containing a catechol moiety, exhibited the most potent DPPH radical-scavenging activity. Amide (**1**) also displayed tyrosinase inhibitory effect toward L-tyrosine as the substrate (≈50 %). The synthesized compounds were also investigated for their *in vitro* inhibitory activity against the replication of influenza virus A (H3N2).

Keywords: *N*-hydroxycinnamoylamides; influenza antivirals; mushroom tyrosinase; monophenolase activity; antioxidant activity; anti-influenza activity.

INTRODUCTION

Phenolics are secondary plant metabolites, important not only for the functional aspects of plant life, but also they have a potential impact on public health. Amongst the main families of phenolic compounds, hydroxycinnamic acids (*e.g.*, ferulic, *p*-coumaric, caffeic acids, *etc.*) and their derivatives (esters, amides and glycosides) have become an emergent topic of many research groups and hence the subject of our interest.^{1–4}

* Corresponding author. E-mail: mayabg2002@yahoo.com
doi: 10.2298/JSC130222103C

Hydroxycinnamic acid amides, both natural and synthetic, possess diverse physiological activities, such as being potent antioxidants,^{5–12} antimicrobials,^{3,4,6,13,14} inhibitors of hepatotoxic and proliferative activity,^{15–18} acting as inhibitors of HIV integrase,^{19–22} inhibitors of α -glucosidase,^{23,24} and tyrosinase,^{1,25,26} *etc.*

A huge amount of data on various polyhydroxy tyrosinase inhibitors exists in the literature. Tyrosinase inhibition is an important strategy in many medicinal, food and agricultural areas. Hyperpigmentation of the human skin and enzymatic browning in fruits and mushrooms are the results of two distinct reactions of tyrosinase (EC 1.14.18.1) – the hydroxylation of tyrosine by monophenolase action to 3,4-dihydroxyphenylalanine (L-DOPA), and further L-DOPA oxidation to *o*-dopaquinone (diphenolase activity). This copper-containing enzyme is widely present in bacteria, fungi and higher plants (mushrooms, bananas, apples, pears, potatoes, *etc.*).^{27,28}

In order to overcome the instability and low degree of percutaneous absorption of natural polyphenols in cosmetic compositions, synthesized *N*-hydroxycinnamoyl amantadine amides, which manifested increased antioxidant, melanin inhibitory and procollagen inducing effects, were synthesized.²⁹

The incorporation of the lipophilic adamantyl moiety in another class of small molecules, such as *N*-benzylbenzamide, appeared to be also an important element for enhanced depigmentation activity.³⁰

Since 1960s, the aminoadamantanes (amantadine, rimantadine) have been representatives of the first class of antivirals, approved for prophylaxis and treatment of influenza. They are known to inhibit virus replication by blocking the proton channel of the M2 structural protein of the virion (M2 blockers).³¹ As only the influenza A viruses possess this structural M2 ion channel protein, aminoadamantanes are not effective against influenza B viruses, since the latter do not encode for M2 protein.^{32,33}

In the quest for therapeutic agents with a broader spectrum that are active against both types (A and B) of influenza viruses, neuraminidase inhibitors (oseltamivir and zanamivir) were discovered as the second class of anti-influenza antivirals.^{34,35} They interfere with viral neuraminidase, which is essential for the release of newly synthesized infective virus progeny.

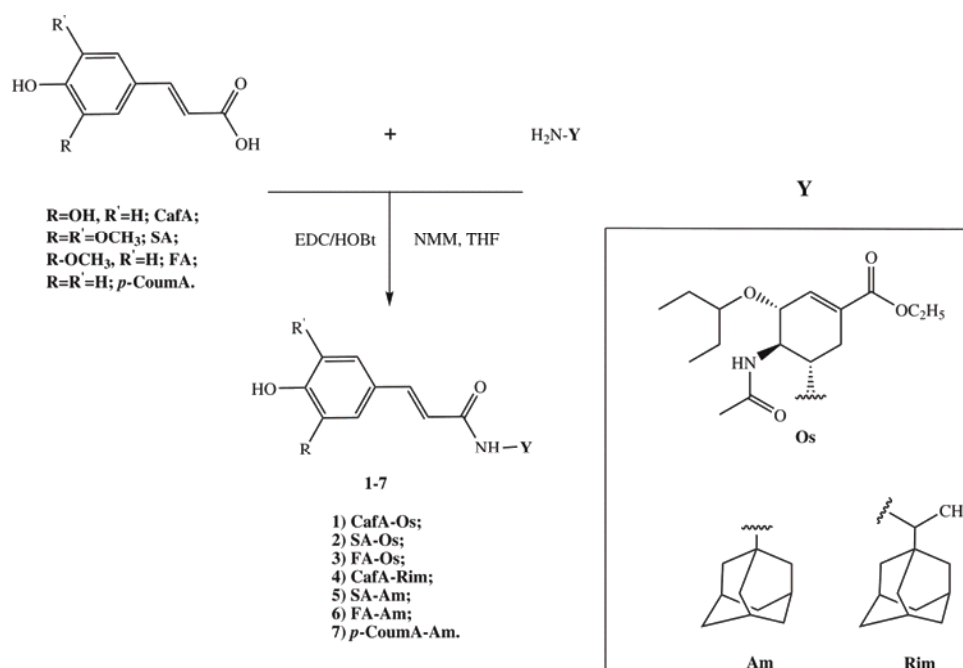
A set of polyphenol compounds (*e.g.*, resveratrol; curcumin and isoquercetin) was reported to inhibit both influenza viruses type A and B *in vitro*.³⁶ However one of the latest investigations on the matter revealed that the mentioned polyphenols possess an antiviral activity only against influenza A virus replication.³⁷

It was found that the reception of a combination of antioxidants (*e.g.*, polyphenolics) with influenza drugs synergized on the reduction of viral replication.^{38,39}

The above findings encouraged us to link chemically antioxidant-functioning hydroxycinnamic acids with anti-influenza drugs (amantadine, rimantadine and oseltamivir) and to study some of their biological activities.

RESULTS AND DISCUSSION

Seven *N*-hydroxycinnamoylamides were synthesized from hydroxycinnamic acids (ferulic, caffeic, sinapic and *p*-coumaric acids) and influenza antivirals (amantadine, rimantadine and oseltamivir) by a previously described procedure.⁷ Unlike the three-step (reactions of the hydroxycinnamoyl amide synthesis, provided previously,²⁹ the present synthetic route (Scheme 1) was performed by 1-[3-(dimethylamino)propyl]-3-ethylcarbodiimide/1-hydroxybenzotriazole (EDC/HOBt) coupling, without preliminary protection and further deprotection steps of the phenolic hydroxyl groups.



Scheme 1. EDC/HOBt-coupling in preparation of *N*-hydroxycinnamoylamides.

After purification by column or preparative thin-layer chromatography, the compounds were obtained in moderate to good yields. The geometry of the double bond in the cinnamoyl residue was confirmed by ¹H-NMR spectroscopy, where the resonance of olefinic protons in all *N*-hydroxycinnamoylamides was observed at 6.19–6.51 ppm and at 7.19–7.55 ppm as two doublets with $J \approx 15.5$ Hz. These signals are evidence that all of the synthesized amides present were *E*-diastereoisomers.

The yields of the compounds, and the analytic and complete spectral data for the synthesized compounds are given in the Supplementary material to this paper.

Scavenging effect on DPPH radicals

Since it is well known⁴⁰ that the DPPH test gives a rough, primary index of antioxidant activity, by measuring the ability of DPPH to scavenge an electron or hydrogen radical of the tested compounds (scavengers) *in vitro*, a myriad of articles have been published.

DPPH scavenging activity of the synthesized *N*-hydroxycinnamoylamides, as well as the used standards caffeic, ferulic, sinapic and *p*-coumaric acids, displayed an activity at 12, 24 and 48 μM in a concentration dependent manner (Table I). As shown in Table I (data for 12 and 24 μM concentration are not presented), the evaluated scavenging activity of the compounds decreased in the following order: CafA \approx CafA-Os (**1**) > CafA-Rim (**4**) > SA > SA-Os (**2**) > FA > FA-Os (**3**) \approx SA-Am (**5**) > FA-Am (**6**) > *p*-CoumA > *p*-CoumA-Am (**7**) \approx Os > Rim > Am.

TABLE I. DPPH radical scavenging activity of *N*-hydroxycinnamoylamides, antivirals and the tested references at a concentration of 48 μM . The given values are the means \pm confidence interval, calculated at the level of significance 0.05 ($n = 3$)

Compound	DPPH radical scavenging activity, %
1	91.83 \pm 5.08
2	48.10 \pm 1.23
3	31.75 \pm 3.77
4	72.58 \pm 8.26
5	30.37 \pm 2.58
6	20.28 \pm 1.04
7	3.00 \pm 0.60
Caffeic acid	92.65 \pm 2.90
Sinapic acid	60.73 \pm 0.62
Ferulic acid	44.30 \pm 0.10
<i>p</i> -Coumaric acid	6.10 \pm 0.04
Oseltamivir	3.51 \pm 0.90
Amantadine hydrochloride	1.75 \pm 0.21
Rimantadine hydrochloride	2.48 \pm 0.30

Amongst the tested newly synthesized amides, *N*-caffeoylamides (**1** and **4**) revealed the best activity, commensurable with that of the free caffeic acid at 3.6 mM concentration. It is not surprising that the latter compounds are the most active ones. The presence of a catechol moiety is the structural feature, responsible for their better radical quenching abilities.⁴¹ All the newly synthesized compounds demonstrated a higher radical scavenging activity than amantadine, rimantadine and oseltamivir, which do not possess DPPH scavenging ability at all. The reported results are in agreement with earlier findings for the disability of

rimantadine to scavenge superoxide radicals,⁴² although its antioxidant effect has been observed *in vivo*. Moreover, the existence of the more polar substituted nucleus of ethyl cyclohex-1-ene-1-carboxylate (*i.e.*, the skeleton of oseltamivir) in the *N*-hydroxycinnamoylamides seems to be more efficient in radical scavenging than the corresponding amides of the hydrophobic aminoadamantanes.

Effect of N-hydroxycinnamoylamides on mushroom tyrosinase

Considering substituted cinnamic acids and their derivatives as potential tyrosinase inhibitors,^{25,43–46} the effects of the obtained *N*-hydroxycinnamoylamides on the monophenolase activity of mushroom tyrosinase (using L-tyrosine as substrate) at 23 μ M concentration was studied herein.

The results of the evaluated activity of the amides, presented as percentage (%) of mushroom tyrosinase inhibition, are outlined in Table II. Hydroquinone was used as a reference compound.

TABLE II. Tyrosinase inhibitory activity of *N*-hydroxycinnamoylamides at a concentration of 23 μ M. The given values are the means \pm confidence interval, calculated at the level of significance 0.05 ($n = 3$); NA –not analyzed; N.I. – no inhibition

Compound	Tyrosinase inhibition, %
Hydroquinone	98.61 \pm 3.45
CafA-Os (1)	49.32 \pm 9.37
SA-Os (2)	N.I.
FA-Os (3)	N.I.
CafA-Rim (4)	N.I.
SA-Am (5)	N.I.
FA-Am (6)	N.I.
<i>p</i> -CoumA-Am(7)	NA

Amongst the tested compounds, the amide CafA-Os (1) was found to inhibit the enzyme with half the activity of the used standard tyrosinase inhibitor hydroquinone.

Despite the fact that both amides (CafA-Os (1) and CafA-Rim (4)) contain the same caffeoyl moiety (catechol entity) in their structure, the inhibitory activity *in vitro* toward mushroom tyrosinase was lost in amide 4, which could be attributed to the sterically hindered adamantane rest.

The obtained results confirmed the finding that the inhibitory activity of *p*-coumaric acid varies from weaker to stronger in comparison with kojic acid and arbutin, depending on the tyrosinase source (mushroom, human or murine).⁴⁷

The data of the present investigation do not correspond to the developmental work on a study of tyrosinase inhibition by *N*-feruloylamantadine amide and related analogues, which possessed similar or greater melanin inhibitory effect than the positive controls – kojic acid and hydroquinone, in cell-based environments.²⁹

Effect of the chemically connected hydroxycinnamic acids with rimantadine, amantadine and oseltamivir against the influenza virus A/Aichi/2/68 (H3N2)

Earlier studies showed that antioxidant therapy could be successfully used as a potential approach to influenza-associated complications.^{39,48–50} The existence of these findings is connected with the synergistic combination of antioxidants with approved influenza antivirals, but antioxidants and antivirals have never been combined chemically until now.

Therefore, the newly synthesized *N*-hydroxycinnamoylamides, were evaluated for their antiviral activity against influenza virus A/Aichi/2/68 (H3N2). The newly synthesized compounds did not reveal a significant inhibitory effect against the *in vitro* replication of influenza A virus H3N2.

EXPERIMENTAL

Materials and methods

1-Adamantylamine hydrochloride (amantadine hydrochloride), 1-(1-adamantyl)ethylamine hydrochloride (rimantadine hydrochloride), (*E*)-4-hydroxy-3-methoxycinnamic (ferulic, FA), (*E*)-3,4-dihydroxycinnamic (caffeic, CafA), (*E*)-4-hydroxy-3,5-dimethoxycinnamic (sinapic, SA), (*E*)-4-hydroxycinnamic (*p*-coumaric, *p*-CoumA) acids, 1-[3-(dimethylamino)propyl]-3-ethylcarbodiimide hydrochloride (EDC), *N*-methylmorpholine (NMM), mushroom tyrosinase (EC 1.14.18.1) and 1,1-diphenyl-2-picrylhydrazyl (DPPH) radical were from Sigma-Aldrich. Hydroquinone was obtained from Ferak (Germany) and L-tyrosine was obtained from Merck (Germany). Ethyl (3*R*,4*R*,5*S*)-4-acetamido-5-amino-3-(1-ethylpropoxy)-1-cyclohexene-1-carboxylate (oseltamivir) was purchased from Aopharm (China). All solvents were of reagent grade and used without further purification and the water used was deionized.

Apparatus

The structures and purity of all newly synthesized amides were confirmed by spectral methods, *i.e.*, UV, ¹H- and ¹³C-NMR spectroscopy and ESI-MS. The ¹H- and ¹³C-NMR spectra were acquired on a Bruker Avance III 400 spectrometer, operating at 400.15 MHz for protons and 100.62 MHz for carbons. The UV spectra of the amides were measured with an Agilent 8453 UV-Vis spectrophotometer. Elemental analyses for C, H and N were realized on a Perkin Elmer 2400 analyzer. The ESI mass spectra were obtained on an Esquire3000 plus instrument.

General procedure for the preparation of N-hydroxycinnamoylamides

In a typical preparation, to a solution of substituted cinnamic acid (3.2 mmol), EDC (0.61 g, 3.2 mmol) and 1-hydroxybenzotriazole (0.43 g, 3.2 mmol) in 10 mL THF, after 10 min stirring at 0 °C, the antiviral compound (3.2 mmol) and NMM (0.35 mL, 3.2 mmol), dissolved in 7 mL THF were added. The resultant reaction mixture was stirred for 1 h at 0 °C and then for 24 h at room temperature, under a nitrogen atmosphere. After completion of the reaction (TLC control – CH₂Cl₂/CH₃OH (3:0.2; 3:0.3); CH₂Cl₂/EtOAc/CH₃OH (3:0.1:0.1)), the THF was evaporated *in vacuo*, and the residue was diluted with EtOAc and then was successively washed with 5 % NaHSO₄, NaHCO₃ and brine, dried over anhydrous Na₂SO₄ and evaporated *in vacuo*. The residue was purified by column chromatography or preparative TLC on silica gel (CH₂Cl₂/CH₃OH) to give the desired compound.

DPPH radical scavenging assay

The free DPPH scavenging assay was performed according to the Nenadis method.⁵¹

The vanishing of the deep violet color of the DPPH radical was accomplished by mixing 2.96 mL 0.1 mM ethanolic DPPH solution with 40 μ L of a free radical scavenger (antioxidant) at the reaction mixture concentrations: 12, 24 and 48 μ M. The decrease in absorbance at 516 nm was measured after 20 min incubation in the dark at room temperature.

The measurements were performed in triplicate and results are presented as the percentage of radical scavenging activity, calculated as follows:

$$\text{Free radical scavenging activity (\%)} = 100(A_{\text{DPPH}} - A_{\text{sample}})/A_{\text{DPPH}}$$

Mushroom tyrosinase inhibition assay

Inhibition of tyrosinase activity was determined spectrophotometrically by a modified dopachrome method²⁵ using L-tyrosine as the substrate.

The reaction media (3 mL) contained: phosphate buffer (1.0 mL, 0.1 M, pH 6.8); L-tyrosine (1.0 mL, 1.5 mM) dissolved in deionized water; inhibitor (0.350 mL, 0.2 mM) dissolved in DMSO; deionized water (0.350 mL); an aqueous mushroom tyrosinase solution (0.300 mL, 192 U mL⁻¹). After adding the mushroom tyrosinase solution, the reaction mixture was incubated at 37 °C for 20 min, and thereafter, the UV absorbance of the reaction mixture was measured at 475 nm. Results were compared with a reference solution consisting of 0.350 mL of DMSO instead of a sample (inhibitor).

The percentage of mushroom tyrosinase inhibitory activity was calculated using the following equation:

$$\text{Inhibition (\%)} = 100(A_{\text{refs}} - A_{\text{sample}})/A_{\text{refs}}$$

where, A_{refs} is the absorbance of the reference solution and A_{sample} is the absorbance of the test sample solution).

Each experiment was performed in triplicate and averaged. Results were evaluated at a level of significance 0.05. Hydroquinone was used as the positive control.

Antiviral activity assay

Cells and viruses. MDCK cells for the propagation of influenza virus A originated from the collection of the Stephan Angeloff Institute of Microbiology, Bulgarian Academy of Sciences, Sofia, Bulgaria, and were grown in a growth medium containing Dulbecco modified Eagles' medium (DMEM) (Gibco BRL, USA), supplemented with 10 % fetal bovine serum, 10 mM HEPES buffer (Merck, Germany) and antibiotics (penicillin 100 IU mL⁻¹ and streptomycin 100 μ g mL⁻¹). The cells were cultured as confluent monolayers in a humidified atmosphere containing 5 % CO₂ at 37 °C.

Influenza virus A/Aichi/2/68 (H3N2) from the collection of the Stephan Angeloff Institute of Microbiology, Bulgarian Academy of Sciences, was grown in MDCK cells in a maintenance medium of Dulbecco modified Eagles' medium (DMEM) (Gibco BRL, USA), containing 0.5 % fetal bovine serum, 10 mM HEPES buffer and antibiotics, as well as 3 mg mL⁻¹ trypsin (Gibco BRL).

Cytopathic effect (CPE) inhibition test. Monolayer MDCK cells in 96-well microplates (Costar, USA) were inoculated, following the removal of the growth medium, with 0.1 mL virus suspension containing 100 CCID₅₀ (cell culture infectious dose 50 %). After 1 h at 37 °C for virus adsorption, the inoculum was washed out and replaced by 0.1 mL of non-cytotoxic 0.5 log₁₀ dilutions in the maintenance medium of the newly synthesized compounds. Each dilution was applied in quadruplicate. Cells that were not inoculated with virus were left for

cell controls (with only maintenance medium) and toxicity controls (with respective dilution of the compound in the maintenance medium). Cells inoculated with virus but not treated with a compound were left for virus controls. Then cells were incubated for 48 h in a humidified atmosphere with 5 % CO₂ at 37 °C or until the virus specific cytopathic effect had destroyed 100 % of the cells in the virus control wells. Then cells were stained according to the neutral red uptake procedure and the percentage of CPE inhibition, if present, was calculated using the following formula: % CPE = $(OD_{\text{test sample}} - OD_{\text{virus control}}) / (OD_{\text{toxicity control}} - OD_{\text{virus control}}) - 100$.

CONCLUSIONS

Seven *N*-(hydroxycinnamoyl)amides were synthesized and identified, six of which were new. The compounds were evaluated for their anti-influenza, DPPH scavenging and mushroom tyrosinase inhibitory activities. The results indicated that amides **1** and **4**, containing the catechol moiety, were the most active as DPPH radical-scavengers. In addition, CafA-Os (**1**) was found to be the most active as a tyrosinase inhibitor (≈ 50 %) *in vitro*.

SUPPLEMENTARY MATERIAL

Analytic and spectral data for the synthesised compounds are available electronically from <http://www.shd.org.rs/JSCS/>, or from the corresponding author on request.

Acknowledgment. This work was supported by the Bulgarian Science Fund (contract DMU 03/2).

ABBREVIATIONS

DPPH – 1,1-diphenyl-2-picrylhydrazyl radical;
 ROS – reactive oxygen species;
 DMSO – dimethyl sulfoxide;
 EDC – 1-[3-(dimethylamino)propyl]-3-ethylcarbodiimide;
 HOBt – 1-hydroxybenzotriazole;
p-CoumA – *p*-coumaric acid;
 FA – ferulic acid;
 SA – sinapic acid;
 CafA – caffeic acid;
 Os – oseltamivir;
 Rim – rimantadine;
 Am – amantadine;
 % RSA – percentage of radical scavenging activity.

ИЗВОД

СИНТЕЗА И БИОЛОШКА АКТИВНОСТ ХИДРОКСИЦИНАМОИЛ АНТИВИРУСНИХ ЛЕКОВА

MAYA G. CHOCHKOVA¹, ASSYA P. GEORGIEVA¹, GALYA I. IVANOVA², NADYA NIKOLOVA³, LUCHIA MUKOVA³,
 LUBOMIRA NIKOLAEVA-GLOMB³ И TSENKA S. MILKOVA¹

¹South-West University "Neofit Rilski", Blagoevgrad, Bulgaria, ²Departamento de Química, Faculdade de Ciências, Universidade do Porto, Porto, Portugal and ³The Stephan Angeloff Institute of Microbiology, Bulgarian Academy of Sciences, Sofia, Bulgaria

Синтетисано је седам *N*-хидроксицинамоил-амида EDC/HOBt катализованим куповањем одговарајућих супституисаних циметних киселина (*p*-кумаринска, ферулинска,

синапинска и кафена киселина) са једињењима која показују антивиралну активност (амантадин, римантидин и оселтамивир). Испитивана је *in vitro* способност пресретања 1,1-дифенил-2-пикрилхидразил (DPPH) радикала и инхибиција активности тирозиназе гљива (употребом L-тирозина као супстрата). Од синтетисаних једињења, деривати *N*-[(*E*)-3-(3,4-дихидроксифенил)-2-пропеноил]оселтамивир (**1**) и *N*-[(*E*)-3-(3,4-дихидроксифенил)-2-пропеноил]римантидин (**4**), који садрже катехолски фрагмент, показују најбољу способност пресретања DPPH радикала. Такође, амид **1** показује инхибиторни ефекат према тирозинази (око 50 %). Испитивана је *in vitro* инхибиторна активност синтетисаних једињења према вирусу грипа А (H3N2).

(Примљено 22. фебруара, ревидирано 24. јуна, прихваћено 1. октобра 2013)

REFERENCES

1. L. Georgiev, M. Chochkova, I. Totseva, K. Seizova, E. Marinova, G. Ivanova, M. Ninova, H. Najdenski, T. Milkova, *Med. Chem. Res.* **22** (2012) 4173
2. L. Georgiev, M. Chochkova, G. Ivanova, H. Najdenski, M. Ninova, T. Milkova, *Riv. Ital. Sost. Grasse* **89** (2012) 91
3. M. G. Chochkova, E. Y. Chorbadzhiyska, G. I. Ivanova, H. Najdenski, M. Ninova, T. Milkova, *Nat. Prod. J.* **2** (2012) 50
4. M. Spasova, S. Philipov, L. Nikolaeva-Glomb, A. S. Galabov, T. Milkova, *Bioorg. Med. Chem.* **16** (2008) 7457
5. L. Georgiev, I. Totseva, K. Seizova, E. Marinova, M. Chochkova, T. Milkova, in *Proceedings of the 31st European Peptide Symposium*, Copenhagen, Denmark, 2010, p. 60
6. M. Sova, *Mini Rev. Med. Chem.* **12** (2012) 749
7. M. Spasova, V. Kortenska-Kancheva, I. Totseva, G. Ivanova, L. Georgiev, T. Milkova, *J. Pept. Sci.* **12** (2006) 369
8. H. S. Seo, S. Y. Kwak, Y. S. Lee, *Bioorg. Med. Chem.* **20** (2010) 4266
9. S. Y. Kwak, H. S. Seo, Y. S. Lee, *J. Pept. Sci.* **15** (2009) 634
10. S. Y. Kwak, S. Lee, J. K. Yang, Y. S. Lee, *Food Chem.* **130** (2012) 847
11. Q.-Y. Wei, H. Jiang, J.-X. Zhang, C. Zhang, P.-F. Guo, *Asian J. Chem.* **24** (2012) 2383
12. P. Rajan, I. Vedernikova, P. Cos, D. V. Berghe, K. Augustyns, A. Haemers, *Bioorg. Med. Chem. Lett.* **11**, (2001) 215
13. B. Narasimhan, D. Belsare, D. Pharande, V. Mourya, A. Dhake, *Eur. J. Med. Chem.* **39** (2004) 827
14. P. De, G. K. Yoya, P. Constant, F. Bedos-Belval, H. Duran, N. Saffon, M. Daff, M. Baltas, *J. Med. Chem.* **54** (2011) 1449
15. P. De, M. Baltas, F. Bedos-Belval, *Curr. Med. Chem.* **18** (2011) 1672
16. K. Matsushige, K. Hase, S. Kadota, T. Namba, *Biol. Pharm. Bull.* **19** (1996) 655
17. T. Nagaoka, A. H. Banskota, Q. Xiong, Y. Tezuka, S. Kadota, *J. Trad. Med.* **18** (2001) 183
18. Y.-J. Chen, M.-S. Shiao, M.-L. Hsu, T.-H. Tsai, S.-Y. Wang, *J. Agric. Food Chem.* **49** (2001) 5615
19. K. Zhu, M. L. Cordeiro, J. Atienza, W. E. Robinson Jr., S. A. Chow, *J. Virol.* **73** (1999) 3309
20. B. McDougall, J.-P. King, B.-W. Wu, Z. Hostomsky, M. G. Reinecke, W. E., Robinson, Jr., *Antimicrob. Agents Chemother.* **42** (1998) 140
21. J.-P. King, G. Ma, W. Miao, Q. Jia, B. R. McDougall, M. G. Reinecke, C. Cornell, J. Kuan, T.-R. Kim, W. E., Robinson, Jr., *J. Med. Chem.* **42** (1999) 497

22. H.-C. Kwon, C.-M. Jung, C.-G. Shin, J.-K. Lee, S.-U. Choi, S.-Y. Kim, K.-R. Lee, *Chem. Pharm. Bull.* **48** (2000) 1796
23. S. Adisakwattana, K. Sookkongwaree, S. Roengsumran, A. Petsom, N. Ngamrojnavanich, W. Chavasiri, S. Deesamer, S. Yibchok-anuna, *Bioorg. Med. Chem. Lett.* **14** (2004) 2893
24. T. Takahashi, M. Miyazawa, *Med. Chem. Res.* **21** (2012) 1762
25. S. Y. Kwak, S. Lee, H. R. Choi, K. C. Park, Y. S. Lee, *Bioorg. Med. Chem. Lett.* **21** (2011) 5155
26. Q. Fan, H. Jiang, E. D. Yuan, J. X. Zhang, Z. X. Ning, S. J. Qi, Q. Y. Wei, *Food Chem.* **134** (2012) 1081
27. M. R. Loizzo, R. Tundis, F. Menichini, *Compr. Rev. Food Sci. Food Saf.* **11** (2012) 378
28. H. J. Kim, S. H. Seo, B. G. Lee, Y. S. Lee, *Planta Med.* **71** (2005) 785
29. H. S. Baek, J. W. You, G. W. Nam, S. M. Ahn, B. M. Kim, H. S. Rho, D. H. Kim, WIPO Patent No. 2008018683 (2008)
30. H. S. Baek, Y. D. Hong, C. S. Lee, H. S. Rho, S. S. Shin, Y.-H. Park, Y. H. Joo, *Bioorg. Med. Chem. Lett.* **22** (2012) 2110
31. C. Scholtissek, G. Quack, H. D. Klenk, R. G. Webster, *Antiviral Res.* **37** (1998) 83
32. A. J. Hay, *Sem. Virol.* **3** (1992) 21
33. L. H. Pinto, L. J. Holsinger, R. A. Lamb, *Cell* **69** (1992) 517
34. A. Moscona, *N. Engl. J. Med.* **353** (2005) 1363
35. A. Moscona, *N. Engl. J. Med.* **353** (2005) 2633
36. Y. Kim, S. Narayanan, K.-O. Chang, *Antiviral Res.* **88** (2010) 227
37. R. Fioravanti, I. Celestino, R. Costi, G. C. Crucitti, L. Pescatori, L. Mattiello, E. Novelino, P. Checconi, A. T. Palamara, L. Nencioni, R. Di Santo, *Bioorg. Med. Chem.* **20** (2012) 5046
38. M. Haidaria, M. Alia, S. W. Casscells III, M. Madjid, *Phytomedicine* **16** (2009) 1127
39. N. Uchide, H. Toyoda, *Molecules* **16** (2011) 2032
40. M. S. Blois, *Nature* **181** (1958) 1199
41. E. Graf, *Free Rad. Biol. Med.* **13** (1992) 435
42. M. Mileva, V. Hadjimitova, L. Tantcheva, T. Traykov, A. S. Galabov, V. Savov, S. Ribarov, *Z. Naturforsch. C.* **55** (2000) 824
43. C. Gómez-Cordovés, B. Bartolomé, W. Vieira, V. M. Virador, *J. Agric. Food Chem.* **49** (2001) 1620
44. J. S. Roh, J. Y. Han, J. H. Kim, J. K. Hwang, *Biol. Pharm. Bull.* **27** (2004) 1976
45. S. Okombi, D. Rival, S. Bonnet, A. M. Mariotte, E. Perrier, A. Boumendjel, *Bioorg. Med. Chem. Lett.* **16** (2006) 2252
46. Q. Fan, H. Jiang, E. D. Yuan, J. X. Zhang, Z. X. Ning, S. J. Qi, Q. Y. Wei, *Food Chem.* **134** (2012) 1081
47. S. M. An, J. S. Koh, Y. C. Boo, *Phytother. Res.* **24** (2010) 1175
48. A. Garozzo, G. Tempera, D. Ungheri, R. Timpanaro, A. Castro, *Int. J. Immunopathol. Pharmacol.* **20** (2007) 349
49. P. Ghezzi, D. Ungheri, *Int. J. Immunopathol. Pharmacol.* **17** (2004) 99
50. M. Mileva, R. Bakalova, L. Tantcheva, A. S. Galabov, S. Ribarov, *Comp. Immunol. Microbiol. Inf. Dis.* **25** (2002) 1
51. N. Nenadis, M. Tsimidou, *J. Am. Oil Chem. Soc.* **79** (2002) 1191.



SUPPLEMENTARY MATERIAL TO
**Synthesis and biological activity of hydroxycinnamoyl-
-containing antiviral drugs**

MAYA G. CHOCHKOVA^{1*}, ASSYA P. GEORGIEVA¹, GALYA I. IVANOVA²,
NADYA NIKOLOVA³, LUCHIA MUKOVA³, LUBOMIRA NIKOLAEVA-GLOMB³
and TSENKA S. MILKOVA¹

¹South-West University “Neofit Rilski”, Blagoevgrad, Bulgaria, ²Departamento de Química,
Faculdade de Ciências, Universidade do Porto, Porto, Portugal and ³The Stephan Angeloff
Institute of Microbiology, Bulgarian Academy of Sciences, Sofia, Bulgaria

J. Serb. Chem. Soc. 79 (5) (2014) 517–526

ANALYTIC AND SPECTRAL DATA FOR THE SYNTHESIZED COMPOUNDS

N-[(*E*)-3-(3',4'-Dihydroxyphenyl)-2-propenoyl]oseltamivir (**1**). Yield: 48 %; Anal. Calcd. for C₂₅H₃₄N₂O₇: C, 63.27; H 7.22; N, 5.90 %. Found: C, 63.31; H, 7.18; N, 5.89 %; ¹H-NMR (400.15 MHz, CDCl₃, δ / ppm): 0.82 (3H, *t*, *J* = 7.3 Hz, -CHCH₂CH₃), 0.87 (3H, *t*, *J* = 7.3 Hz, -CHCH₂CH₃), 1.26 (3H, *t*, *J* = 7.3 Hz, -O-CH₂CH₃), 1.49 (4H, *q*, *J* = 7.3 Hz, 2 × -CHCH₂CH₃), 1.84 (3H, *s*, -C(O)CH₃), 2.73 (1H, *m*, -CHCH₂CH_{2a}), 2.78 (1H, *m*, -CHCH₂CH_{2b}), 3.35 (1H, *m*, -CHCH₂CH₃), 4.15–4.17 (3H, *m*, 2 × -O-CH₂CH₃ + 1 × -CHCH₂CH₂), 4.31 (1H, *brs*, -CHCH₂CH₂), 6.19 (1H, *d*, *J* = 15.5 Hz, =CH-C(O)-), 6.68 (2H, *s*, 2 × *o*-CH), 6.75 (1H, *brs*, =CH), 6.97 (1H, *s*, *m*-CH), 7.32 (2H, *brs*, 2 × NH), 7.38 (1H, *d*, *J* = 15.5 Hz, =CH-Ph), 8.18 (2H, *brs*, 2 × OH); ¹³C-NMR (100.62 MHz, CDCl₃, δ / ppm): 172.9 (COOC₂H₅), 167.8 (HNCO), 166.3, 146.9, 144.8, 142.1 (=CH-Ph), 137.7 (=CHCHCH), 129.2 (C_q), 127.1 (C_q), 121.9 (*o*-CH), 117.3 (=CH-CO), 116.0 (*o*-CH), 114.8 (CH), 82.8 (-O-CHCH₂CH₃), 75.8 (-OCH), 61.0 (-O-CH₂CH₃), 55.3 (-C(O)HN-CH), 48.4 (-HN-CH), 30.6 (-CHCH₂CH₂), 26.4 (-CHCH₂CH₃), 25.8 (-CHCH₂CH₃), 22.9 (-O)CCH₃, 14.2 (-O-CH₂CH₃), 9.5 (-CHCH₂CH₃), 9.5 (-CHCH₂CH₃); ESI-MS (*m/z*): 475 ([M+H]⁺), 497 ([M+Na]⁺), 949 ([2M+H]⁺); UV-Vis (EtOH) (λ_{max} / nm (ε / L mol⁻¹ cm⁻¹): 203 (32490), 218 (30971), 297 (17434), 325 (20457).

N-[(*E*)-3-(3',5'-Dimethoxy-4'-hydroxyphenyl)-2-propenoyl]oseltamivir (**2**). Yield: 42 %; Anal. Calcd. for C₂₇H₃₈N₂O₈: C, 62.53; H 7.39; N, 5.40 %. Found: C, 62.47; H, 7.41; N, 5.67 %; ¹H-NMR (400.15 MHz, CDCl₃, δ / ppm): 0.92 (3H, *t*, *J* = 7.2 Hz, -CHCH₂CH₃), 0.90 (3H, *t*, *J* = 7.2 Hz, -CHCH₂CH₃), 1.29

* Corresponding author. E-mail: mayabg2002@yahoo.com

(3H, *t*, $J = 7.2$ Hz, $-\text{O}-\text{CH}_2\text{CH}_3$), 1.53 (4H, *q*, $J = 7.2$ Hz, $2 \times -\text{CHCH}_2\text{CH}_3$), 1.96 (3H, *s*, $-\text{C}(\text{O})\text{CH}_3$), 2.37 (1H, *dd*, $J = 16.8, 9.6$ Hz, $-\text{CHCHCH}_2\text{a}$), 2.86 (1H, *dd*, $J = 16.8, 5.6$ Hz, $-\text{CHCHCH}_2\text{b}$), 3.41 (1H, *m*, $-\text{CHCH}_2\text{CH}_3$), 3.88 (6H, *s*, $2 \times \text{OCH}_3$), 4.05-4.40 (5H, *m*, $-\text{O}-\text{CH}_2\text{CH}_3$, $-\text{CHCHCH}_2$, $-\text{CHCHCH}_2$, $-\text{CHCHCHCH}_2$), 5.82 (1H, *s*, OH), 6.18 (1H, *d*, $J = 8.3$ Hz, NH), 6.25 (1H, *d*, $J = 15.1$ Hz, $=\text{CH}-\text{C}(\text{O})-$), 6.71 (2H, *s*, $2 \times o\text{-CH}$), 6.75 (1H, *d*, $J = 9.6$ Hz, NH), 6.82 (1H, *brs*, $=\text{CH}$), 7.48 (1H, *d*, $J = 15.1$ Hz, $=\text{CH}-\text{Ph}$); ^{13}C -NMR (100.62 MHz, CDCl_3 , δ / ppm): 172.9 (COOC_2H_5), 167.8 (HNCO), 166.3, 147.2, 146.6, 141.7 ($=\text{CH}-\text{Ph}$), 137.4 ($=\text{CHCHCH}$), 136.7 (Cq), 129.5 (Cq), 126.0 (Cq), 118.2 ($=\text{CH}-\text{CO}$), 104.8 ($2 \times o\text{-CH}$), 82.8 ($-\text{O}-\text{CHCH}_2\text{CH}_3$), 75.6 ($-\text{OCH}$), 61.0 ($-\text{O}-\text{CH}_2$), 56.2 ($2 \times \text{OCH}_3$), 54.5 ($-\text{C}(\text{O})\text{HN}-\text{CH}$), 48.8 ($-\text{HN}-\text{CH}$), 30.9 ($-\text{CHCHCH}_2$), 26.3 ($-\text{CHCH}_2\text{CH}_3$), 25.8 ($-\text{CHCH}_2\text{CH}_3$), 23.3 ($-(\text{O})\text{CCH}_3$), 14.2 ($-\text{O}-\text{CH}_2\text{CH}_3$), 9.5 ($-\text{CHCH}_2\text{CH}_3$), 9.2 ($-\text{CHCH}_2\text{CH}_3$); ESI-MS (m/z): 519.2 ($[\text{M}+\text{H}]^+$), 541 ($[\text{M}+\text{Na}]^+$); UV-Vis (EtOH) (λ_{max} / nm (ϵ / $\text{L mol}^{-1}\text{cm}^{-1}$): 203 (56915), 225 (42016), 323 (24306).

N-[(E)-3-(3'-Methoxy-4'-hydroxyphenyl)-2-propenoyl]oseltamivir (**3**). Yield: 31.4 %; Anal. Calcd. for $\text{C}_{26}\text{H}_{36}\text{N}_2\text{O}_7$: C, 63.92; H 7.43; N, 5.40 %. Found: C, 63.84; H, 7.39; N, 5.36 %; ^1H -NMR (400.15 MHz, CDCl_3 , δ / ppm): 0.89 (3H, *t*, $J = 7.5$ Hz, $-\text{CHCH}_2\text{CH}_3$), 0.92 (3H, *t*, $J = 7.5$ Hz, $-\text{CHCH}_2\text{CH}_3$), 1.29 (3H, *t*, $J = 7.5$ Hz, $-\text{O}-\text{CH}_2\text{CH}_3$), 1.53 (4H, *q*, $J = 7.5$ Hz, $2 \times -\text{CHCH}_2\text{CH}_3$), 1.94 (3H, *s*, $-\text{C}(\text{O})\text{CH}_3$), 2.37 (1H, *dd*, $J = 18.0, 9.7$ Hz, $-\text{CHCHCH}_2\text{a}$), 2.86 (1H, *dd*, $J = 18.0, 5.3$ Hz, $-\text{CHCHCH}_2\text{b}$), 3.41 (1H, *m*, $-\text{CHCH}_2\text{CH}_3$), 3.87 (3H, *s*, OCH_3), 4.05-4.40 (5H, *m*, $-\text{O}-\text{CH}_2\text{CH}_3$, $-\text{CHCHCH}_2$, $-\text{CHCHCH}_2$, $-\text{CHCHCHCH}_2$), 6.10 (1H, *brs*, OH), 6.24 (1H, *d*, $J = 15.3$ Hz, $=\text{CH}-\text{C}(\text{O})-$), 6.30 (1H, *d*, $J = 8.5$ Hz, NH), 6.80 (2H, NH + $=\text{CH}$), 6.85 (1H, *d*, $J = 7.7$ Hz, *m*-CH), 6.95 (1H, *d*, $J = 2.0$ Hz, *o*-CH), 6.99 (1H, *dd*, $J = 7.7, 2.0$ Hz, *o*-CH), 7.50 (1H, *d*, $J = 15.3$ Hz, $=\text{CH}-\text{Ph}$); ^{13}C -NMR (100.62 MHz, CDCl_3 , δ / ppm): 171.8 (COOC_2H_5), 166.7 (HNCO), 165.9, 147.2, 146.6, 141.4 ($=\text{CH}-\text{Ph}$), 137.5 ($=\text{CHCHCH}$), 129.4 (Cq), 127.1 (Cq), 122.5 (*o*-CH), 117.9 ($=\text{CH}-\text{CO}$), 114.7 (*m*-CH), 109.2 (*o*-CH), 82.8 ($-\text{O}-\text{CHCH}_2\text{CH}_3$), 75.7 ($-\text{OCH}$), 61.0 ($-\text{O}-\text{CH}_2\text{CH}_3$), 55.9 (OCH_3), 54.5 ($-\text{C}(\text{O})\text{HN}-\text{CH}$), 48.8 ($-\text{HN}-\text{CH}$), 30.8 ($-\text{CHCHCH}_2$), 26.3 ($-\text{CHCH}_2\text{CH}_3$), 25.7 ($-\text{CHCH}_2\text{CH}_3$), 23.3 ($-(\text{O})\text{CCH}_3$), 14.2 ($-\text{O}-\text{CH}_2\text{CH}_3$), 9.5 ($-\text{CHCH}_2\text{CH}_3$), 9.2 ($-\text{CHCH}_2\text{CH}_3$); ESI-MS (m/z): 489.5 ($[\text{M}+\text{H}]^+$), 511 ($[\text{M}+\text{Na}]^+$), 977 ($[\text{2M}+\text{H}]^+$); UV-Vis (EtOH) (λ_{max} / nm (ϵ / $\text{L mol}^{-1}\text{cm}^{-1}$): 203 (48276), 218 (45018), 295 (25826), 322 (33300).

N-[(E)-3-(3',4'-Dihydroxyphenyl)-2-propenoyl]rimantadine (**4**). Yield: 68.1 %; Anal. Calcd. for $\text{C}_{21}\text{H}_{27}\text{NO}_3$: C, 73.87; H 7.97; N, 4.10 %. Found: C, 73.64; H, 7.91; N, 4.12 %; ^1H -NMR (400.15 MHz, $\text{DMSO}-d_6$, δ / ppm): 1.08 (3H, *d*, $J = 7.0$ Hz, CH_3), 1.4-1.9 (12H, *m*, $6 \times -\text{CH}_2$), 1.98 (3H, CH, cyclo), 3.83 (1H, *m*, $-\text{CHCH}_3$), 5.67 (1H, *d*, $J = 10.0$ Hz, NH), 6.25 (1H, *d*, $J = 15.8$ Hz, $=\text{CH}$), 6.76 (1H, *brs*, OH), 6.86 (1H, *d*, $J = 8.2$ Hz, *m*-CH), 6.96 (1H, *dd*, $J = 8.2$ Hz, 1.8 Hz,

o-CH), 7.18 (1H, *d*, $J = 1.8$ Hz, *o*-CH), 7.55 (1H, *d*, $J = 15.8$ Hz, =CH), 8.15 (1H, *s*, OH); ^{13}C -NMR (100.62 MHz, DMSO- d_6 , δ / ppm): 166.9 (CO), 146.8, 144.3, 142.3 (CH), 127.0 (Cq), 120.3 (*o*-CH), 117.5 (=CH), 115.8 (*o*-CH), 115.4 (*m*-CH), 53.7 (CHCH₃), 38.4 (CH₂, cycle), 37.0 (CH₂, cycle), 28.2 (CH, cycle), 14.5(CHCH₃); ESI-MS (m/z): 342.1 ([M+H]⁺), 364.5 ([M+Na]⁺); UV-Vis (EtOH) (λ_{max} / nm (ϵ / L mol⁻¹cm⁻¹)): 220 (61680), 242 (52404), 296 (54191), 322 (58566).

N-[(*E*)-3-(3',5'-Dimethoxy-4'-hydroxyphenyl)-2-propenoyl]amantadine (**5**). Yield: 53 %; Anal. Calcd. for C₂₁H₂₇NO₄: C, 70.56; H 7.61; N, 3.92 %. Found: C, 70.58; H, 7.47; N, 3.96 %; ^1H -NMR (400.15 MHz, DMSO- d_6 , δ / ppm): 1.62 (6H, *s*, cycle), 1.9–2.1 (9H, *m*, cycle), 3.86 (6H, *s*, 2×OCH₃), 5.70 (1H, *s*, NH), 6.51 (1H, *d*, $J = 15.6$ Hz, HC=), 6.86 (2H, *s*, Ar-H(_o)), 7.24 (1H, *d*, $J = 15.6$ Hz, HC=), 9.80 (1H, *s*, OH); ^{13}C -NMR (100.62 MHz, DMSO- d_6 , δ / ppm): 165.9 (CO), 148.1, 153.4 (ArOH), 141.2 (=CH-Ar), 127.0 (Cq-Ar), 122.2 (HN-CH=), 115.3 (=CH), 105.3 (2×Ar-ortho-CH), 57.2 (OCH₃), 53.1 (HN-CH), 50.9 (Cq, cycle), 42.6 (CH₂, cycle), 37.3 (CH₂), 30.4 (CH, cycle); ESI-MS (m/z): 358 ([M+H]⁺), 380 ([M+Na]⁺), 715 ([2M+H]⁺), 737.1 ([2M+Na]⁺); UV-Vis (EtOH) (λ_{max} / nm (ϵ / L mol⁻¹ cm⁻¹)): 201 (32395), 235 (34457), 320 (30539).

N-[(*E*)-3-(3'-methoxy-4'-hydroxyphenyl)-2-propenoyl]amantadine (**6**). Yield: 42.1 %; Anal. Calcd. for C₂₀H₂₅NO₃: C, 73.37; H 7.70; N, 4.28 %. Found: C, 73.41; H, 7.73; N, 4.56 %; ^1H -NMR (400.15 MHz, DMSO- d_6 , δ / ppm): 1.49 (6H, *s*, cycle), 1.93–2.30 (9H, cycle), 3.82 (3H, *s*, OCH₃), 6.46 (1H, *d*, $J = 15.5$ Hz, HC=), 6.82 (1H, *d*, $J = 8.1$ Hz, Ar-H(*m*)), 7.12 (1H, *d*, $J = 1.8$ Hz, Ar-H(*o*)), 7.28 (1H, *s*, Ar-H(*o*)), 7.31 (1H, *s*, NH), 7.52 (1H, *d*, $J = 15.5$ Hz, HC=), 9.02 (1H, *s*, OH); ^{13}C -NMR (100.62 MHz, DMSO- d_6 , δ / ppm): 166.1(CO), 152.6, 141.0 (=CH), 129.1 (2C, Ar-CH), 126.1 (Cq), 120.2 (=CH), 115.7 (2C, Ar-CH), 56.3 (OCH₃), 53.3 (HN-CH), 42.6 (CH₂, cycle), 37.3 (CH₂), 30.4 (CH, cycle); ESI-MS (m/z): 328 ([M+H]⁺), 350 ([M+Na]⁺), 390 ([M+Na+K]⁺); UV-Vis (EtOH) (λ_{max} / nm (ϵ / L mol⁻¹ cm⁻¹)): 218 (97221), 234 (91575), 293 (102106), 321 (120575).

N-[(*E*)-3-(4'-hydroxyphenyl)-2-propenoyl]amantadine (**7**). Yield: 40 %; Anal. Calcd. for C₁₉H₂₃NO₂: C, 76.74; H 7.80; N, 4.71 %. Found: C, 76.71; H, 7.84; N, 4.49 %; ^1H -NMR (400.15 MHz, DMSO- d_6 , δ / ppm): 1.62 (6H, *s*, cycle), 1.9–2.1 (9H, *m*, cycle), 6.43 (1H, *d*, $J = 15.6$ Hz, HC=), 6.76 (2H, *d*, $J = 8.38$ Hz, *p*-H), 7.19 (1H, *d*, $J = 15.6$ Hz, HC=), 7.32 (2H, *d*, $J = 8.38$ Hz, *o*-H), 7.42 (1H, *s*, NH), 9.80 (1H, *s*, OH); ^{13}C -NMR (100.62 MHz, DMSO- d_6 , δ / ppm): 164.6 (CO), 158.6, 138.0 (=CH), 129.1 (2C, Ar-CH), 126.1 (Cq), 120.2 (=CH), 115.7 (2C, Ar-CH), 50.9 (Cq, cycle), 41.3 (CH₂, cycle), 35.9 (CH₂), 28.9 (CH, cycle); ESI-MS (m/z): 298 ([M+H]⁺), 320 ([M+Na]⁺); UV-Vis (EtOH) (λ_{max} / nm): 212 (30565), 224 (25452), 293 (20254).



J. Serb. Chem. Soc. 79 (5) 527–531 (2014)
JSCS–4604

SHORT COMMUNICATION

**Iodine-mediated one-pot synthesis of 3-cyanocoumarins and
3-cyano-4-methylcoumarins**

DINESH SHARMA^{1*} and JAGDISH K. MAKRANDI²

¹Department of Chemistry, BRCM College of Engineering & Technology, Bahal-127028,
India and ²Department of Chemistry, Maharshi Dayanand University, Rohtak-124001, India

(Received 27 January, accepted 21 November 2013)

Abstract: 2-Hydroxybenzaldehydes **1a–e** on reaction with malononitrile (**2**) in the presence of iodine as catalyst give 3-cyanocoumarins **3a–e** in one step under thermal heating as well as under microwave irradiation. The latter conditions are much more efficient in terms of time (2–5 min) and yield as compared to the thermal conditions (2–2.5 h). Following a similar procedure, 3-cyano-4-methylcoumarins **3f–i** were also prepared by the reaction of 2-hydroxyacetophenones **1f–i** with **2**.

Keywords: 3-cyanocoumarin/3-cyano-4-methylcoumarin; malononitrile; iodine; microwave irradiation; one-pot reaction.

INTRODUCTION

3-Cyanocoumarins (2-oxo-2H-chromene-3-carbonitriles) constitute an important class of compounds because of their biological activities,¹ such as antimicrobial properties² and inhibition of α -chymotripsin.³ These compounds have also been used as intermediates for the preparation of methine dyes,⁴ cephalosporins,⁵ modified penicillins,⁶ oxygen-bridged tetrahydropyridones⁷ and isoureas.⁸

3-Cyanocoumarins were earlier prepared by the reaction of 2-hydroxybenzaldehydes with malononitrile or with ethyl cyanoacetate under basic conditions using various bases, such as pyridine,⁹ piperidine,¹⁰ aqueous alkali,¹¹ Mg–Al hydrotalcite,¹² MgO¹³ and ionic liquids.^{14,15} In addition, these reactions have been performed under phase transfer catalysed conditions.¹⁶ In recent reports, these compounds were obtained by the condensation of 2-hydroxybenzaldehydes with malononitrile using ZrCl₄/[bmim]BF₄¹⁷ and SiCl₄ in ethanol.¹⁸

* Corresponding author. E-mail: dksharma_84@rediffmail.com
doi: 10.2298/JSC130127140S

However, these methods suffer from one or other limitations. The former reaction between 2-hydroxybenzaldehyde and malononitrile gives 2-imino-2*H*-chromene-3-carbonitrile as an intermediate that has to be hydrolysed under acidic conditions.¹⁶ In the latter method, 3-carboxycoumarins are also formed along with 3-cyanocoumarins.¹⁹

In recent years, molecular iodine was used as a mild and efficient condensing agent in various organic reactions.^{20–23} Thus, it was thought worthwhile to study the reaction of 2-hydroxybenzaldehydes and malononitrile using iodine as catalyst, which led to the synthesis of 3-cyanocoumarins in a single step.

RESULTS AND DISCUSSION

A solution of 2-hydroxybenzaldehyde (**1a**) and malononitrile (**2**) in dimethylformamide (DMF) was refluxed in the presence of a catalytic amount of iodine, and the reaction was found to proceed to completion in 2 h, as evidenced by thin layer chromatography (TLC), affording a colourless compound that was identified as 3-cyanocoumarin (**3a**) based on its IR, ¹H-NMR and ¹³C-NMR spectral data.

As the reactions are known to be improved when they are performed under microwave irradiations,²⁴ the above reaction was repeated using microwave irradiation and it was found to be completed in 2 min and 3-cyanocoumarin was obtained in 90 % yield.

Using the above conditions, 3-cyano-4-methylcoumarins **3f–i** were also prepared by the reaction of 2-hydroxyacetophenones **1f–i** with **2** using iodine as catalyst under both thermal and microwave conditions.

The optimum conditions of the reaction were checked by varying the amount of iodine and 0.12 mmol of iodine was found to be sufficient for completion of the reaction. No reaction was found to take place in the absence of the catalyst. It appears that initial condensation between 2-hydroxybenzaldehyde and malononitrile was catalysed by iodine, which is known to act as a condensing agent due to its Lewis acidity.²⁵ Excessive amounts of iodine (20–40 mol %) were found excessive, as no further improvement of the reaction was found either in terms of the yield or the reaction time.

The methods reported earlier could not be used successfully for the preparation of 3-cyano-4-methylcoumarins involving reaction of 2-hydroxyacetophenones with malononitrile as it required stringent conditions and the yields were very poor. However, these compounds could be obtained in excellent yield (85–90 %) using the present method. The success of the method was established by the synthesis of various substituted 3-cyanocoumarins and 3-cyano-4-methylcoumarins **3a–i**. The identity of all the compounds was checked by their IR and ¹H-NMR spectral data, given in the Supplementary material to this paper, and comparison of the melting points with literature values, Table I.

EXPERIMENTAL

The melting points of **3a-i** were determined in open capillaries. The IR spectra were recorded on a Perkin-Elmer spectrum BX series FT-IR spectrophotometer using the KBr pellets technique. The ^1H - and ^{13}C -NMR spectra were recorded on a Bruker Avance (400 MHz) instrument using TMS as an internal standard. The reactions were performed in a microwave oven (Samsung, model CE1031LFB, output energy 900 W, frequency 2450 MHz) with a temperature control arrangement maintaining the temperature of the oven at 100 °C using 50 % power for all the experiments.

TABLE I. Physical data of 3-cyanocoumarins and 3-cyano-4-methylcoumarins; method A: thermal conditions; method B: microwave conditions

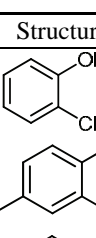
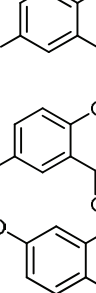
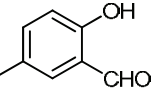
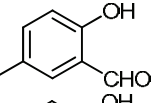
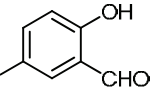
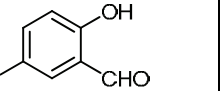
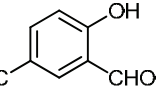
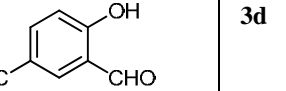
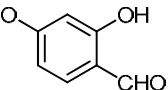
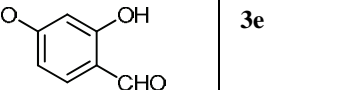
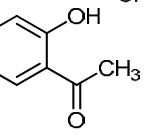
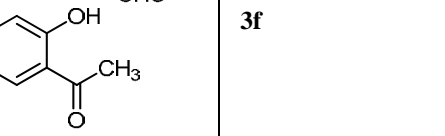
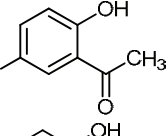
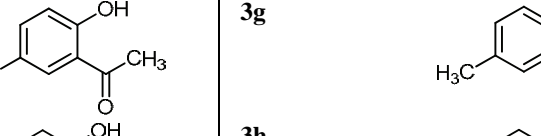
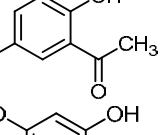
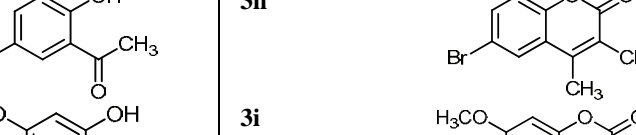
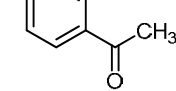

Compound	Structure	Compound	Structure
1a		3a	
1b		3b	
1c		3c	
1d		3d	
1e		3e	
1f		3f	
1g		3g	
1h		3h	
1i		3i	

TABLE I. Continued

Compound	R	R ₁	R ₂	Method A		Method B		M.p. / °C
				Time, h	Yield, %	Time, min	Yield, %	
3a	H	H	H	2	85	2	90	179–181 ¹⁰
3b	H	H	Br	2	92	2.5	95	195–196 ²⁶
3c	H	H	Cl	2	86	2.5	92	190–192 ²⁷
3d	H	H	CH ₃	2	80	3	85	204–206 ²⁸
3e	H	OCH ₃	H	2	82	3	86	223–226 ²⁹
3f	CH ₃	H	H	2.5	86	4	92	190–192 ³⁰
3g	CH ₃	H	CH ₃	2.5	90	5	95	200–201 ²⁶
3h	CH ₃	H	Br	2.5	90	4	95	178–180 ²⁶
3i	CH ₃	OCH ₃	H	2.5	85	5	87	220–222 ²⁹

General procedure for the synthesis of 3-cyano-/3-cyano-4-methyl-coumarins 3a–i

Method A (thermal conditions). A mixture of 2-hydroxybenzaldehydes/2-hydroxyacetophenones **1a–i** (4.71 mmol), malononitrile (**2**, 0.32 g, 4.71 mmol), iodine (0.03 g, 0.12 mmol) and dimethylformamide (10 mL) in a round bottom flask (50 ml) was heated in an oil bath at 140–145 °C for 2–2.5 h. Completion of the reaction was monitored by thin layer chromatography (silica gel plates using the solvent benzene: acetone, 1:1). The reaction mixture was cooled and ice-cold sodium thiosulphate solution (10 %, 30 mL) was added to remove any iodine present in the reaction mixture. The solid that separated out was filtered, washed with water and recrystallised from aqueous ethanol to give **3a–i**.

Method B (microwave conditions): A mixture of 2-hydroxybenzaldehydes/2-hydroxyacetophenones **1a–i** (4.71 mmol), malononitrile (**2**, 0.32 g, 4.71 mmol), iodine (0.03 g, 0.12 mmol) and dimethylformamide (5 mL) taken in a loosely stoppered round bottom flask was subjected to microwave irradiation for 2–5 min. Completion of the reaction was controlled by thin layer chromatography and the work-up was as described above to give **3a–i**.

CONCLUSION

In conclusion, the presented method appears to be extremely simple and highly efficient giving 3-cyano- and 3-cyano-4-methyl-coumarins in a single step.

SUPPLEMENTARY MATERIAL

Spectral data for the synthesised coumarins are available electronically from <http://www.shd.org.rs/JSCS/>, or from the corresponding author on request.

ИЗВОД

ЈЕДНОСТАВНА СИНТЕЗА 3-ЦИЈАНОКУМАРИНА И 3-ЦИЈАНО-4-МЕТИЛКУМАРИНА У ПРИСУСТВУ ЈОДА

DINESH SHARMA¹ и JAGDISH K. MAKRANDI²

¹Department of Chemistry, BRCM College of Engineering & Technology, Bahal-127028, India и ²Department of Chemistry, Maharshi Dayanand University, Rohtak-124001, India

2-Хидроксибензалдехиди **1a–e** у реакцији са малондинитрилом (**2**), у присуству јода као катализатора, под условима термалног загревања или микроталасног озрачивања, као производ дају 3-цијанокумарине **3a–e**. Реакције под микроталасима трају знатно краће време (2–5 min) у поређењу са термичким загревањем (2–2,5 h). При-

меном сличних реакционих услова, 3-цијано-4-метилкумарини **3f-i** су добијени полазећи од 2-хидроксиацетофена **1f-i** и **2**.

(Примљено 27. јануара, прихваћено 21. новембра 2013)

REFERENCES

1. S. Fomine, E. Rivera, L. Fomina, A. Oritz, T. Ogawa, *Polymer* **39** (1998) 3551
2. A. A. Zaha, A. Hazem, *New Microbiol.* **25** (2002) 213
3. C. Doucet, L. Pochet, N. Thierry, B. Pirotte, J. Delarge, M. R. Rovaux, *J. Med. Chem.* **42** (1999) 4161
4. J. D. Kendall, A. J. Axford, Brit Patent 672741 (1952) (CA 1955, 49, 84)
5. L. Bonsignore, F. Cottiglia, H. Elkhaili, F. Jehl, S. M. Lavagna, G. Loy, F. Manna, H. Monteil, D. Pompei, D. Secci, *Farmaco* **53** (1998) 425
6. L. Bonsignore, A. Delogu, G. Loy, S. M. Lavagna, D. Secci, *Eur. J. Med. Chem.* **29** (1994) 479
7. D. Jonsson, M. Erlandsson, A. Unden, *Tetrahedron Lett.* **42** (2001) 6953.
8. L. Bonsignore, F. Cottiglia, S. M. Lavagna, G. Loy, D. Secci, *Heterocycles* **50** (1999) 469
9. E. Clingolani, *Gazz. Chim. Ital.* **84** (1954) 843
10. W. Baker, C. S. Howas, *J. Chem. Soc.* (1953) 119
11. F. Fringuelli, O. Piermatti, F. Pizzo, *Synthesis* **15** (2003) 2331
12. A. Ramani, B. M. Chanda, S. Sivasankar, *Green Chem.* **1** (1999) 163
13. H. Valizadeh, A. Fakhari, *J. Heterocycl. Chem.* **46** (2009) 1392
14. H. Valizadeh, H. Gholipour, *Synth. Commun.* **40** (2010) 1477
15. M. M. Heravi, P. Ansari, M. Saeedi, N. Karimil, N. T. Hosseini, *Bull. Chem. Soc. Ethiop.* **35** (2011) 315
16. Seema, S. Kumar, J. K. Makrandi, *Indian J. Chem., B* **44** (2005) 1307
17. H. Valizadeh, M. Mahmoodian, H. Gholipour, *J. Heterocycl. Chem.* **48** (2011) 799
18. T. A. Salama, M. A. Ismail, A. G. M. Khalil, S. S. Elmorsy, *ARKIVOC* (2012) 242
19. F. Fringuelli, O. Piermatti, F. Pizzo, *J. Chem. Educ.* **81** (2004) 874
20. J. S. Yadav, P. K. Chand, S. Anjaneyulu, *Tetrahedron Lett.* **43** (2002) 3783
21. R. A. Periana, O. Mirinov, D. J. Taube, S. Gamble, *J. Chem. Soc. Chem. Commun.* (2002) 2376
22. D. Bandyopadhyay, J. Cruz, R. N. Yadav, B. K. Banik, *Molecules* **17** (2012) 11570
23. Y. Hanzawa, Y. Kasashima, K. Tomono, T. Mino, M. Sakamoto, T. Fujita, *J. Oleo Sci.* **61** (2012) 393.
24. F. M. Moghaddam, Z. Mirjafary, H. Saeidian, *Sci. Iran., Trans. C* **16** (2009) 12
25. A. Parveen, M. R. S. Ahmed, K. A. Shaikh, S. P. Deshmukh, R. P. Pawar, *ARKIVOC* (2007) 12
26. S. Kumar, *Orient. J. Chem.* **25** (2009) 1145
27. J. M. Bruce, D. Creed, K. Davas, *J. Chem. Soc.* (1971) 3749
28. R. Clinging, F. M. Dean, L. E. Houghton, *J. Chem. Soc.* (1970) 897
29. S. S. Lele, M. G. Patel, S. Sethna, *J. Org. Chem.* **27** (1962) 637
30. C. H. Schroeder, K. P. Link, *J. Am. Chem. Soc.* **75** (1953) 1886.



SUPPLEMENTARY MATERIAL TO
**Iodine-mediated one-pot synthesis of 3-cyanocoumarins and
3-cyano-4-methylcoumarins**

DINESH SHARMA^{1*} and JAGDISH K. MAKRANDI²

¹Department of Chemistry, BRCM College of Engineering & Technology, Bahal-127028,
India and ²Department of Chemistry, Maharshi Dayanand University, Rohtak-124001, India

J. Serb. Chem. Soc. 79 (5) (2014) 527–531

SPECTRAL DATA FOR THE SYNTHESISED COUMARINS

3-Cyanocoumarin (3a). IR (KBr, λ_{\max} / cm^{-1}): 1725 (C=O), 2226 (C \equiv N); ¹H-NMR (400 MHz, CDCl₃, δ / ppm): 7.30–7.60 (2H, *m*), 7.68–8.0 (2H, *m*), 8.75 (1H, *s*); ¹³C-NMR (100 MHz, CDCl₃, δ / ppm): 101.5, 113.6, 114.8, 119.7, 122.8, 126.1, 128.8, 131.8, 154.8, 161.2.

6-Bromo-3-cyanocoumarin (3b). IR (KBr, λ_{\max} / cm^{-1}): 1737 (C=O), 2235 (C \equiv N); ¹H-NMR (400 MHz, CDCl₃, δ / ppm): 7.35 (1H, *d*, *J* = 9.0 Hz), 7.83–7.85 (1H, *dd*, *J* = 9.0 Hz, *J* = 2.5 Hz), 7.90 (1H, *d*, *J* = 2.5 Hz), 8.55 (1H, *s*); ¹³C-NMR (100 MHz, CDCl₃, δ / ppm): 101.2, 113.2, 117.8, 118.2, 118.5, 118.8, 130.9, 136.6, 154.2, 161.0.

6-Chloro-3-cyanocoumarin (3c). IR (KBr, λ_{\max} / cm^{-1}): 1726 (C=O), 2228 (C \equiv N); ¹H-NMR (400 MHz, CDCl₃, δ / ppm): 7.50 (1H, *d*, *J* = 9.0 Hz), 7.82–7.84 (1H, *dd*, *J* = 9.0 Hz, *J* = 2.5 Hz), 7.95 (1H, *d*, *J* = 2.5 Hz), 8.72 (1H, *s*); ¹³C-NMR (100 MHz, CDCl₃, δ / ppm): 101.4, 113.4, 116.8, 120.6, 122.8, 130.2, 131.0, 132.6, 154.8, 161.5.

3-Cyano-6-methylcoumarin (3d). IR (KBr, λ_{\max} / cm^{-1}): 1725 (C=O), 2225 (C \equiv N); ¹H-NMR (400 MHz, CDCl₃, δ / ppm): 2.48 (3H, *s*, CH₃), 7.22–7.72 (3H, *m*), 8.22 (1H, *s*); ¹³C-NMR (100 MHz, CDCl₃, δ / ppm): 21.6, 101.4, 113.7, 117.8, 118.5, 119.7, 128.6, 134.2, 137.4, 155.2, 162.1.

3-Cyano-7-methoxycoumarin (3e). IR (KBr, λ_{\max} / cm^{-1}): 1715 (C=O), 2215 (C \equiv N); ¹H-NMR (400 MHz, CDCl₃, δ / ppm): 3.45 (3H, *s*), 7.18 (1H, *d*, *J* = 2.5 Hz), 7.82–7.85 (2H, *m*), 8.92 (1H, *s*); ¹³C-NMR (100 MHz, CDCl₃, δ / ppm): 56.2, 101.8, 102.2, 111.4, 112.6, 113.4, 119.8, 132.6, 156.4, 159.8, 164.4.

3-Cyano-4-methylcoumarin (3f). IR (KBr, λ_{\max} / cm^{-1}): 1725 (C=O), 2230 (C \equiv N); ¹H-NMR (400 MHz, CDCl₃, δ / ppm): 2.72 (3H, *s*), 7.20–7.52 (4H, *m*);

*Corresponding author. E-mail: dksharma_84@rediffmail.com

^{13}C -NMR (100 MHz, CDCl_3 , δ / ppm): 18.1, 96.2, 113.2, 120.4, 122.8, 124.6, 126.8, 129.8, 155.6, 157.4, 165.1.

3-Cyano-4,6-dimethylcoumarin (3g). IR (KBr, λ_{max} / cm^{-1}): 1735 (C=O), 2234 (C \equiv N); ^1H -NMR (400 MHz, CDCl_3 , δ / ppm): 2.45 (3H, s), 2.75 (3H, s), 7.32 (1H, d, J = 9.0 Hz), 7.45–7.70 (2H, m); ^{13}C -NMR (100 MHz, CDCl_3 , δ / ppm): 17.8, 21.4, 96.4, 112.8, 118.2, 120.8, 129.8, 133.4, 136.4, 156.1, 157.2, 164.8.

6-Bromo-3-cyano-4-methylcoumarin (3h). IR (KBr, λ_{max} / cm^{-1}): 1738 (C=O), 2236 (C \equiv N); ^1H -NMR (400 MHz, CDCl_3 , δ / ppm): 2.72 (3H, s), 7.35 (1H, d, J = 9.0 Hz), 7.20–8.15 (2H, m); ^{13}C -NMR (100 MHz, CDCl_3 , δ / ppm): 18.2, 95.8, 113.1, 114.8, 118.8, 121.8, 132.6, 136.2, 152.6, 157.2, 164.1.

3-Cyano-7-methoxy-4-methylcoumarin (3i). IR (KBr, λ_{max} / cm^{-1}): 1720 (C=O), 2227 (C \equiv N); ^1H -NMR (400 MHz, CDCl_3 , δ / ppm): 2.70 (3H, s), 3.95 (3H, s), 6.85–7.05 (2H, m), 7.68 (1H, d, J = 9.0 Hz); ^{13}C -NMR (100 MHz, CDCl_3 , δ / ppm): 18.1, 21.4, 96.2, 105.2, 112.2, 112.8, 116.6, 125.4, 152.1, 157.1, 160.6, 164.2.



J. Serb. Chem. Soc. 79 (5) 533–543 (2014)
JSCS–4605

Immobilization of β -glucosidase onto a mesoporous silica support: physical adsorption and covalent binding of the enzyme

DARJANA Ž. IVETIĆ, VLADIMIR V. SRDIĆ[#] and MIRJANA G. ANTOV^{*#}

*University of Novi Sad, Faculty of Technology, Bulevar cara Lazara 1,
21000 Novi Sad, Serbia*

(Received 4 October, revised 20 December, accepted 27 December 2013)

Abstract: In this study, the immobilization of β -glucosidase onto mesoporous silica support by physical adsorption and covalent binding was investigated. The immobilization was performed onto micro-sized silica aggregates with an average pore size of 29 nm. During physical adsorption, the highest yield of immobilized β -glucosidase was obtained with an initial protein concentration of 0.9 mg mL⁻¹. The addition of NaCl increased 1.7-fold, while the addition of Triton X-100 decreased 6-fold adsorption yield in comparison to the one obtained without any addition. Covalently bonded β -glucosidase, *via* glutaraldehyde previously bonded to silanized silica, had a higher yield of immobilized enzyme as well as higher activity and substrate affinity in comparison to the one physically adsorbed. Covalent binding did not considerably change pH and temperature stability of the obtained biocatalyst in range of values that are commonly used in reactions in comparison to the unbound enzyme. Furthermore, covalent binding provided a biocatalyst that retained over 70 % of its activity after 10 cycles of reuse.

Keywords: β -glucosidase; immobilization; physical adsorption; chemical binding; mesoporous silica.

INTRODUCTION

The enzymatic modification of cellulose is a field of great interest in many processes due to the numerous applications of one of its degradation products, glucose. A cellulose polymer is degraded to glucose through the cooperative actions of a complex of cellulolytic enzymes. Cellobiohydrolases hydrolyze the cellulose polymer from the ends, releasing cellobiose as the product, while endoglucanases randomly hydrolyze the internal β -1,4-linkages creating more free ends for the action of cellobiohydrolases.¹ Finally, β -glucosidases hydrolyze the cellobiose to glucose. Cellobiohydrolases and endoglucanases are often inhibited

* Corresponding author. E-mail: mantov@uns.ac.rs

[#] Serbian Chemical Society member.

doi: 10.2298/JSC131004154I



by cellobiose, making β -glucosidases the key enzyme for efficient hydrolysis of cellulose in terms of avoiding decreased hydrolysis rates over time due to cellobiose accumulation.^{2,3}

However, the cellulases complexes from the main fungal producers normally contain amounts of β -glucosidase that are not sufficient to hydrolyze all the released cellobiose.^{3,4} Thus, during enzymatic hydrolysis of cellulose in order to prevent limitation of the overall hydrolysis rate by accumulated cellobiose, β -glucosidase often must be additionally supplemented to the reaction mixture.⁵ However, enzyme cost is one of the major obstacles in the path of large-scale commercialization of the enzymatic hydrolysis of cellulose. Enzyme recovery and recycling, which is achievable by immobilization, is one of the most important and effective ways of increasing the efficiency of an enzymatic hydrolysis process.⁶ With respect to cellulose hydrolysis, immobilization of β -glucosidase might be especially beneficial to process economy, considering the necessity for its addition to regular complex cellulases.

The variety of enzyme immobilization methods can be reduced to two main approaches, *i.e.*, physical adsorption and covalent binding with a carrier, both of which have advantages and shortcomings. Physical adsorption is simple to perform, cheap and tends to be less destructive to the enzyme than chemical binding, but interactions formed between the enzyme and the supports are unstable. In covalent binding, the bonds between the carrier and enzyme are very strong resulting in a highly stable conjugate, but, very often, the enzyme activity drops considerably.⁵ Many supports have been tested for their ability to immobilize β -glucosidase, of which porous silica, the most commonly used material for enzyme immobilization, was proven to be suitable for the immobilization of β -glucosidase.^{5,7}

The aim of this study was to investigate the immobilization of a new commercial β -glucosidase, which is part of the Novozymes Cellulosic Ethanol Enzyme Kit (Novozymes, Denmark), onto a mesoporous silica support using physical adsorption and covalent binding. The biocatalysts obtained by physical adsorption and covalent binding were compared with respect to the immobilization yield, activity and substrate affinity. Then, in next set of experiments, the biocatalyst that provided the best results for these parameters was tested for stability and reusability in a real system with carboxymethyl cellulose as the substrate.

MATERIALS AND METHODS

β -Glucosidase and enzyme assay

In this study β -glucosidase NS22118 from Novozymes Cellulosic Ethanol Enzyme Kit, a kind gift of Novozymes (Novozymes, Denmark), was used for the immobilization experiments. The protein concentration in the enzyme solution was 26.7 mg mL⁻¹, while its activity was 558 U mL⁻¹, which were determined as described below.

A sample of enzyme solution or obtained biocatalyst (support with immobilized enzyme) was added to 1 mL of 50 mM citrate buffer (pH 5.0) containing 2 mM 4-nitrophenyl- β -D-glucopyranoside.³ The reaction mixture was incubated for 10 min at 50 °C. After addition of 2 mL Na₂CO₃ solution (1 M), the absorbance was read at 405 nm. A standard curve was obtained from the released *p*-nitrophenol. One unit of enzyme activity was defined as 1 mM *p*-nitrophenol produced per minute under the assay conditions and it is expressed per mL of enzyme solution or per gram of material containing the immobilized enzyme.

The protein concentration of enzyme preparation and solutions (supernatant obtained after separation of the support) were determined by the Bradford method using bovine serum albumin as the standard.⁸

The experimental results are the mean value of at least three measurements (the accuracy was ± 5 %) on a minimum of three replicas for every experimental point.

Support material

Mesoporous silica particles were used as the support for β -glucosidase immobilization. The materials were synthesized from highly basic sodium silicate solutions of three different SiO₂ concentrations as reported by Filipović *et al.*^{9,10} Sulfuric acid was slowly added into the well stirred sodium silicate solutions at 90 °C to precipitate silica particles. Finally, the pH was adjusted at value of 4 to prevent dissolution process. The white precipitated powders were washed with distilled water, separated from liquid phase by filtration and finally dried at 120 °C for 1 day.⁹ The obtained silica powders were calcined at 500 °C for one hour in order to remove the synthesizing template.

The particle size was measured by dynamic light scattering on Zetasizer Nano ZS, (Malvern Instruments, UK). The specific surface area (according to the BET method), pore size distribution (according to the BJH method) and pore volume of the as-synthesized particles were measured by low temperature nitrogen adsorption using a Autosorb-3B instrument (Quantachrome, USA). The size and morphology of the particles were examined using a scanning electron microscope (JEOL JSM 6460 LV, Japan).

Immobilization of β -glucosidase

In the experiments of physical adsorption of β -glucosidase onto a silica support, 25 mg of silica and 4 mL of a β -glucosidase solution in 50 mM citrate buffer, pH 4.7 were used. Adsorption was conducted at the room temperature for one hour under magnetic stirring. The experiments were performed with the aim of determining the influence of the initial enzyme concentration, in the range 0.54–2.70 mg mL⁻¹, on the physical adsorption of β -glucosidase. In order to investigate the influence of poly(ethylene) glycol-*p*-(1,1,3,3-tetramethylbutyl)-phenyl ether (Triton X-100) or NaCl on the physical adsorption of β -glucosidase, the immobilization was conducted under the previously mentioned conditions at an initial enzyme concentration 0.9 mg mL⁻¹, in 50 mM citrate buffer containing 0.1 vol. % Triton X-100 or 0.8 M NaCl.

The chemical immobilization of β -glucosidase onto the silica support was conducted through covalent bonding as reported by Weetall.¹¹ The support material was first functionalized through silanization with a 0.5 vol. % solution of 3-amino-propyltriethoxysilane (APTS) for 3 h at 75 °C.¹¹ Subsequently, the material was washed three times with distilled water and dried for 15 h at 105 °C. Activation of functionalized material was conducted with 2.5 vol. % solution of glutaraldehyde in sodium phosphate buffer (pH 7.0) for 45 min at 20 °C and washed three times with distilled water. Finally, immobilization of β -glucosidase (protein concentration 20 mg mL⁻¹ in 0.01 M phosphate buffer, pH 6.8) was realized through contact of the enzyme with functionalized and activated support (0.1 g) for 15 h at 20 °C.¹¹

After each immobilization reaction, the silica support (with immobilized β -glucosidase) was separated through centrifugation at 14,000 rpm for 5 min (Mini Spin Plus, Eppendorf) and the protein concentration in the supernatant was measured in order to calculate the amount of β -glucosidase immobilized on the silica support (q_i / mg β -glucosidase g^{-1} dry silica) using the following equation:

$$q_i = \frac{V(c_0 - c_s)}{w} \quad (1)$$

where V is the volume of the aqueous phase (mL), c_0 and c_s (mg β -glucosidase mL^{-1} solution) are the concentrations of β -glucosidase initially added and in the supernatant obtained after immobilization, respectively, and w is the weight of dry silica (g).

Stability and reuse

Effect of pH on the relative stability of the covalently bonded β -glucosidase was investigated during 1 h exposure to pH values in the range 2–9 (Britton–Robinson buffer), while effect of temperature was investigated during 1 h exposure to temperatures in the 20–80 °C for both the free and immobilized enzyme.

The reusability of the covalently bonded β -glucosidase was investigated by performing successive reactions with the biocatalyst (for 30 min each). The biocatalyst was supplemented to a cellulase complex (Celluclast 1.5 L, Novozymes) and used for the degradation of a 2 vol. % solution of carboxymethyl cellulose (as substrate) in 50 mM citrate buffer (pH 4.7) at a temperature of 40 °C under gentle mixing (50 rpm).

RESULTS AND DISCUSSION

Physical adsorption of β -glucosidase

In order to determine the most suitable silica support for the adsorption of β -glucosidase mesoporous silica supports with different characteristics were used. The mesoporous silica supports were synthesized as described earlier^{9,10} and their characteristics regarding pore size, specific surface area and total pore volume were determined.¹⁰ The tested silica particles were micro-sized aggregates (Fig. 1). The pore size distribution of the silica supports donated as Snv-90, Sns-90 and Snn-90, with an average pore size of 29, 24 and 16 nm, respectively, are presented in Fig. 2.

The results obtained for the amounts of enzyme physically adsorbed onto the different silica supports are shown in Fig. 3. The highest amount of adsorbed β -glucosidase was obtained with the silica support having the largest average pore size (29 nm),¹⁰ which also had the widest pore size distribution (Fig. 2). It was found that β -glucosidase from *Aspergillus niger* has an unsymmetrical, so-called tadpole-like shape with a diameter of 15 nm (*i.e.*, maximum diameter) and a radius of gyration of 4.2 nm.¹² Accordingly and depending of the molecule orientation, it might be that the enzyme requires more space for entrance into the pores than is defined by its diameter. As result, the highest amount of adsorbed enzyme was obtained on the support with the largest investigated pore size and this material was used for the further experiments. In all experiments of physical

adsorption, the conditions with respect to the pH value of the reaction were chosen to prevent electrostatic repulsion between silica and the enzyme (pH 4.7).

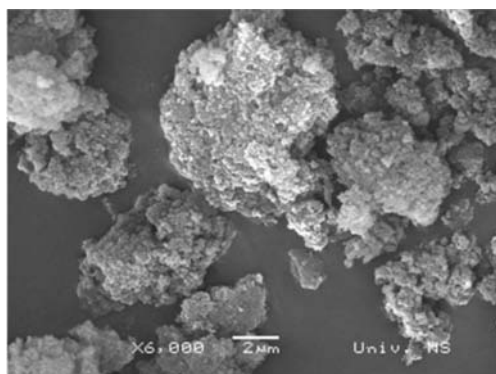


Fig. 1. Scanning electron micrograph of the mesoporous silica aggregates.

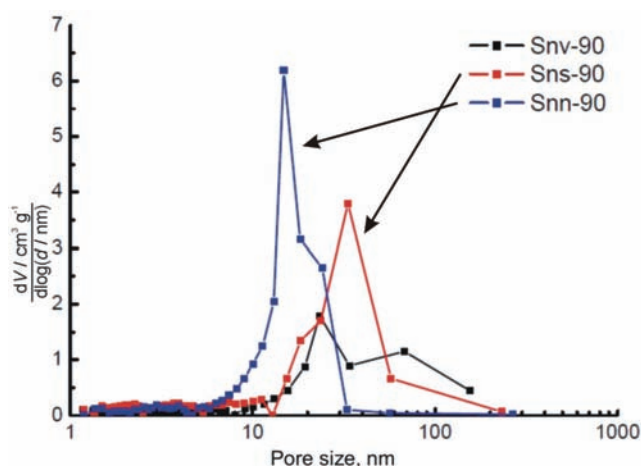


Fig. 2. Pore size distribution for tested silica particles (data for Snv-90 from the literature¹⁰).

Considering that the concentration gradient is an important driving force for physical adsorption, the influence of the initial β -glucosidase concentration on adsorption was investigated. In the investigated range of loaded enzyme, the highest amount of adsorbed β -glucosidase was obtained at a protein concentration of 0.9 mg mL^{-1} (data not shown), while higher values did not lead to an increase in the amount of adsorbed β -glucosidase. This might be due to saturation of the binding sites, suggesting that the available sites on the silica surface are the limiting factor for the adsorption, as was reported for other proteins.¹³

Physical adsorption provided a yield of immobilized enzyme of 20.1 mg of β -glucosidase per gram of silica support. The obtained biocatalyst had an activity of 7.65 U per gram of silica support and an affinity towards the substrate of 15.06 mM (Table I).

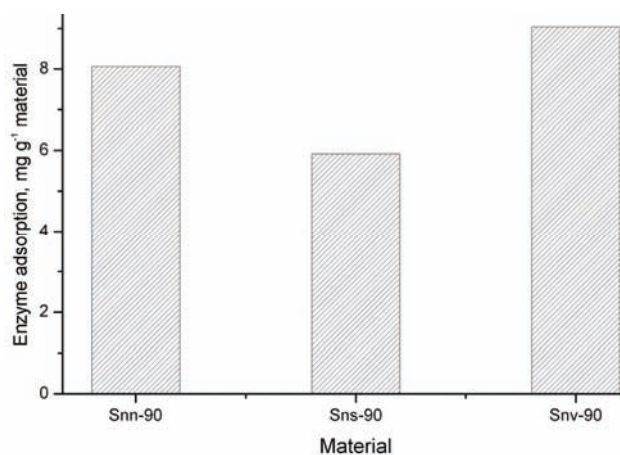


Fig. 3. Adsorption of β -glucosidase onto different silica supports.

TABLE I. Characteristics of physically adsorbed and covalently bonded β -glucosidase onto mesoporous silica support (pore size 29 nm)

β -Glucosidase	Physically adsorbed	Covalently bonded
Amount of adsorbed enzyme, mg g ⁻¹ material	20.10	42.00
Activity, U g ⁻¹ material	7.65	15.58
K_M / mM	15.63	11.06

Influence of Triton X-100 and NaCl on the physical adsorption of β -glucosidase

In order to reveal the mechanism of β -glucosidase adsorption onto the surface of silica, the effect of salt and detergent on the adsorption efficiency was investigated. The adsorption was performed in citrate buffer (pH 4.7) containing 0.8 M NaCl or 0.1 vol. % Triton X-100 and compared with adsorption in citrate buffer alone (Fig. 4). Presence of 0.8 M NaCl increased β -glucosidase adsorption by 1.7-fold in comparison to the adsorption yield obtained in its absence. On the other hand, the addition of 0.1 vol.% Triton X-100 decreased the β -glucosidase adsorption 6-fold in comparison to the adsorption in its absence (Fig. 4).

Generally, protein adsorption is the result of the action of electrostatic and van der Waals forces (between two dissimilar surfaces) and it would be expected that electrostatics play an important role in the adsorption process. However, the change of concentration of the supporting electrolyte may have surprising effects as recently demonstrated for cytochrome c¹⁴ and lysozyme.¹⁵ The increase of the adsorption upon NaCl addition might be explained by its influence on the charge on both the support and enzyme. Namely, the charge density on silica increases with increasing NaCl concentration while the effective charge on the surface of the enzyme might be strongly affected by the anion type and concentration (as shown for lysozyme).¹⁵ As a result, the increase in ionic strength reduces the Debye length and consequently weakens the electrostatic attractive forces between

the protein and the silica-based surface. This favors van der Waals attractive interactions, which are stronger than expected because of the adsorption of Cl^- at the charged interface of the protein.¹⁵

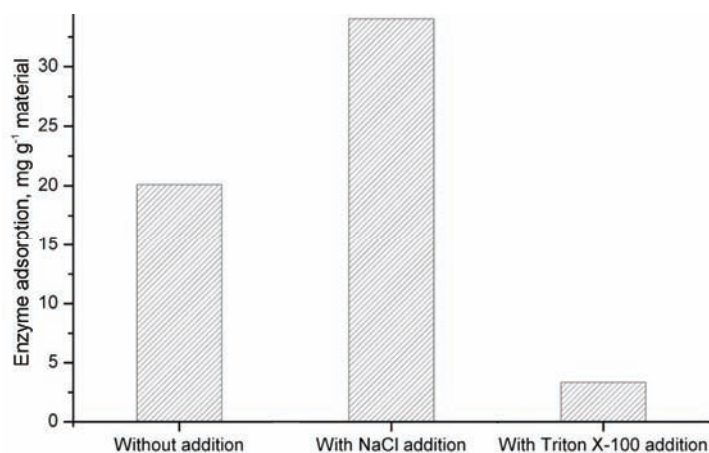


Fig. 4. Physical adsorption of β -glucosidase onto mesoporous silica support (pore size 29 nm).

On the other hand, in the presence of Triton X-100, the adsorption efficiency was reduced by more than six fold. This might be explained by the possible competition for regions where interactions with β -glucosidase might have occurred on the silica surface and additional physical hindrance of the silica surface by the formation of small aggregates, which are characteristic for the initial phase of detergent adsorption.¹⁶ Furthermore, the presence of Triton X-100 might weaken van der Waals forces, which are one of the driving forces for β -glucosidase adsorption besides electrostatic interaction.¹⁷

Thus, presented results might indicate that physical adsorption of β -glucosidase onto silica support under investigated conditions (pH 4.7 and room temperature) could be result of synergistic effect of at least two types of interaction – electrostatic and van der Waals forces.

Covalent binding of β -glucosidase

Covalent binding is known to have the advantage of forming strong and stable linkages between an enzyme and the carrier, which consequently eliminates the loss of activity caused by enzyme leakage from the support.⁵ Thus, with the aim of improving the characteristics and yield of bonded enzyme, covalent binding of β -glucosidase onto the silica support was performed. β -Glucosidase was covalently bonded onto silica material *via* glutaraldehyde, which had previously been attached to the functionalized silica support.

Covalent binding provided a yield of bonded enzyme of 42 mg per gram of silica support, which was 2.1-fold higher in comparison to the amount obtained

by physical adsorption (Table I). In addition, the covalently bonded β -glucosidase had a higher activity of enzyme per gram of material (15.58 U g^{-1}) in comparison to that physically adsorbed, while the biocatalyst obtained by covalent binding had a lower K_M value (11.06 mM), *i.e.*, a higher affinity towards the substrate (Table I). A similar yield of β -glucosidase covalently bonded onto silica gel was reported by Karagulyan *et al.*,⁵ while Wang *et al.*⁷ obtained a considerably higher yield with respect to the amount of bonded β -glucosidase, although its activity was similar to the that obtained in this study.

Stability and reusability of covalently bonded β -glucosidase

Due to better immobilization yield and better characteristics of the biocatalyst obtained by covalent binding, such as higher enzyme activity per gram of material and lower K_M value, the biocatalyst was subjected to an investigation of its pH and temperature stability, as well as its reusability.

The stability of the covalently bonded β -glucosidase was investigated under different conditions with respect to temperature and pH. Within the investigated range of the temperatures ($20\text{--}80 \text{ }^\circ\text{C}$), covalent binding of β -glucosidase did not considerably affect the profile of temperature stability in comparison to that of the free enzyme (Fig. 5). On the other hand, at the screened values of pH ($2\text{--}9$), the stability profile of the covalently bonded enzyme was changed in comparison to that of free β -glucosidase (Fig. 6). However, the activity of the immobilized β -glucosidase was similar to that of the free enzyme in the pH range $4\text{--}5$ that are commonly used in cellulase reactions (Fig. 6).

Recycling and reuse of an immobilized enzyme is one of the most important aims of its immobilization with respect to the economy of processes involving

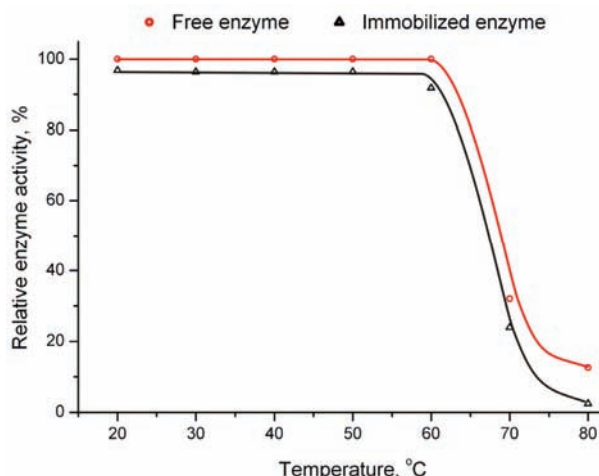


Fig. 5. Temperature stability of β -glucosidase covalently bonded onto mesoporous silica support (pore size 29 nm).

reactions with this kind of biocatalyst. Thus, the biocatalyst obtained by covalent binding of β -glucosidase onto silica was subjected to successive reactions (for 30 min each) with carboxymethyl cellulose as the substrate under mild conditions that were appropriate for the enzyme and at the same time not destructive for the material.¹⁸

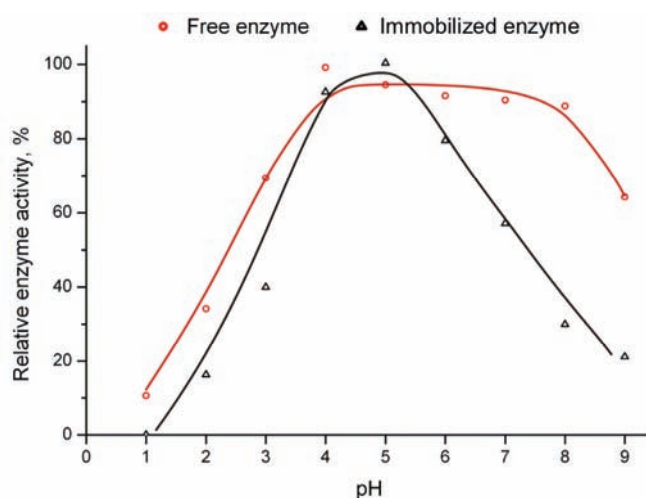


Fig. 6. pH stability of β -glucosidase covalently bonded to the mesoporous silica support (pore size 29 nm).

Ten cycles of biocatalyst were performed and the obtained results are shown in Fig. 7. It could be noticed that after ten cycles of use, the covalently bonded β -

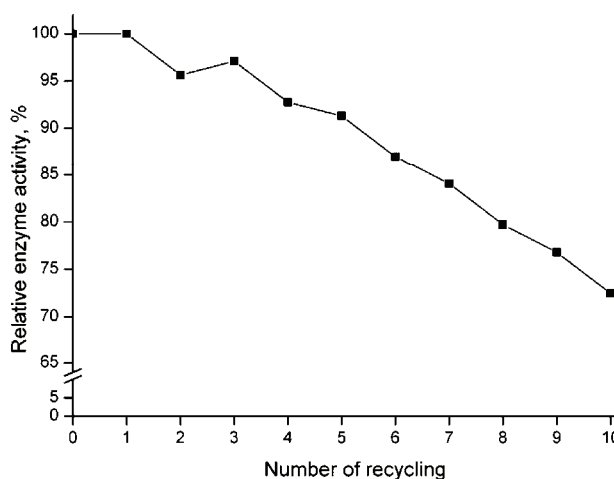


Fig. 7. Repeated use of covalently bonded β -glucosidase onto the mesoporous silica support (pore size 29 nm).

glucosidase had retained more than 70 % of its initial activity. Similar result within ten cycles of reuse of covalently immobilized β -glucosidase onto different silica-derived nanoparticles was previously reported.⁷

CONCLUSIONS

This paper presents preliminary results of an investigation of immobilization of a new commercial β -glucosidase (from Novozymes Cellulosic Ethanol Enzyme Kit). Considering process economy, immobilization of this β -glucosidase might be very beneficial because it is intended to be used for supplementation of cellulase complexes involved in the hydrolytic degradation of cellulose in (ligno)cellulosic biomass. The immobilization was performed on chosen micro-sized, mesoporous silica particles with an average pore size of 29 nm. Physical adsorption was conducted under conditions that prevented repulsion between the enzyme and support. The addition of NaCl increased, while the addition of Triton X-100 decreased the amount of physically adsorbed enzymes, indicating the mechanism involved in the process. Covalent bonding of β -glucosidase through silanization of the silica support and binding of enzyme *via* glutaraldehyde gave higher yields of bonded β -glucosidase 2.1-fold in comparison to that physically adsorbed. Furthermore, covalently bonded β -glucosidase had a higher activity (per gram of silica support) and higher affinity towards the substrate in comparison to the physically adsorbed enzyme, while it retained its thermal and pH stability in comparison to the free enzyme in the range of these parameters commonly used for cellulase reactions. Furthermore, the obtained biocatalyst retained high activity (more than 70 % of its initial activity) after ten times of recycling.

Acknowledgement. Financial support from the Ministry of Education, Science and Technological Development of the Republic of Serbia (Grant No. III 45021) is gratefully acknowledged. The authors also acknowledge Novozymes for their kind gift of β -glucosidase from Novozymes Cellulosic Ethanol Enzyme Kit.

ИЗВОД

ИМОБИЛИЗАЦИЈА β -ГЛУКОЗИДАЗЕ НА МЕЗОПОРОЗНИ СИЛИКА НОСАЧ: ФИЗИЧКА АДОРПЦИЈА И КОВАЛЕНТНО ВЕЗИВАЊЕ ЕНЗИМА

ДАРЈАНА Ж. ИВЕТИЋ, ВЛАДИМИР В. СРДИЋ и МИРЈАНА Г. АНТОВ

Универзитет у Новом Саду, Технолошки факултет, Булевар цара Лазара 1, 21 000 Нови Сад

У овом раду је испитана имобилизација β -глукозидазе на мезопорозном силика носачу применом физичке адсорпције и ковалентног везивања. Имобилизација је извршена на силика микро-агрегатима са просечном величином пора од 29 nm. Током физичке адсорпције највећи принос имобилизоване β -глукозидазе је добијен при почетној концентрацији протеина од 0,9 mg ml⁻¹. Додатак NaCl је 1,7 пута повећавао, а додатак детергента Triton X-100 6 пута смањио принос адсорпције у односу на принос остварен без додавања. Ковалентно везана β -глукозидаза, путем глутараледхида који је везан за претходно силанизовану силику, имала је виши принос имобилизованог ен-

зима, као и вишу активност и афинитет према супстрату у поређењу са физички везаном β -глюкозидазом. У поређењу са слободним ензимом ковалентно везивање није значајно променило рН и температурну стабилност добијеног биокатализатора при вредностима ових параметра које се уобичајено користе у реакцијама. Осим тога, ковалентно везивање је обезбедило добијање биокатализатора који је задржао преко 70 % активноти након 10 циклуса узастопне употребе.

(Примљено 4. октобра, ревидирано 20. децембра, прихваћено 27. децембра 2013)

REFERENCES

1. Y.-P. Zhang, L. R. Lynd, *Biotechnol. Bioeng.* **88** (2004) 797
2. M. F. Vieira, A. M. S. Vieira, G. M. Zanin, P. W. Tardioli, C. Mateo, J. M. Guisán, *J. Mol. Catal., B* **69** (2011) 47
3. B. Flachner, A. Brumbauer, K. Reczey, *Enzyme Microb. Technol.* **24** (1999) 362
4. A. Allen, D. Sternberg, *Biotechnol. Bioeng. Symp.* **10** (1980) 189
5. H. K. Karagulyan, V. K. Gasparyan, S. R. Decker, *Appl. Biochem. Biotechnol.* **146** (2008) 39
6. S. Das, D. Berke-Schlessel, H.-F. Ji, J. McDonough, Y. Wei, *J. Mol. Catal., B* **70** (2011) 49
7. P. Wang, X. Hu, S. Cook, H.-M. Hwang, *Appl. Biochem. Biotechnol.* **158** (2009) 88
8. M. M. Bradford, *Anal. Biochem.* **72** (1976) 248
9. R. Filipović, Z. Obrenović, I. Stijepović, Lj. M. Nikolić, V. V. Srdić, *Ceram. Int.* **35** (2009) 3347
10. R. Filipović, D. Lazić, M. Perušić, I. Stijepović, *Process. Appl. Ceram.* **4** (2010) 265
11. H. H. Weetall, *Appl. Biochem. Biotechnol.* **41** (1993) 157
12. M. A. Lima, M. Oliveira-Neto, M. A. S. Kadowaki, F. R. Rosseto, E. T. Prates, F. M. Squina, A. F. P. Leme, M. S. Skaf, I. Polikarpov, *J. Biol. Chem.* **288** (2013) 32991
13. Y. K. Chang, L. Chu, J. C. Tsai, S. J. Chiu, *Process. Biochem.* **41** (2006) 1864
14. L. Medda, A. Salis, E. Magner, *Phys. Chem. Chem. Phys.* **14** (2012) 2875
15. D. Steri, M. Monduzzi, A. Salis, *Microporous Mesoporous Mater.* **170** (2013) 164
16. J. Zhao, W. Brown, *Langmuir* **11** (1995) 2944
17. C. C. Ruiz, J. A. Molina-Bolívar, J. Aguiar, *Langmuir* **17** (2001) 6831
18. C. Schilde, A. Kwade, *J. Mater. Res.* **27** (2012) 672.



J. Serb. Chem. Soc. 79 (5) 545–556 (2014)
JSCS–4606

Synthesis, characterization and crystal structure of Cu(II) complex with a diimine-dioxime ligand, [Cu₂(LH)₂](ClO₄)₂. Influence of the weak Cu···O(perchlorate) interaction on the structure of the Cu₂N₂O₂ metallocycle

MARIJA MIRKOVIĆ¹, NADEŽDA NIKOLIĆ^{1#}, DUŠAN MIJIN^{2#},
MILKA AVRAMOV IVIĆ^{3#}, AGNEŠ KAPOR⁴ and ZORAN D. TOMIĆ^{1*}

¹Vinča Institute of Nuclear Sciences, University of Belgrade, P. O. Box 522, 11001 Belgrade, Serbia, ²Faculty of Technology and Metallurgy, University of Belgrade, Karnegijeva 4, P. O. Box 3503, 11120 Belgrade, Serbia, ³ICTM – Department of Electrochemistry, University of Belgrade, Njegoseva 12, Belgrade, Serbia and ⁴Department of Physics, Faculty of Sciences, University of Novi Sad, Trg Dositeja Obradovića 4, 21000 Novi Sad, Serbia

(Received 10 September, revised 28 October, accepted 31 October 2013)

Abstract: The diimine–dioxime ligand, 3,3'-(1,4-butanediyl-dinitrilo)bis-2-pentanone, 2,2'-dioxime (LH₂), containing a N₄ donor set was prepared by the Schiff base condensation of 2-hydroxyimino-3-pentanone and 1,4-diaminobutane in two ways: in a protic and in an aprotic solvent. A higher yield of the (LH₂) imine was obtained when the synthesis was performed using a protic solvent (C₂H₅OH) instead of aprotic benzene (78 and 30 %, respectively). The Cu(II) metal complex of diimine–dioxime was synthesized in CH₃OH from the perchlorate salt of LH₂ in a 1:1 mole ratio. The isolated complex was characterized by the elemental analysis, IR spectroscopy and cyclic voltammetry. The structure of [Cu₂(LH)₂](ClO₄)₂ was determined by single-crystal X-ray diffraction analysis. Comparison with structurally related diimine–dioxime Cu(II) complexes revealed the influence of a weak Cu···O(perchlorate) interaction on the geometry of the metallocycle.

Keywords: Cu(II) complex; weak interactions; supramolecular aggregates; diimine–dioxime ligand.

INTRODUCTION

Schiff bases are typically formed by the condensation of primary amines and aldehydes.^{1,2} Schiff base ligands containing strong donor sites, such as phenoxo oxygen atoms or imine nitrogen atoms, have been shown to exhibit a broad range of biological properties, including antifungal,^{3,4} antibacterial⁵ and antitumor^{6,7}

* Corresponding author. E-mail: zorant@vin.bg.ac.rs

Serbian Chemical Society member.

doi: 10.2298/JSC130910120M

activities. They are used as pigments and dyes, catalysts, polymer stabilizers, intermediates in organic synthesis⁸ and extractants for metal ions in solvent extractions.⁹ Schiff bases represent an important class of chelating agents with the capability of forming stable complexes with most transition metals.¹⁰

Transition metal complexes of polydentate Schiff base ligands, especially tetradentate Schiff bases, are applicable in catalysis and material chemistry,^{11,12} and played a significant role in various reactions for the enhancement of the yield and product selectivity.¹³ The Schiff base ligands readily form complexes with the transition metals.^{14–16} Recent studies have focused particularly on the development of new Schiff bases containing the diimine–dioxime functionality, a potential ligand for ⁶⁴Cu radiopharmaceuticals.¹⁷ These studies also included investigations of lipophilic, cationic copper(II) complexes of diimino–dioxime as potential positron emission tomography (PET) radiopharmaceuticals for imaging myocardial perfusion and multi-drug resistance in cancer.¹⁸ Of particular interest is the capability of the deprotonated diimine–dioximes to form bridges between metal ions giving rise to complexes of different nuclearity.¹⁹ These complexes are of current interest in connection with the ability of oximate bridges to mediate strong antiferromagnetic interaction between metal centers.²⁰ During complex formation, one of the oxime groups loses a proton and a hydrogen bond is formed between the two oxime groups. The strength of the hydrogen bond is dependent on the size of the metal ion, the length of the methylene linkage and chemical environment around the metal ion.²¹ A number of these studies were based on the analysis of the crystal structures and subsequent identification of the bonding and non-bonding interactions relevant for the explanation of the molecular and crystal properties.²²

A particular problem arises concerning the use of copper in the synthesis of metal complexes. Copper is known for its flexible coordination behavior associated with the capability to form weak bonds, a property termed “plasticity”.²³ This problem becomes more pronounced in the studies of weaker non-bonding interactions.²⁴ Detailed analysis of the copper environment followed by computational or database studies²⁵ may provide additional insight into the non-bonding contacts relevant for the properties of copper complexes. One of the ligands frequently used in the synthesis of copper complexes is the perchlorate group. As a ligand, the ClO₄[−] group may appear in various bonding arrangements, however its steric properties limit its coordinating ability in the presence of smaller potential ligands.²⁶ Recently the coordinating properties of ClO₄[−] bonded to Cu were studied.^{27,28} However, in most of the crystal structures, ClO₄[−] is present as a non-coordinated ion.

In the present study, the copper(II) complex of the 3,3′-(1,4-butanediyl-dinitrilo)bis-2-pentanone, 2,2′-dioxime ligand was chosen for study to enable comparison with the previously studied copper(II) complex^{29,30} of the closely related ligand with two methyl groups in place of the present two ethyl groups.

EXPERIMENTAL

General

All reagents obtained from commercial sources were of analytical grade and used without further purification. The infrared spectra were obtained using a FTIR BOMEM MB 100 Hartmann Braun Fourier transform infrared spectrometer. The samples were analyzed in the form of KBr pellets after removal of the liquid under high vacuum at a low temperature. Elemental analysis (C, H, N) of the samples were performed using a VARIO EL III elemental analyzer. The melting points (uncorrected) were determined on Mel-Temp melting point apparatus (Laboratory Devices Inc., USA).

The electrochemical experiments were performed using standard equipment for cyclic voltammetry measurements and a three electrode electrochemical cell, as described in detail previously, was used.^{31,32} Glassy carbon (Pine rotating disc electrode) served as the working electrode (only for the stationary measurements) and a gold wire was used as the counter electrode while a saturated calomel electrode (SCE) was the reference electrode. The glassy carbon electrode (surface area 0.500 cm²) was polished with diamond paste, cleaned with a mixture of 18 M Ω -water and sulfuric acid and further cleaned with 18 M Ω -water in an ultrasonic bath. The Cu(II) complex and the diimine-dioxime ligand containing a donor set of N₄ were examined in 0.05 M NaHCO₃. The complex is soluble in 0.05 M NaHCO₃ while ligand was dissolved in 1 mL of methanol before addition into the electrolyte. The methanol was electrochemically inactive under the described experimental conditions. Prior to the addition of the Cu(II) complex and ligand, the electrolyte was deoxygenated by purging with nitrogen. Cyclic voltammetry was performed at a sweep rate of 50 mV s⁻¹. The potential range applied was between -0.5 and 0.8 V. All the potentials are given vs. SCE. All the experiments were performed at room temperature.

Synthesis

2-Hydroxyimino-3-pentanone (KO) was synthesized as described earlier³³ in 75 % yield. The diimine-dioxime ligand, 3,3'-(1,4-butanediyl-dinitrilo)bis-2-pentanone, 2,2'-dioxime (LH₂), was prepared in two ways: in aprotic (benzene) and in protic (ethanol) solvents. The synthesis in benzene was realized using a previously described method³⁴ in 30 % yield. The synthesis and characterization of the ligand LH₂ in ethanol was described elsewhere³⁵ (78 % yield).

Synthesis of [Cu₂(LH)₂](ClO₄)₂. Copper(II) acetate monohydrate (110 mg, 0.625 mmol), suspended in 10 mL of CH₃OH was added to a hot CH₃OH suspension of the ligand LH₂ (175 mg, 0.625 mmol). The reaction mixture was then refluxed for 3 h. The reddish-brown product was isolated as the perchlorate salt by the addition of a saturated aqueous solution of NaClO₄. The reaction mixture was allowed to stand at room temperature for 3 days, when brown crystals were formed. The crystals were collected and dried in a desiccator. Crystals suitable for X-ray diffraction were grown by slow diffusion of a saturated aqueous solution of NaClO₄ into a methanolic solution of the product. Yield 68 %; mp: >225 °C explosive. Anal. Calcd. for C₂₈H₅₀Cl₂Cu₂N₈O₁₂: C, 37.84; H, 5.67; N, 12.61 %. Found: C, 37.67; H, 5.99; N, 12.38 %. Selected IR data (KBr, cm⁻¹): $\nu_{C=N}$ 1521.92 *m*, 1624.97 *w* (*m*, medium; *w*, weak).

Crystallography

Single-crystal X-ray diffraction data were collected on an Oxford Diffraction Gemini S four-circle diffractometer equipped with a Sapphire CCD detector, using graphite-monochromated MoK α radiation ($\lambda = 0.71073$ Å) at room temperature. The data reduction was realized using the Oxford Diffraction program CRYCALISPRO.³⁶ Empirical absorption

corrections were applied using spherical harmonics implemented in the SCALE3 ABSPACK³⁶ scaling algorithm. The structure was solved by direct methods using the SIR92 program³⁷ as implemented in the WinGX program system.³⁸ One of the O atoms from the ClO₄ is disordered over two positions at 70 % and 30 % occupancy. All non-hydrogen atoms were refined anisotropically using SHELXL-97³⁹ by applying a full-matrix least-squares method based on F^2 , including all reflections. The hydrogen atoms were placed in the idealized positions and refined riding on their parent atoms. The geometrical calculations were performed using the programs PARST⁴⁰ and PLATON.⁴¹ The programs CAMERON,⁴² Mercury⁴³ and ORTEP⁴⁴ were employed for graphical presentations of the structure. The crystal data and refinement parameters are summarized in Table I.

TABLE I. Crystal data and structure refinement for [Cu₂(LH)₂](ClO₄)₂

Formula	C ₂₈ H ₅₀ Cl ₂ Cu ₂ N ₈ O ₁₂
Formula weight	888.74
Crystal system	Monoclinic
Space group	P21/n
<i>a</i> , <i>b</i> , <i>c</i> / Å	7.6214(2), 20.2174(6), 12.4894(3)
α , β , γ / °	90, 94.204(3), 90
<i>V</i> / Å ³	1919.25(9)
<i>Z</i>	2
<i>D</i> _{calc} / g cm ⁻³	1.538
μ (MoK α) / mm ⁻¹	1.315
Crystal size, mm	0.20 × 0.22 × 0.26
Temperature, K	293
λ (MoK α) / Å	0.71073
θ Range, °	3.4–29.1
Reflections collected	8595
Unique reflections	4399
Reflections observed, (<i>I</i> > 2 σ (<i>I</i>))	3013
<i>R</i> _{int}	0.024
Data / restraints / parameters	4399 / 0 / 246
Goodness-of-fit on F^2	0.940
Final <i>R</i> indices (<i>I</i> > 2 σ (<i>I</i>))	<i>R</i> 1 = 0.0371, <i>wR</i> 2 = 0.0870
<i>R</i> indices (all data)	<i>R</i> 1 = 0.0620, <i>wR</i> 2 = 0.0918
Largest diff. peak and hole, e Å ⁻³	0.431 and –0.322

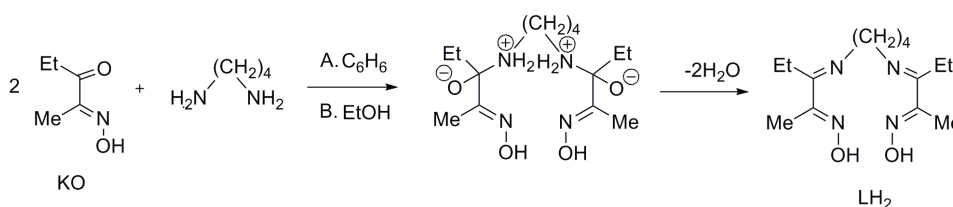
RESULTS AND DISCUSSION

Syntheses

The diimine–dioxime ligand (LH₂) and its Cu(II) complex were synthesized and characterized. In the present study, synthesis of a linear alkyl derivative of the diimine–dioxime ligand system was performed according to published procedures^{34,35} in two ways: in aprotic (A) and in protic (B) solvents (Scheme 1).

A higher yield of imine (78 %) was obtained when the synthesis was performed using the protic solvent (C₂H₅OH). In the case of the aprotic benzene, a poor yield of imine (30 %) was achieved. The synthesis of a Schiff base (imine)

is accomplished *via* the condensation reaction of a carbonyl compound with a primary amine.⁴⁵ In this addition–elimination reaction, a fast nucleophilic attack of the amine nitrogen on the carbonyl carbon is followed by the slow elimination of water. The synthesis of the Cu(II) complex was readily accomplished when the reaction was performed in CH₃OH. The IR spectrum of the ligand showed a $\nu(\text{C}=\text{N})$ peak at 1622 cm⁻¹ and the absence of a $\nu(\text{C}=\text{O})$ peak at around 1700 cm⁻¹, which is indicative of a Schiff base condensation. After formation of the complex, two C=N bonds are discernable. The two $\nu(\text{C}=\text{N})$ were observed at lower frequencies than that in the free ligand, in accordance with coordination at the oxime and imine nitrogens.



Scheme 1. Synthetic route for the ligand LH₂ in aprotic (A) and protic (B) solvents.

Electrochemical behavior of [Cu₂(LH)₂](ClO₄)₂

The cyclic voltammogram of glassy carbon electrode in 0.05 M NaHCO₃ (dashed line) and after the addition of Cu(II) complex (full line) are presented in Fig. 1.

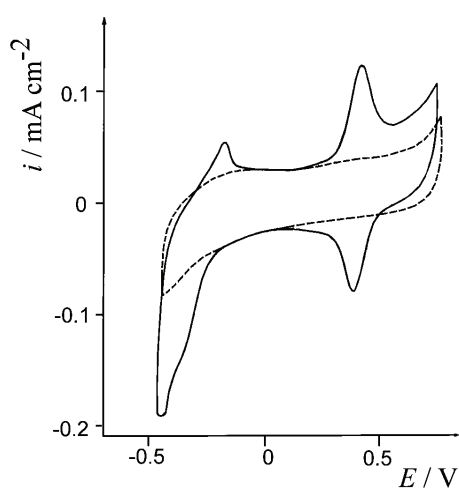


Fig. 1. Cyclic voltammogram of a glassy carbon electrode in 0.05 M NaHCO₃ (dashed line) and after the addition of the Cu(II) complex, concentration 2.0×10^{-3} mg·cm⁻³ (full line), sweep rate: 50 mV·s⁻¹. Only the first sweep was recorded.

In Fig. 1, the reversible oxido-reduction processes of the Cu(II) complex can be observed at 0.45 V, while the reduction reaction occurred between -0.3 V and

–0.5 V. It could be supposed that the observed electrochemical processes should be attributed to reactions on the reactive groups of the ligand. In order to check this assumption, under the same experimental conditions, the LH₂ ligand containing a donor set of N₄ was investigated. It was shown that the diimine–dioxime ligand exhibits the same reversible oxido reduction processes at 0.45 V. Thus, the Cu(II) complex is electrochemically characterized by the reversible oxido reduction processes at 0.45 V, which proceeds on the ligand. Additionally, the Cu(II) complex exhibits the beginning of an additional oxidation reaction at 0.7 V, which could be attributed to the central copper atom.^{46,47} Moreover, a very apparent reduction reaction was observed between –0.3 and –0.5 V and small anodic peak at –0.30 V, which could be attributed to the interaction of central copper atom with the ligand. In Fig. 1, only the first sweep is shown because the decreases in the peak current values during sweeping were negligible.

Crystal structure analyses

In the complex, Cu(II) is five coordinated by the four imine nitrogen atoms of LH[–] and the oximate oxygen from the neighboring cationic complex. Selected bond lengths and angles are given in Table II.

TABLE II. Selected bond lengths (Å) and angles (°); symmetry code: $i = 1-x, -y, 1-z$

Cu1–O1 ⁱ 2.318(2)	N1–C1 1.288(3)	N1–Cu1–N2 80.54(8)	O1 ⁱ –Cu1–N3 92.23(7)
Cu1–N1 1.954(2)	N4–C4 1.281(3)	N1–Cu1–N3 174.26(9)	O1 ⁱ –Cu1–N4 96.21(7)
Cu1–N2 1.970(2)	N2–C2 1.277(3)	N1–Cu1–N4 94.52(9)	O1 ⁱ –Cu1–O4 174.71(8)
Cu1–N3 1.992(2)	N2–C5 1.464(3)	N2–Cu1–N3 103.13(8)	O4–Cu1–N1 90.23(8)
Cu1–N4 1.977(2)	N3–C8 1.473(4)	N2–Cu1–N4 153.98(9)	O4–Cu1–N2 75.98(9)
Cu1–O4 2.947(3)	N3–C3 1.275(4)	N3–Cu1–N4 80.25(9)	O4–Cu1–N3 86.43(9)
O1–N1 1.341(2)		O1 ⁱ –Cu1–N2 109.31(7)	O4–Cu1–N4 78.53(8)
O2–N4 1.378(3)		O1 ⁱ –Cu1–N1 90.68(7)	Cu1–O1–Cu1 ⁱ 97.76(5)

Two cationic fragments related by a center of inversion are assembled into binuclear units with the Cu(II) centers bridged by deprotonated oxime fragments (Fig. 2).

Similar features were previously observed in structurally related oximate-bridged dinuclear copper(II) complexes.²⁰ The pentacoordinate geometry can be described using the distortion parameter τ ,⁴⁸ where $\tau = 1$ corresponds to an ideal trigonal bipyramid and $\tau = 0$ to an ideal square pyramid. According to the trigonality index $\tau = 0.34$ for the title compound, the coordination geometry around a Cu(II) ion could be described as a severely distorted square pyramid. The basal plane is formed by N1, N2, N3 and N4 atoms, and the metal ion deviates by 0.24 Å from this plane, towards the apical positions occupied by oxime oxygen O1. The intra-molecular Cu⋯Cu separation is 3.9424(4). In order to gain more insight into the structural features of the title compound **I**, the obtained results

were compared with those for similar crystal structures of Cu complex cations containing a diimine–dioxime ligand and $(\text{ClO}_4)^-$ as the counter ion, *i.e.*, the two polymorphs of the Cu(II) complex of the deprotonated anion of 3,3'-(1,4-butanediyl-dinitrilo)bis-2-pentanone, 2,2'-dioxime (**II**),^{29,30} and the Cu(II) complex with a thio-oxime ligand (**III**)⁴⁹ (Scheme 2).

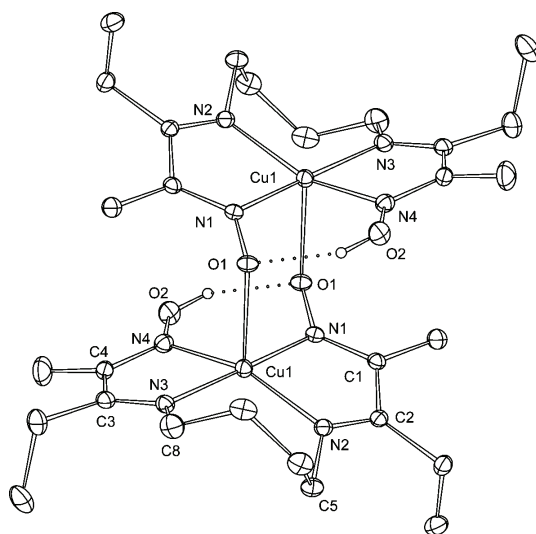
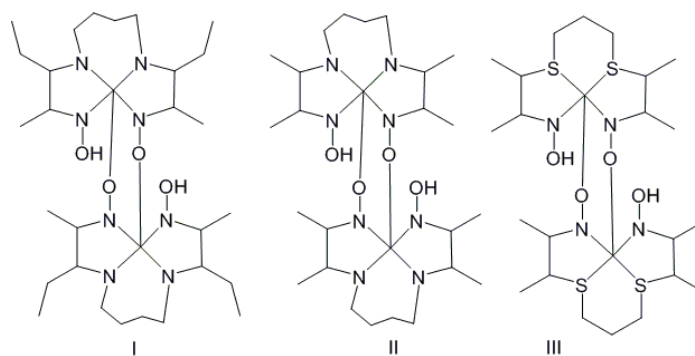


Fig. 2. Molecular diagram and atom numbering scheme of $[\text{Cu}_2(\text{LH})_2]^{2+}$. Methyl and methylene hydrogens are excluded for clarity. Intramolecular O–H...O hydrogen bonds are depicted by dotted lines.



Scheme 2. Structural formulas of the cationic complexes used for comparison.

The three complexes differ in the presence of an ethyl instead of a methyl substituent at the five-membered chelate ring in **I**, and the presence of a six-membered chelate ring and sulfur instead of nitrogen in the diimine–dioxime ligand in **III**. Comparison of geometric parameters of **I**, **II** and **III** indicate similarity of the $\text{Cu}_2\text{O}_2\text{N}_2$ ring conformation and the shape of the coordination polyhedron in all three complexes. The overlay of the three solid state structures presented in Fig. 3 illustrates their similarity.

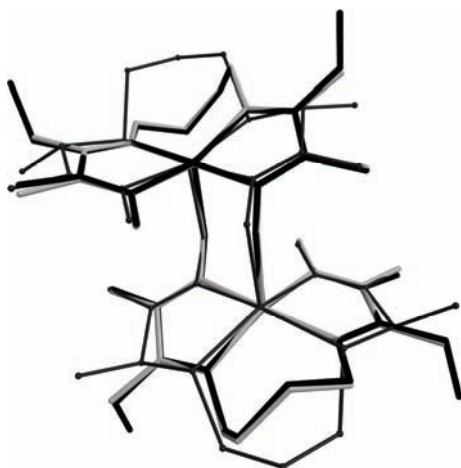


Fig. 3. Overlay of the solid-state structures of **I** (black), **II** (light grey) and **III** (dark grey, thin line).

Although the overall structures of **I**, **II** and **III** are similar, subtle differences in the geometry of the metallocycle were observed. These differences are caused mainly by differences in the Cu–O1 bond (Fig. 2). In **I** and **III**, these Cu–O bonds are 2.318(2) and 2.293 Å, respectively, which is longer than 2.266/2.262 Å found in the two polymorphs of **II**. While these differences in the axial Cu–O bonds could be attributed to the “plasticity”²³ of the copper coordination sphere, it is interesting to examine the possible influence of the closest perchlorato fragment on these bonds. In the crystal structures of **I** and **III**, the closest perchlorato oxygen is at Cu–O distances of 2.947(3) and 2.907 Å, respectively. These are on the borderline of values that have been reported for a semi-coordinated perchlorato group.^{50,51} In the crystal structure of **II** however, the closest perchlorato oxygen is at a rather larger distance of 3.767/3.766 Å and cannot be considered as semi-coordinated to Cu. If the presence of the semicoordinative bond Cu–O(perchlorate) *trans* to the Cu–O(oximate) bond is taken into account, the elongation of the Cu–O bonds in **I** and **III** relative to **II** could be attributed to the *trans* influence of the weakly coordinated perchlorato oxygen. The nearest intermolecular Cu···Cu separation in **I** is 7.621(5) Å. This is longer than the corresponding values of 6.484/6.480 and 6.016 Å found in **II** and **III**, respectively. Bearing in mind the overall similarity of these compounds (Fig. 3), this difference could be attributed to the difference in the molecular volume, caused mainly by the presence of the additional methyl groups in the molecule of the title compound. This complex exhibits an intramolecular hydrogen bond (Fig. 2) between *cis* oxime groups with an O···O distance of 2.593(3) Å, H···O = 1.83 Å and O–H···O angle of 154°. The role of O1 as an acceptor of a hydrogen bond is associated with the different geometry of two N–O bonds. Both the N1–O1 and N1–Cu1 bonds are shorter than the N4–O2, and N4–Cu1 bonds, respectively. This finding implies more multiple bond character in the fragment O1–N1–Cu1,

relative to O2–N4–Cu1. Bearing in mind the association of molecules in the solid state, it is interesting to note the lack of strong hydrogen bonding donors. There is only one strong donor O2–H, which is involved in the intradimer hydrogen bond to O1 (Fig. 2). Due to steric requirements, it is highly unlikely that the O2–H bond could be involved in additional, intermolecular, contacts. Hence, it was anticipated that intermolecular contacts between the C–H donors and perchlorate oxygens would govern the association of molecules in the crystal. Inspection of the intermolecular geometry confirms that the ClO_4^- anions participate in weak hydrogen bonds in the cationic complex through C–H \cdots O interactions. Fig. 4 illustrates the role of the weak Cu–O(perchlorate) interaction and the C–H \cdots O contacts (Table III) in the packing of molecules in the crystal structure.

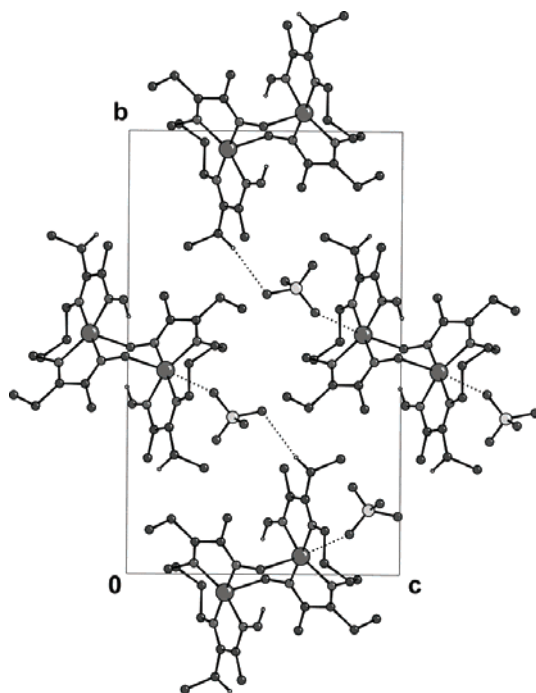


Fig. 4. Part of the crystal structure showing the contacts relevant for the association of molecules in the crystal structure of $[\text{Cu}_2(\text{LH})_2](\text{ClO}_4)_2$. Hydrogen atoms not involved in the non-bonding contacts have been excluded for clarity.

TABLE III. Geometry of the hydrogen bonds; symmetry code: $i = x-1/2, -y+1/2, +z-1/2$

D–H \cdots A	H \cdots A / Å	D–H \cdots A / °
O2–H1 \cdots O1	1.83	154
C13–H5 \cdots O61 ⁱ	2.67	171
C12–H36 \cdots O6 ⁱ	2.67	145

CONCLUSIONS

The complex $[\text{Cu}_2(\text{LH})_2](\text{ClO}_4)_2$ was prepared by reaction of copper(II) acetate monohydrate and 3,3'-(1,4-butanediyl-dinitilo)bis-2-pentanone, 2,2'-dioxime

(LH₂) in CH₃OH, followed by the addition of NaClO₄. The compound was characterized by elemental analysis, IR spectroscopy, cyclic voltammetry and single-crystal X-ray crystallography. The crystal structure consists of centrosymmetric [Cu₂(LH)₂]²⁺ and perchlorato anions. The copper(II) atom is in a distorted square-pyramidal coordination with four imine-nitrogen atoms comprising the basal plane and the bridging oximate-oxygen from the other half of the dimer in the axial position. During complex formation, one oxime proton is lost, and a hydrogen bond between the two oxime groups of the same ligand is formed. Comparison with structurally related diimine–dioxime complexes indicates that the geometry of the metallocycle could be influenced by the presence of a weakly coordinated perchlorato anion.

SUPPORTING INFORMATION

CCDC 881203 contains the supplementary crystallographic data for this paper. These data can be obtained free of charge from The Cambridge Crystallographic Data Centre *via* www.ccdc.cam.ac.uk/data_request/cif.

Acknowledgements. This research work was financially supported by the Ministry of Education, Science and Technological Development of the Republic of Serbia, Grant Nos. 45015, 172013, 172065 and 172014. We are indebted to Prof. Vladimir Divjaković from the Department of Physics, Faculty of Sciences, University of Novi Sad, for the crystallographic results and useful suggestions.

ИЗВОД

СИНТЕЗА, КАРАКТЕРИЗАЦИЈА И КРИСТАЛНА СТРУКТУРА [Cu₂(LH)₂](ClO₄)₂. УТИЦАЈ СЛАБЕ Cu···O(ПЕРХЛОРАТО) ИНТЕРАКЦИЈЕ НА СТРУКТУРУ Cu₂N₂O₂ МЕТАЛОЦИКЛА

МАРИЈА МИРКОВИЋ¹, НАДЕЖДА НИКОЛИЋ¹, ДУШАН МИЛИН², МИЛКА АВРАМОВ ИВИЋ³, АГНЕШ КАПОР⁴
и ЗОРАН Д. ТОМИЋ¹

¹Институт за нуклеарне науке „Винча“, Универзитет у Београду, п. бр. 522, 11001 Београд,

²Технолошко–металуршки факултет, Универзитет у Београду, Карнегијева 4, п. бр.3503, 11120

Београд, ³ИХТМ – Центар за електрохемију, Универзитет у Београду, Њетошева 12, Београд и

⁴Депарتمان за Физику, Природно–математички факултет, Универзитет у Новом Саду,
Три Досијеја Обрадовића 4, 21000 Нови Сад

Лиганд 3,3'-(1,4-бутандиил-динитрило)бис-2-пентанон, 2,2'-диоксим (LH₂), синтетисан је у реакцији 2-хидроксиимино-3-пентанона и 1,4-диаминобутана. Утврђено је да постоји разлика у приносу у зависности од поларности растварача. Када се реакција одиграва у етанолу принос је 78 %, а уколико се користи бензен принос је 30 %. Реакцијом бакар(II)-ацетата и лиганда LH₂ добијен је бинуклеарни центросиметрични комплекс чија је формула [Cu₂(LH)₂](ClO₄)₂. Једињење је окарактерисано елементалном анализом, инфрацрвеном спектроскопијом и цикличном волтаметријом. Структура комплекса у чврстом стању је одређена применом метода рендгенско–структурне анализе на монокристалу. Поређење кристалне структуре добивеног једињења са структурно сличним бакар(II) комплексима указује на утицај слабе Cu···O(перхлорато) интеракције на структурна својства Cu₂O₂N₂ металоцикла.

(Примљено 10. септембра, ревидирано 28. октобра, прихваћено 31. октобра 2013)

REFERENCES

1. S. Plentz-Meneghetti, J. Kress, P. J. Lutz, *Macromol. Chem. Phys.* **201** (2000) 1823
2. Z. Guan, P. M. Cotts, E. F. McCord, S. J. McLain, *Science* **283** (1999) 2059
3. K. Singh, M. S. Barwa, P. Tyagi, *Eur. J. Med. Chem.* **41** (2006) 147
4. P. Panneerselvam, R. B. Nair, G. Vijayalakshmi, E. H. Subramanian, S. K. Sridhar, *Eur. J. Med. Chem.* **40** (2005) 225
5. A. A. Abu-Hussen, *J. Coord. Chem.* **59** (2006) 157
6. R. Mladenova, M. Ignatova, N. Manolova, T. Petrova, I. Rashkov, *Eur. Polym. J.* **38** (2002) 989
7. M. Verma, S. N. Pandeya, K. N. Singh, J. P. Stables, *Acta Pharm.* **54** (2004) 49
8. D. N. Dhar, C. L. Taploo, *J. Sci. Ind. Res.* **41** (1982) 501
9. B. Dede, F. Karipcin, M. Cengiz, *J. Hazard. Mater.* **163** (2009) 1148
10. M. K. Taylor, J. Reglinski, D. Wallace, *Polyhedron* **23** (2004) 3201
11. A. B. Oki, S. J. Hodgson, *Inorg. Chim. Acta* **170** (1990) 65
12. E. J. Larson, V. L. Pecoraro, *J. Am. Chem. Soc.* **113** (1991) 3810
13. K. C. Gupta, A. K. Sutar, *Coord. Chem. Rev.* **252** (2008) 1420
14. S. Kiani, R. J. Staples, S. T. Treves, A. B. Packard, *Polyhedron* **28** (2009) 775
15. S. Choubey, S. Roy, K. Bhar, R. Ghosh, P. Mitra, C. Lin, J. Ribas, B. K. Ghosh, *Polyhedron* **55** (2013) 1
16. M. Sutradhar, T. R. Barman, J. Klanke, M. G. B. Drew, E. Rentschler, *Polyhedron* **53** (2013) 48
17. A. B. Packard, J. F. Kronauge, E. Barbarics, S. Kiani, S. T. Treves, *Nucl. Med. Biol.* **29** (2002) 289
18. A. B. Packard, J. F. Kronauge, P. J. Day, S. T. Treves, *Nucl. Med. Biol.* **25** (1998) 531
19. P. Chaudhuri, *Coord. Chem. Rev.* **243** (2003) 143
20. B. Cervera, R. Ruiz, F. Lloret, M. Julve, J. Cano, J. Faus, C. Bois, J. Mrozinski, *J. Chem. Soc., Dalton Trans.* (1997) 395
21. P. Kitiphaisalnont, S. Thohinung, P. Hanmungtum, N. Chaichit, S. Patrarakorn, S. Siripaisarnpipat, *Polyhedron* **25** (2006) 2710
22. J. Lewinski, J. Zacharaa, I. Justyniak, M. Dranka, *Coord. Chem. Rev.* **249** (2005) 1185
23. B. Murphy, B. Hathaway, *Coord. Chem. Rev.* **243** (2003) 237
24. Z. D. Tomić, V. M. Leovac, S. V. Pokorni, D. Zobel, S. D. Zarić, *Eur. J. Inorg. Chem.* **6** (2003) 1222
25. Z. D. Tomić, S. B. Novaković, S. D. Zarić, *Eur. J. Inorg. Chem.* **11** (2004) 2215
26. J. L. Pascal, F. Favier, *Coord. Chem. Rev.* (1998) 865
27. S. Schnitzler, M.-D. Serb, U. Englert, *Acta Crystallogr., C* **68** (2012) m251
28. I. Banerjee, M. Dolai, A. D. Jana, K. K. Das, M. Ali, *Cryst. Eng. Comm.* **14** (2012) 4972
29. J. H. Timmons, J. W. L. Martin, A. E. Martell, P. Rudolf, A. Clearfield, R. C. Buckley, *Inorg. Chem.* **20** (1981) 3056
30. Y. M. Wang, C. C. Wang, S. L. Wang, C. S. Chung, *Acta Crystallogr., C* **46** (1990) 1770
31. M. L. Avramov Ivić, S. D. Petrović, D. Ž. Mijin, F. Vanmoos, D. Ž. Orlović, D. Ž. Marjanović, V. V. Radović, *Electrochim. Acta* **54** (2008) 649
32. K. M. Drljević-Djurić, V. D. Jović, U. Č. Lacnjevac, M. L. Avramov Ivić, S. D. Petrović, D. Ž. Mijin, S. B. Djordjević, *Electrochim. Acta* **56** (2010) 47
33. L. R. Canning, D. P. Nowotnik, R. D. Neirinckx, I. M. Piper, Amersham International Plc., United States Patent 4,789,736, (1988)
34. R. D. Neirinckx, L. R. Canning, I. M. Piper, D. P. Nowotnik, R. D. Pickett, R. A. Holmes, W. A. Volkert, A. M. Forster, P. S. Weisner, J. A. Marriott, *J. Nucl. Med.* **28** (1987) 191

35. M. Mirković, D. Janković, S. Vranješ-Đurić, M. Radović, D. Stanković, D. Mijin, N. Nikolić, *Appl. Organomet. Chem.* **26** (2012) 347
36. Oxford Diffraction, CrysAlisPro version 1.171.32.24, Oxford Diffraction Ltd., Abingdon, 2008
37. A. Altomare, G. Cascarano, C. Giacovazzo, A. Guagliardi, *J. Appl. Crystallogr.* **26** (1993) 343
38. L. J. Farrugia, *J. Appl. Crystallogr.* **32** (1999) 837
39. G. M. Sheldrick, *Acta Crystallogr., A* **64** (2008) 112
40. M. Nardelli, *J. Appl. Crystallogr.* **28** (1995) 659
41. A. L. J. Spek, *J. Appl. Crystallogr.* **36** (2003) 7
42. D. J. Watkin, C. K. Prout, L. J. Pearce, *CAMERON*, Chemical Crystallography Laboratory, University of Oxford, Oxford, UK, 1996
43. J. Bruno, J. C. Cole, P. R. Edgington, M. K. Kessler, C. F. Macrae, P. McCabe, J. Pearson, R. Taylor, *Acta Crystallogr., B* **58** (2002) 389
44. L. J. Farrugia, *J. Appl. Crystallogr.* **30** (1997) 565
45. R. B. Moffett, in *Organic Syntheses Coll. Vol. 4*, N. Rabjohn, Ed., Wiley, New York, 1963, p. 605
46. R. R. Gagne, J. L. Allison, R. S. Gall, C. A. Coval, *J. Am. Chem. Soc.* **99** (1977) 7170
47. Y. Sulfab, F. M. Al-Sogair, *Transit. Metal Chem.* **27** (2002) 299
48. A. W. Addison, T. N. Rao, J. Reedijk, J. Vanrijn, G. C. Verschoor, *J. Chem. Soc., Dalton Trans.* (1984) 1349
49. M. J. Prushan, A. W. Addison, R. J. Butcher, L. K. Thompson, *Inorg. Chim. Acta* **358** (2005) 3449
50. S. Youngme, G. A. van Albada, H. Kooijman, O. Roubeau, W. Somjitsripunya, A. L. Spek, C. Pakawatchai, J. Reedijk, *Eur. J. Inorg. Chem.* (2002) 2367
51. A. M. Schuitema, P. G. Aabel, I. A. Koval, M. Engelen, W. L. Driessen, J. Reedijk, M. Lutz, A. L. Spek, *Inorg. Chim. Acta* **355** (2003) 374.



J. Serb. Chem. Soc. 79 (5) 557–563 (2014)
JSCS–4607

Relating the *ABC* and harmonic indices

IVAN GUTMAN^{1,2*#}, LINGPING ZHONG³ and KEXIANG XU³

¹Faculty of Science, University of Kragujevac, P. O. Box 60, 34000 Kragujevac, Serbia,
²Department of Chemistry, Faculty of Science, King Abdulaziz University, Jeddah 21589,
Saudi Arabia and ³Department of Mathematics, Nanjing University of Aeronautics and
Astronautics, Nanjing 210016, P. R. China

(Received 30 September, accepted 30 December 2013)

Abstract: The atom–bond connectivity (*ABC*) index is a much-studied molecular structure descriptor, based on the degrees of the vertices of the molecular graph. Recently, another vertex–degree-based topological index, the harmonic index (*H*), has attracted attention and gained popularity. It is shown how *ABC* and *H* are related.

Keywords: topological index; degree-based topological index; atom–bond connectivity index; *ABC* index; harmonic index.

INTRODUCTION

In contemporary theoretical chemistry, a great variety of graph-based molecular structure descriptors, so-called “topological indices”, are studied and used.^{1–4} Of these, about two dozens are defined in terms of vertex degrees.^{5–8} Comparative testing of the vertex–degree-based topological indices^{6,7} revealed that from a practical point of view, one of the best is the “atom–bond connectivity (*ABC*) index”. Its applicability, especially for modeling thermochemical properties of saturated organic compounds, is nowadays well documented.^{6,9,10}

The *ABC* index is defined as:

$$ABC = ABC(G) = \sum_{u,v} \sqrt{\frac{d(u) + d(v) - 2}{d(u)d(v)}} \quad (1)$$

where $d(u)$ denotes the degree of the vertex u , and the summation goes over all pairs of adjacent vertices of the molecular graph G . Recall¹¹ that the degree of a vertex is the number of its first neighbors (in the underlying graph); in graphs

* Corresponding author. E-mail: gutman@kg.ac.rs

Serbian Chemical Society member.

doi: 10.2298/JSC130930001G



representing organic molecules, the vertex degrees may assume only values 1, 2, 3 or 4.

Another way of expressing the *ABC* index is:⁵

$$ABC = \sum_{i \leq j} \sqrt{\frac{i+j-2}{ij}} m_{ij} \quad (2)$$

where m_{ij} denotes the number of edges connecting a vertex of degree i with a vertex of degree j .

Details of the theoretical investigation of the *ABC* index can be found in a survey,¹² recent papers,¹³⁻¹⁸ and the references cited therein.

Using the same notation as in Eq. (1), the harmonic index is defined as:

$$H = H(G) = \sum_{u,v} \frac{2}{d(u) + d(v)} \quad (3)$$

and, in analogy, Eq. (2) can be written as:⁵

$$H = \sum_{i \leq j} \frac{2}{i+j} m_{ij} \quad (4)$$

Although this quantity was first mentioning in a mathematical paper¹⁹ from 1987, it did not attract the attention of scholars until quite recently. On the other hand, in the last few years, a remarkably large number of studies of the properties of the harmonic index have appeared,²⁰⁻²⁸ amongst them some by two of the present authors.^{20,21,24} The chemical applicability of the harmonic index was also recently investigated.^{6,7}

In view of the great current research activity on the *ABC* and harmonic indices, and in view of the mathematical similarity of Eqs. (2) and (4), it could be of some interest to search for relations between them. This task is accomplished in the two subsequent sections.

RELATIONS BETWEEN *THE ABC* AND HARMONIC INDICES – GENERAL GRAPHS

In order to establish relations between the two considered topological indices, bearing in mind Eqs. (2) and (4), an auxiliary function $Q = Q(x, y)$ is introduced:

$$Q(x, y) = \frac{\sqrt{\frac{x+y-2}{xy}}}{\frac{2}{x+y}} = \frac{x+y}{2} \sqrt{\frac{x+y-2}{xy}} \quad (5)$$

As the variables x and y pertain to vertex degrees, for any connected graph G with n vertices, they must satisfy the condition $1 \leq x \leq y \leq n-1$. In addition, it

cannot be $x = y = 1$ (except in the trivial case $n = 2$, which is ignored), *i.e.*, y must be ≥ 2 .

By direct calculation, one obtains:

$$\frac{\partial Q(x, y)}{\partial y} = \frac{x(y+2) + (y^2 - x^2) + y(y-2)}{4y\sqrt{xy(x+y-2)}}$$

that evidently is positive-valued for all $y \geq 2$. Thus, $Q(x, y)$ is a monotonically increasing function in the variable y . Consequently, its minimal value is either $Q(1, 2)$ or $Q(2, 2)$, and its maximal value is $Q(x, n-1)$ for some x , which still needs to be determined.

Since:

$$Q(1, 2) = \frac{3}{2\sqrt{2}} \approx 1.061$$

and:

$$Q(2, 2) = \sqrt{2} \approx 1.414$$

it is concluded that Q is minimal for $x = 1, y = 2$.

The first derivative of $Q(x, n-1)$ is found to be:

$$\frac{\partial Q(x, n-1)}{\partial x} = \frac{2x^2 + (n-3)x - (n-1)(n-3)}{4x\sqrt{(n-1)x(x+n-3)}}$$

A detailed analysis shows that for $n = 3$ and $n = 4$, the function $Q(x, n-1)$ monotonically increases and, therefore, its greatest value is $Q(n-1, n-1)$. For $n \geq 5$, this function has a minimum in the interval $(1, n-1)$ and, therefore, the greatest value of $Q(x, n-1)$ is either $Q(1, n-1)$ or $Q(n-1, n-1)$. As:

$$Q(1, n-1) = \frac{n}{2} \sqrt{\frac{n-2}{n-1}}$$

and

$$Q(n-1, n-1) = \sqrt{2n-4}$$

by direct checking one finds that for $n \leq 6$ the greatest value of the function Q is $Q(n-1, n-1)$, whereas for $n \geq 7$ its greatest value is $Q(1, n-1)$.

Return now to the topological indices ABC and H , Eqs. (1) and (3). Let G be a graph with n vertices. An edge of G is said to be of the (i, j) -type if its end-vertices have degrees i and j .

Bearing in mind Eqs. (2) and (4) and the Form (5) chosen for the function Q , it is seen that the ratio $ABC(G)/H(G)$ will be minimal if all edges of G are of the $(1, 2)$ -type. In connected graphs, this is only possible if $n = 3$ and then G is

just the molecular graph P_3 of propane. Thus, the first relation, valid for all graphs, is obtained:

$$\frac{ABC(G)}{H(G)} \geq Q(1,2) = \frac{3}{2\sqrt{2}} \quad (6)$$

with equality (for connected graphs) if and only if $G = P_3$.

In the same manner, it could be concluded that for $n \leq 6$, the ratio $ABC(G)/H(G)$ will be maximal if all edges of G are of the $(n-1, n-1)$ -type, whereas for $n \geq 7$, all edges should be of the $(1, n-1)$ -type.

Therefore, if $n \leq 6$, then:

$$\frac{ABC(G)}{H(G)} \leq Q(n-1, n-1) = \sqrt{2n-4} \quad (7)$$

with equality if and only if G is a complete graph.¹¹

If $n \geq 7$, then:

$$\frac{ABC(G)}{H(G)} \leq Q(1, n-1) = \frac{n}{2} \sqrt{\frac{n-2}{n-1}} \quad (8)$$

with equality if and only if G is a star graph.¹¹

Summarizing the relations (6)–(8), the first main result can be stated:

Proposition 1. Let G be any graph with n vertices, $n > 2$. Then:

$$\gamma_1 H(G) \leq ABC(G) \leq \gamma_2 H(G) \text{ and } \delta_1 ABC(G) \leq H(G) \leq \delta_2 ABC(G)$$

where:

$$\gamma_1 = \frac{3}{2\sqrt{2}}, \gamma_2 = \sqrt{2}, 2, \sqrt{6}, 2\sqrt{2} \text{ and } \frac{n}{2} \sqrt{\frac{n-2}{n-1}}$$

for $n = 3, 4, 5, 6$, and $n \geq 7$, respectively, and:

$$\delta_1 = \frac{1}{\gamma_2} \text{ and } \delta_2 = \frac{1}{\gamma_1}.$$

Equality cases are specified at Eqs. (6)–(8).

RELATIONS BETWEEN ABC AND HARMONIC INDICES – MOLECULAR GRAPHS

In the case of molecular graphs, the analysis of the relation between the ABC and harmonic indices is much simpler, thanks to the fact that these graphs may have only 9 different types of edges. The respective Q -values are given in Table I.

Using the values from Table I and an analogous, yet simpler, reasoning as in the preceding section, second main result is straightforwardly deduced:

Proposition 2. Let G be any molecular graph with n vertices, $n > 2$. Then:

$$Q(1,2)H(G) \leq ABC(G) \leq Q(4,4)H(G) \text{ and}$$

$$\frac{1}{Q(4,4)}ABC(G) \leq H(G) \leq \frac{1}{Q(1,2)}ABC(G)$$

where the values of $Q(i, j)$ are given in Table I. The equality $ABC(G) = Q(1,2)H(G)$ occurs if and only if G is the molecular graph of propane. In the case of ordinary molecular graphs, the equality $ABC(G) = Q(4,4)H(G)$ is not possible, but could be satisfied if G is the graph representation of a diamond-like nanostructure.^{29,30}

For benzenoid systems, in which only (2,2)-, (2,3)- and (3,3)-type edges occur (*i.e.*, in Eqs. (2) and (4) the only non-zero multipliers are m_{22}, m_{23}, m_{33}),^{5,31-33} the following special case of Proposition 2 holds:

Proposition 3. Let G be the molecular graph of a benzenoid system. Then:

$$Q(2,2)H(G) \leq ABC(G) \leq Q(3,3)H(G) \text{ and}$$

$$\frac{1}{Q(3,3)}ABC(G) \leq H(G) \leq \frac{1}{Q(2,2)}ABC(G)$$

where the values of $Q(i, j)$ are given in Table I. The equality $ABC(G) = Q(2,2)H(G)$ occurs if and only if G is the molecular graph of benzene. The equality $ABC(G) = Q(3,3)H(G)$ occurs in the cases of nanotubes and nanotoruses, as well as fullerenes.^{29,30}

TABLE I. The value of the auxiliary function Q , Eq. (5), for all possible edge-types that may occur in molecular graphs; i, j are the degrees of the end-vertices of the respective edge

i, j	$Q(i, j)$	i, j	$Q(i, j)$
1,2	1.061	2,4	2.121
1,3	1.633	3,3	2.000
1,4	2.165	3,4	2.259
2,2	1.414	4,4	2.449
2,3	1.768		

Acknowledgement. The second author was supported by the National Natural Science Foundation of China (Nos. 11001129 and 11226289) and the Fundamental Research Funds for the Nanjing University of Aeronautics and Astronautics (No. NS2013075). The third author was supported by the National Natural Science Foundation of China (No. 11201227), the Natural Science Foundation of Jiangsu Province (No. BK20131357), and a China Post-doctoral Science Foundation Funded Project (No. 2013M530253).

ИЗВОД

ВЕЗЕ ИЗМЕДУ АВС И ХАРМОНИЈСКОГ ИНДЕКСА

ИВАН ГУТМАН¹, LINGPING ZHONG² и KEXIANG XU³

¹Природно-математички факултет Универзитета у Крагујевцу, ²Department of Chemistry, Faculty of Science, King Abdulaziz University, Jeddah 21589, Saudi Arabia и ³Department of Mathematics, Nanjing University of Aeronautics and Astronautics, Nanjing 210016, P. R. China

Индекс повезаности атом-веза (*atom-bond connectivity index*, АВС) је један од највише проучаваних молекулских структурних дескриптора заснованих на степенима чворова молекулског графа. Недавно је један други такав тополошки индекс – хармонијски индекс *H* – привукао пажњу и добио на значају. У раду налазимо везе између АВС и *H*.

(Примљено 30. септембра, прихваћено 30. децембра 2013)

REFERENCES

1. J. Devillers, A. T. Balaban (Eds.), *Topological Indices and Related Descriptors in QSAR and QSPR*, Gordon & Breach, Amsterdam, 1999
2. R. Todeschini, V. Consonni, *Handbook of Molecular Descriptors*, Wiley-VCH, Weinheim, Germany, 2000
3. R. Todeschini, V. Consonni, *Molecular Descriptors for Chemoinformatics*, Vols. 1 and 2, Wiley-VCH, Weinheim, Germany, 2009
4. I. Gutman, B. Furtula (Eds.), *Novel Molecular Structure Descriptors – Theory and Applications*, Vols. 1 and 2, Univ. Kragujevac, Kragujevac, 2010
5. I. Gutman, B. Furtula, *J. Serb. Chem. Soc.* **77** (2012) 1031
6. I. Gutman, J. Tošović, *J. Serb. Chem. Soc.* **78** (2013) 805
7. B. Furtula, I. Gutman, M. Dehmer, *Appl. Math. Comput.* **219** (2013) 8973
8. I. Gutman, *Croat. Chem. Acta* **86** (2013) 351
9. E. Estrada, *Chem. Phys. Lett.* **463** (2008) 422
10. I. Gutman, J. Tošović, S. Radenković, S. Marković, *Indian J. Chem., A* **51** (2012) 690
11. I. Gutman, O. E. Polansky, *Mathematical Concepts in Organic Chemistry*, Springer, Berlin, 1986
12. I. Gutman, B. Furtula, M. B. Ahmadi, S. A. Hosseini, P. Salehi Nowbandegani, M. Zarrinderakht, *Filomat* **27** (2013) 1075
13. I. Gutman, B. Furtula, *MATCH Commun. Math. Comput. Chem.* **68** (2012) 131
14. I. Gutman, B. Furtula, M. Ivanović, *MATCH Commun. Math. Comput. Chem.* **67** (2012) 467
15. W. Lin, X. Lin, T. Gao, X. Wu, *MATCH Commun. Math. Comput. Chem.* **69** (2013) 549
16. M. B. Ahmadi, S. A. Hosseini, P. Salehi Nowbandegani, *MATCH Commun. Math. Comput. Chem.* **69** (2013) 559
17. M. B. Ahmadi, S. A. Hosseini, M. Zarrinderakht, *MATCH Commun. Math. Comput. Chem.* **69** (2013) 565
18. S. A. Hosseini, M. B. Ahmadi, I. Gutman, *MATCH Commun. Math. Comput. Chem.* **71** (2014) 5
19. S. Fajtlowicz, *Congr. Numer.* **60** (1987) 187
20. L. Zhong, *Appl. Math. Lett.* **25** (2012) 561
21. L. Zhong, *Ars Combin.* **104** (2012) 261
22. J. Liu, Q. Zhang, *Util. Math.* **88** (2012) 281
23. X. Xu, *Appl. Math. Sci.* **41** (2012) 2013
24. L. Zhong, K. Xu, *Util. Math.* **90** (2013) 23

25. Y. Zhu, R. Chang, X. Wei, *Ars Comb.* **110** (2013) 97
26. R. Wu, Z. Tang, H. Deng, *Util. Math.* **91** (2013) 65
27. H. Deng, S. Balachandran, S. K. Ayyaswamy, Y. B. Venkatakrishnan, *Discr. Appl. Math.* **161** (2013) 2740
28. R. Wu, Z. Tang, H. Deng, *Filomat* **27** (2013) 51
29. M. V. Diudea, C. L. Nagy, *Periodic Nanostructures*, Springer, Amsterdam, 2007
30. M. V. Diudea, *Nanomolecules and Nanostructures*, Univ. Kragujevac, Kragujevac, 2010
31. J. Rada, R. Cruz, I. Gutman, *Chem. Phys. Lett.* **572** (2013) 154
32. R. Cruz, H. Giraldo, J. Rada, *MATCH Commun. Math. Comput. Chem.* **70** (2013) 501
33. J. Rada, R. Cruz, I. Gutman, *MATCH Commun. Math. Comput. Chem.* **72** (2014) 125.



J. Serb. Chem. Soc. 79 (5) 565–578 (2014)
JSCS–4608

Thermodynamics of the complexation between salicylaldehyde thiosemicarbazone with Cu(II) ions in methanol–1,4-dioxane binary solutions

RASHMIDIPTA BISWAS, DHIRAJ BRAHMAN and BISWAJIT SINHA*

Department of Chemistry, University of North Bengal, Darjeeling-734013, India

(Received 30 July, revised 7 November, accepted 19 November 2013)

Abstract: The complexation reaction between salicylaldehyde thiosemicarbazone, abbreviated as STSC, with Cu(II) ion was studied in binary mixtures of methanol–1,4-dioxane using UV–Vis spectrophotometric and conductometric methods at different temperatures. The formation constants (K_f) for the 1:1 complex, Cu(II)–STSC, were calculated from computer fitting of the absorbance and molar conductance data against various concentrations ratios ($c_M:c_L$ or $c_L:c_M$) in different binary solvent mixtures. A non-linear correlation was observed for the variation of $\log K_f$ for the complex against the solvent compositions. Various thermodynamic parameters (ΔH , ΔS and ΔG) for the formation of the Cu(II)–STSC complex were also determined from the temperature dependence of the formation constants (K_f). The results showed that the complexation reaction is affected by the nature and composition of the mixed solvents.

Keywords: salicylaldehyde thiosemicarbazone; Cu(II); stability constants; binary mixtures; methanol; 1,4-dioxane.

INTRODUCTION

Schiff bases derived from the amines and aldehydes belong to an important class of ligands that coordinate to metal ions through the azomethine nitrogen.^{1–3} In recent years, there has been considerable interest in the chemistry of transition metal complexes of thiosemicarbazone ligands, primarily because of their bio-inorganic relevance.⁴ In the solid state, these thiosemicarbazones exist in the thione form and in solution they tautomerize into the thiol form.⁵ Complexation usually occurs through the dissociation of the acidic proton, resulting in the formation of a five-membered chelate ring and, when an additional donor site is incorporated or linked to the carbonylic carbon by one or two intervening atoms, tricoordination usually occurs.⁵ Thiosemicarbazones of salicylaldehyde and their

* Corresponding author. E-mail: biswachem@gmail.com
doi: 10.2298/JSC130730137B

derivatives constitute a class of versatile tridentate (O, N and S) donors capable of stabilizing both higher and lower oxidation states of transition metal ions.^{6–8} These ligands also have an ion-sensing ability, metal extraction properties, pharmacological properties, *etc.*^{9–13} Among the first row transition metals, copper plays a pivotal role in cell physiology as a catalytic cofactor in the redox chemistry of mitochondrial respiration, iron absorption, free radical scavenging, elastin cross-linking,¹⁴ *etc.* Copper is found in all living organisms and is a crucial trace element in redox chemistry, growth and development.¹⁵ It is important for the function of several enzymes and proteins involved in energy metabolism, respiration and DNA syntheses. Very little information is available in the literature about the thermodynamic stability of the complexes of STSC and its derivatives, most probably due to their low water solubility that limits experimental exploration of their solution equilibria. However, the use of aqueous organic solvent mixtures can be useful for comparing the stability of complexes of different metal ions and a series of ligands in semi aqueous media.^{16–18}

Among the various organic solvents, alcohols in nonpolar solvents can associate by means of hydrogen bonds into a series of *n*-mers. In dilute solutions, the predominant species are the unassociated molecules, while in concentrated solutions, both linear and *n*-mers coexist. In solvents such as 1,4-dioxane (DO) that can form hydrogen bonds with methanol (MeOH), the self-association of alcohols may be reduced or perturbed in favor of hydrogen-bonded structures when mixed together, leading to intermolecular association between MeOH and DO molecules.¹⁹ Papanastasiou *et al.*²⁰ suggested that binary mixtures of DO and MeOH are characterized by the formation of two intermolecular complexes of the types (DO:MeOH) 1:1 and 1:2 and that DO can associate through hydrogen bonds involving either of its two oxygen atoms. Although, numerous literature data are available for complex formation of Schiff bases with metal ions in non-aqueous solvents and mixed solvent systems, thermodynamic data on complex formation of salicylaldehyde thiosemicarbazone (STSC) with Cu(II) ions in pure and mixed non-aqueous or semi aqueous solvents are rather scarce.^{21–26} Hence in this work, the complexation behavior of STSC with Cu(II) ion in different MeOH–DO mixed solvents was studied in order to understand the thermodynamics of complex formation between STSC and Cu(II) in the studied mixed solvents.

EXPERIMENTAL

Materials

Reagent grade thiosemicarbazone (s), salicylaldehyde (l) and copper(II) nitrate trihydrate, $\text{Cu}(\text{NO}_3)_2 \cdot 3\text{H}_2\text{O}$ (s) were procured from Thomas Baker, India, and used as received. Spectroscopic grade methanol (MeOH) and 1,4-dioxane (DO) (each of purity > 99 %, S. D. Fine Chemicals, India) were used without further purification. Salicylaldehyde thiosemicarbazone (STSC) was prepared according to a literature procedure and its purity was checked by spec-

trosopic and other analytical methods.¹¹ The various binary solvent mixtures were prepared by mass and necessary adjustments were performed to achieve exact mass fractions ($w_1 = 0.40, 0.60, 0.80$ and 1.00) of MeOH in the binary solvent mixtures at 298.15 K under atmospheric pressure. The mass measurements were realized on a digital electronic analytical balance (Mettler, AG 285, Switzerland) with a precision of $\pm 0.01\text{ mg}$. The relative error in solvent composition was about 1%. The physical properties of these solvent mixtures are available in the literature.²⁷

Preparation of the ligand

Thiosemicarbazone (0.746 g) was dissolved in 75 mL of doubly distilled deionized water by warming. To the obtained solution, salicylaldehyde (1 g) was added and the reaction mixture was refluxed for $3\text{--}4\text{ h}$. Crystals of STSC were obtained from the solution on cooling. The thus-obtained crystals were separated by filtration, dried under vacuum and further purified by recrystallization from ethanol.

Analytical and spectral data of the ligand

The melting point of the ligand was determined by the open capillary method. The IR spectrum of the ligand salicylaldehyde thiosemicarbazone in the wavenumber range $400\text{--}4000\text{ cm}^{-1}$ was recorded on a Perkin-Elmer FT-IR spectrophotometer (RX-1). Elemental micro-analyses were realized using a Perkin-Elmer (Model 240C) analyzer.

Salicylaldehyde thiosemicarbazone. White crystalline compound; Anal. Calcd. for $\text{C}_8\text{H}_9\text{N}_3\text{OS}$: C, 49.23; H, 4.61; N, 21.53; S, 16.41 %; IR (KBr, cm^{-1}): 3443.87 (3444²⁹), 3320.97 (3321²⁹), 3175.01 (3175²⁹), 1236.84 (1237²⁹), 1035.91 (1036²⁹), 751.76 (752²⁹).

The structure of the synthesized Schiff base is depicted in Fig. 1.

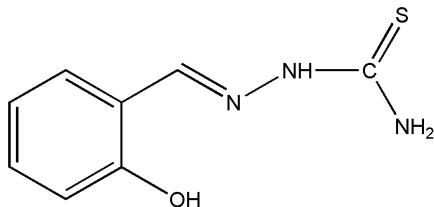


Fig. 1. Structure of salicylaldehyde semicarbazone (STSC).

UV-Vis spectrophotometric titration

The absorbance spectra were recorded on a Jasco V-530 spectrophotometer equipped with a thermostated bath. During the complexation studies, temperature of the quartz cell was maintained at $298.15 \pm 0.1\text{ K}$. For the spectrophotometric titration, the stepwise additions of metal ion solution ($1.3 \times 10^{-3}\text{ mol dm}^{-3}$) to 2 mL of a solution of ligand ($5.0 \times 10^{-5}\text{ mol dm}^{-3}$) were realized using a $10\text{ }\mu\text{L}$ pre-calibrated micropipette. The absorbance (A) of the solution was measured after each addition of metal ion solution to the ligand solution.

Conductometric titration

The conductance measurements were performed with a Systronics-308 conductivity bridge (with a precision $\pm 0.1\%$) and a dip-type immersion conductivity cell (type CD-10) at a frequency of 1 kHz . Measurements were made in a water bath maintained at $\pm 0.01\text{ K}$ of the desired temperatures. The cell was calibrated with standard KCl solution as described earlier³² and the cell constant was 1.16 cm^{-1} . During the conductometric titration, a solution of copper nitrate ($5.0 \times 10^{-4}\text{ mol dm}^{-3}$, 15 mL) was placed in the conductivity cell and the conductance of the solution was measured. A solution of the ligand ($2.5 \times 10^{-2}\text{ mol dm}^{-3}$) was added stepwise

to the conductivity cell with a pre-calibrated micropipette (50 μL) and the conductance of the resulting solution was measured after each addition. Addition of the ligand solution was continued until the total concentration of the ligand was approximately three times greater than that of the metal ion concentration ($c_L:c_M = 3:1$).

RESULTS

UV-Vis spectrophotometric titration

The UV-Vis spectra of the STSC ligand and its Cu(II) complex in pure MeOH and in the binary mixtures of MeOH with DO are presented in Fig. 2, which shows that the absorption spectrum of the solution of STSC ligand (initially $5.0 \times 10^{-5} \text{ mol dm}^{-3}$) underwent marked changes when a solution of Cu(II) cations ($1.3 \times 10^{-3} \text{ mol dm}^{-3}$) was added to the ligand solution in a stepwise fashion until the concentration ratio, $c_M:c_L$, of 3:1 at 298.15 K was achieved. The UV-Vis spectrum of STSC showed two characteristic bands at around 291 and 332 nm. These bands originate from the azomethine chromophore and the phenol moiety, respectively. During the spectrophotometric titration, complex formation was indicated by a gradual decrease in the intensity of the 332 nm peak and by the development of a peak at around 394 nm. These changes in UV-Vis spectra were due to the coordination of Cu(II) ion through imine nitrogen atom, sulfur atom with an additive effect from the deprotonation of the phenolate group upon chelation, resulting in the formation of six and five-membered ring systems between the metal atom and the ligand in the complex.¹⁶ However, the peak at 291 nm overlapped with that of the free NO_3^- at around 298 nm²⁹ and increased gradually in intensity in pure MeOH as more and more electrolyte solution was added, but the peak showed no such changes for the solutions in the binary mixtures; probably due to low dielectric constants of the binary mixtures. Hence, the analysis of the spectrophotometric data was performed with the absorbance values at $\lambda = 394 \text{ nm}$ as shown in Fig. 3. It is evident from Fig. 3 that when the ligand STSC reacted with Cu(II) ions in MeOH and its binary mixtures with DO, a 1:1 complex is formed. The mass balance for the ML complex is given by the relation:³¹



and the formation constant (K_f) could be given by:

$$K_f = \frac{[\text{ML}]}{[\text{M}][\text{L}]} \quad (2)$$

where $[\text{M}]$, $[\text{L}]$ and $[\text{ML}]$ stand for the concentrations of free metal ion, free ligand and formed complex in equilibrium, respectively. The mass balance for Eq. (1) can be solved provided that the following relations for the concentrations of total metal ion and ligand remain valid in equilibrium:

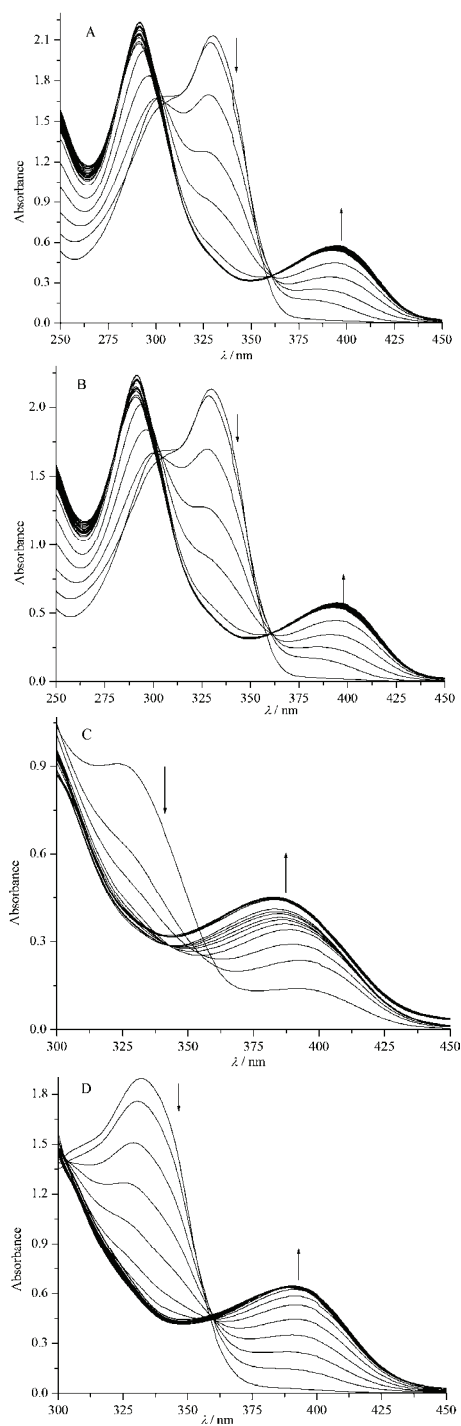


Fig. 2. UV-Vis spectra of the STSC ligand ($5 \times 10^{-5} \text{ mol dm}^{-3}$) in the presence of increasing concentrations of Cu(II) ions in different solvent mixtures with MeOH mass fractions (w_1) at 298.15 K: A, $w_1 = 1.00$; B, $w_1 = 0.80$; C, $w_1 = 0.60$; D, $w_1 = 0.40$.

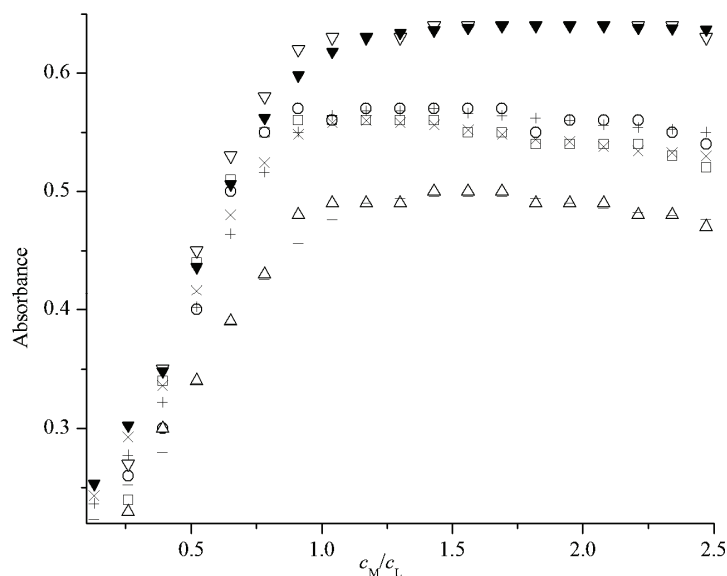


Fig. 3. Absorbance plot (\circ) for the ligand STSC with Cu(II) ion against $c_M:c_L$ for different mass fractions (w_1) of MeOH in different solvent mixtures at 298.15 K. Symbols for the experimental data: \square , $w_1 = 1.00$; \circ , $w_1 = 0.80$; Δ , $w_1 = 0.60$; ∇ , $w_1 = 0.40$. Symbols for the calculated data: \times , $w_1 = 1.00$; $+$, $w_1 = 0.80$; $-$, $w_1 = 0.60$; \blacktriangledown , $w_1 = 0.40$.

$$c_M = [M] + [ML] \quad (3)$$

$$c_L = [L] + [ML] \quad (4)$$

When the $[M]$ and $[L]$ values, obtained from Eqs. (3) and (4), are substituted in Eq. (2), one obtains K_f as:

$$K_f = \frac{[ML]}{(c_M - [ML])(c_L - [ML])} \quad (5)$$

If only the complex absorbs at a particular wavelength, the total absorption (A) at this wavelength can be given by:

$$A = \varepsilon l [ML] = \varepsilon [ML] \quad (6)$$

where ε is the molar absorption coefficient of the complex and the path length $l = 1$ cm. Hence, from the above relation, $[ML]$ is given by:

$$[ML] = A / \varepsilon \quad (7)$$

Therefore, when $c_M \gg c_L$, Eq. (5) can be rearranged as:

$$K_f = \frac{[ML]}{c_M(c_L - [ML])} = \frac{A / \varepsilon}{c_M(c_L - A / \varepsilon)} \quad (8)$$

Rearranging the above relation, one obtains:³¹

$$\frac{c_M c_L}{A} = \frac{c_M}{\epsilon} + \frac{1}{\epsilon K_f} \quad (9)$$

Thus a linear regression of $c_M c_L/A$ against c_M gives the molar absorption coefficient (ϵ) from the slope and K_f from the intercept. Using these ϵ and K_f values, obtained from Eq. (9) as initial guess values, the absorbance ($A_{\text{cald.,}i}$) of each solution was iteratively calculated and then the final ϵ and K_f values were obtained from Eq. (10) by using the Newton–Raphson Method with the aid of a C-program. Eq. (10) was obtained after some rearrangement of Eq. (5):

$$(A/\epsilon)^2 - \{(c_M + c_L) + 1/K_f\}(A/\epsilon) + c_M c_L = 0 \quad (10)$$

The standard errors (σ) in the absorbances were calculated from the following relation:

$$\sigma = \left[\sum_{i=1}^n \{A_{\text{exp.,}i} - A_{\text{cald.,}i}\}^2 / n \right]^{1/2} \quad (11)$$

where n stands for the number of solutions. The obtained standard errors (σ) were 0.035, 0.025, 0.039 and 0.042 in the solvent mixtures with $w_1 = 0.40, 0.60, 0.80$ and 1.00, respectively.

Conductometric titration

It is known that the equilibrium for 1:1 complexation is represented by Eq. (1) and the formation constant (K_f) is given by:

$$K_f = \frac{[\text{ML}]}{[\text{M}][\text{L}]} \frac{f_{\text{ML}}}{f_{\text{M}}f_{\text{L}}} \quad (12)$$

where the f terms stand for the activity coefficients of the species indicated in subscripts. Under the employed dilute concentration range, the activity coefficient of the uncharged ligand (f_L) can be assumed to be unity.^{33,34} According to the Debye–Huckel limiting law $f_M \approx f_{\text{ML}}$, the activity coefficients in Eq. (12) cancel each other.³⁵ The fraction of the total metal ion concentration (α), remaining free at equilibrium, can be expressed by the relation:

$$\alpha = \frac{A_m - A_{\text{ML}}}{A_{\text{MA}} - A_{\text{ML}}} \quad (13)$$

where A_m , A_{MA} and A_{ML} stand for the total molar conductance, and the molar conductance of the electrolyte and the complex, respectively. The A_{ML} values were calculated by a least square linear regression of the data points (A_m vs. c_L/c_M) after the curve changed its slope at higher $c_L:c_M$ ratios (Fig. 4). Then, the α values were calculated from Eq. (13) for each solution and an initial K_f value

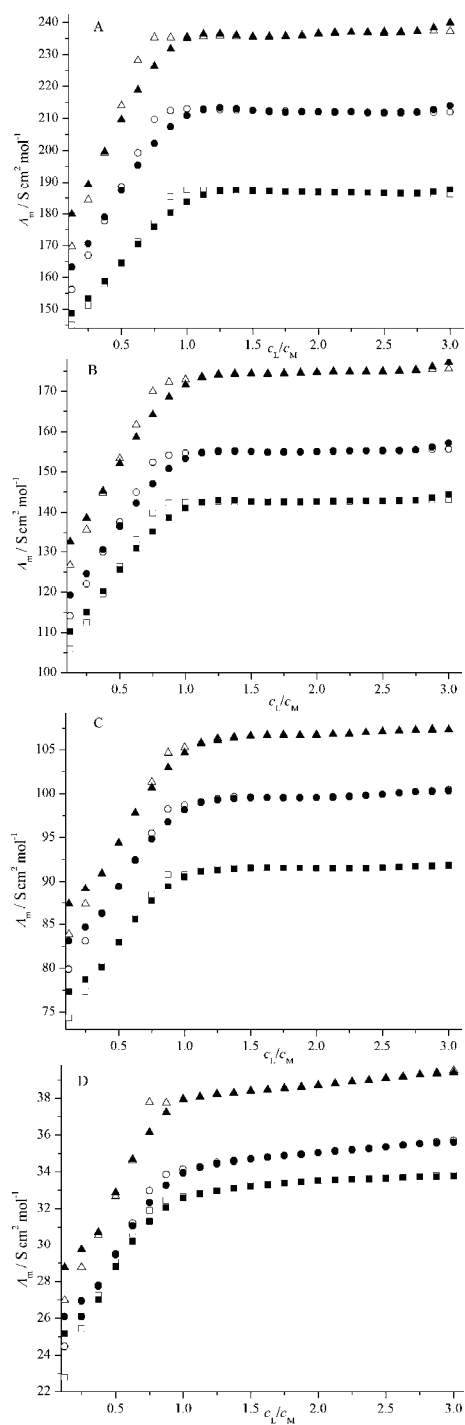


Fig. 4. Molar conductance (Λ_m) vs. mole ratio plot ($c_L:c_M$) for the Cu(II)-STSC complex in pure MeOH and different binary mixtures of MeOH-DO at different temperatures: A, $w_1 = 1.00$; B, $w_1 = 0.80$; C, $w_1 = 0.60$; D, $w_1 = 0.40$. Symbols for the experimental data: \square , $T = 298.15$ K; \circ , $T = 308.15$ K; Δ , $T = 318.15$ K and symbols for the calculated data: \blacksquare , $T = 298.15$ K; \bullet , $T = 308.15$ K; \blacktriangle , $T = 318.15$ K.

for each solution was calculated using the [M] and [L] values. Eq. (12) can also be rearranged as:³⁶

$$K_f[\text{ML}]^2 - \{1 + (c_M + c_L)K_f\}[\text{ML}] + K_f c_M c_L = 0 \quad (14)$$

The final K_f values and [ML] were then calculated iteratively using the Newton–Raphson Method and successive approximations with the aid of a C-program.

DISCUSSION

The nature of a solvent can strongly influence the stoichiometry of a complex and complexation of transition metal ions in solution. The stability of transition metal complexes with polydentate ligand depends on several factors, such as the number and type of the donor sites present in the ligand, the number and size of the chelate rings formed on complexation, *etc.*³⁷ In addition, the stability also depends upon the donor strengths and dielectric constants of solvent–solvent mixtures.³⁸ Although the STSC solution had negligible conductance, its addition to the metal ion solution caused a rather large and continuous increase in molar conductance in all solvents. As can be seen from Fig. 4, the addition of STSC to Cu(II) ions in pure MeOH as well as in the binary solvent mixtures at different temperatures resulted in increases in molar conductivity. This fact indicated that the Cu(II)–STSC complex is more mobile than solvated Cu(II) ions and to the existence of some ion pairs in the initial salt and the release of some high-mobility protons and NO₃[−] into the solution.^{39,40} The slope of Λ_m vs. c_L/c_M plots for all solvent mixtures showed significant changes in slopes when $c_L:c_M$ was about 1 thus indicating the formation of a relatively stable 1:1 complex (ML) between Cu(II) ions and STSC. From Fig. 4, it is also evident that the curvature of the molar conductivity plots for the Cu(II)–STSC complex decreased as the experimental temperature increased. This fact indicated to the formation of a weaker complex at higher temperatures. This is also evident from Table I wherein $\log K_f$ for Cu(II)–STSC complex in pure MeOH as well as in the binary solvent mixtures decreased with increasing temperature. However, slightly higher values of $\log K_f$ were obtained at 318.15 K for solvent mixtures with $w_1 = 0.40$ and 0.60 than those at 308.15 K.

TABLE I. $\log K_f$ values for the Cu(II)–STSC complex obtained from complexometric titrations in MeOH–DO binary mixtures at different temperatures; w_1 is the mass fraction of MeOH in the binary solvent mixtures. Standard errors are given in the parenthesis

w_1	T / K		
	298.15	308.15	318.15
1.00	5.28 (± 0.23)	4.90 (± 0.21)	4.89 (± 0.19)
0.80	5.14 (± 0.21)	4.84 (± 0.18)	4.76 (± 0.16)
0.60	4.92 (± 0.16)	4.75 (± 0.15)	4.80 (± 0.11)
0.40	4.97 (± 0.18)	4.83 (± 0.15)	5.00 (± 0.12)

MeOH has a higher Gutmann donor number ($DN = 19$) than that of DO ($DN = 14.8$).⁴¹ However, a comparison of the stability constants given in Table I and III revealed that Cu(II) ion was weakly solvated and easily complexed by the ligand in the solvent mixtures with higher contents of MeOH and the stability constants decreased with increasing concentration of DO in the binary solvents. This fact is in accordance with the reverse order of their solvating ability as represented by their Gutmann donor numbers. It is known that the solvating ability of the solvent plays an important role in different complexation reactions. Moreover, the stability and selectivity of the formed complexes are affected by a number of molecular factors, such as the number and character of the donor atoms in the Schiff base, the polarizability and charge density of the metal ion, the nature of substituents and the character of the co-anion with the cationic species.^{42,43} In the Cu(II)–STSC complex, the ligand binds a Cu(II) ion through its three binding sites (O, N and S) and the fourth coordination site is most probably occupied by the solvent molecules, *i.e.*, MeOH or DO.¹⁶ However, as per the polarity and steric factors for MeOH and DO, it is expected that MeOH will preferentially occupy the fourth coordination site. Regardless, the variation of the $\log K_f$ for the Cu(II)–STSC complex as a function of solvent composition is presented in Fig. 5, which shows that the changes in the stability constants for Cu(II)–STSC complex *vs.* the solvent composition are not linear. This evidence reflects that changes might be occurring in the structure of the solvent mixtures²⁰ and these changes probably alter solvations of the metal ion, the Schiff base and even the resulting complex as well as the preferential solvation of these species in the mixed solvents.⁴⁴ Preferential solvation of ions by one of the components of a mixed solvent system depends on two factors: the relative donor–acceptor abilities of the

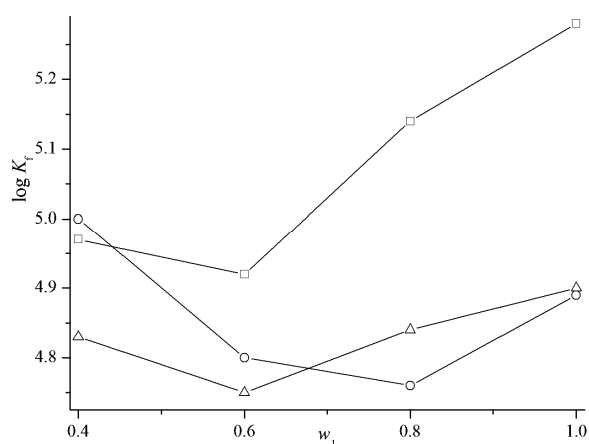


Fig. 5. Variation of formation constants (K_f) for Cu(II)–STSC complex against mass fractions (w_1) of MeOH in the binary solvent mixtures at different temperatures. Symbols: \square , 298.15 K; Δ , 308.15 K; \circ , 318.15 K.

component molecules towards the ion and the interactions between solvent molecules themselves. The solvating properties of the components in mixed solvents can even be significantly modified by solvent–solvent interactions when the energy of the latter is comparable with the energy difference of ion–solvent interactions for both of the components.⁴⁵

Anyway, the stability constants given in Tables I and II have nearly the same order although the formation constants evaluated by the two methods are not the same but are similar in magnitude. This is because the experimental data were analyzed by two different approaches in the two methods used to determine the stability constants (K_f) and they have their own intrinsic error limits.

TABLE II. $\log K_f$ values for the Cu(II)–STSC complex obtained from UV–Vis spectrophotometry in MeOH–DO binary mixed solvents at 298.15 K; w_1 is the mass fraction of MeOH in the binary solvent mixtures. Standard errors are given in the parenthesis

w_1	$\log K_f$
1.00	4.87 (± 0.13)
0.80	4.77 (± 0.12)
0.60	4.76 (± 0.10)
0.40	4.65 (± 0.13)

Thermodynamic parameters

In order to obtain a better understanding of the thermodynamics of the complexation reaction between Cu(II) and STSC, it is useful to determine the contributions of enthalpy and entropy of the reaction. The thermodynamic parameters were calculated from the temperature dependence of the complexation constants (van't Hoff plot):

$$2.303 \log K_f = -\frac{\Delta H}{RT} + \frac{\Delta S}{R}$$

where R is the gas constant. For all the solvent mixtures, the plots of $\log K_f$ vs. $1/T$ were almost linear and the ΔS and ΔH values were determined in the usual way from the slope and the intercept of the plots, respectively. The calculated thermodynamic parameters are listed in Table III. The ΔH and ΔS values associated with the complexation reaction were negative for all the solvent mixtures except for the solvent mixture with $w_1 = 0.40$. The ΔG values for the complexation reaction were negative indicating the spontaneity of the reaction. Thus, it is evident that the reactions were spontaneous and enthalpy-driven except for the solvent mixture with $w_1 = 0.40$. For this solvent mixture, the complexation reaction was observed to be entropy-driven. These trends, as reflected by the thermodynamic parameters for the complexation reaction, are the overall results of several factors, such as solvation/desolvation of the species involved in the complexation reaction and the variation in flexibility of Schiff base during the complex-

ation process, as well as the degree of ion–solvent, ligand–solvent, complex–solvent and solvent–solvent interactions.^{46,47}

TABLE III. Thermodynamic parameters (ΔH , ΔS and ΔG) for the formation of the Cu(II)–STSC complex in different binary mixtures of MeOH with DO

w_1	$\Delta G / \text{kJ mol}^{-1}$			$\Delta H / \text{kJ mol}^{-1}$	$\Delta S / \text{J mol}^{-1} \text{K}^{-1}$
	298.15 K	308.15 K	318.15 K		
1.00	–29.81 (± 0.23)	–29.61 (± 0.22)	–29.41 (± 0.21)	–35.77 (± 0.23)	–19.97 (± 0.22)
0.80	–29.15 (± 0.12)	–28.96 (± 0.12)	–28.78 (± 0.11)	–34.71 (± 0.13)	–18.65 (± 0.13)
0.60	–27.89 (± 0.15)	–28.45 (± 0.13)	–29.01 (± 0.15)	–11.11 (± 0.13)	56.27 (± 0.14)
0.40	–28.09 (± 0.20)	–29.11 (± 0.23)	–30.13 (± 0.22)	2.42 (± 0.20)	102.31 (± 0.23)

CONCLUSIONS

The formation constants for the complexation of Cu(II) ion with STSC were determined conductometrically at different temperatures and spectrophotometrically at 298.15 K. Thermodynamic parameters for the complexation were determined from the temperature dependence of the formation constant. The stoichiometry of the Cu(II)–STSC complex in pure MeOH and in all the MeOH–DO binary mixtures was found to be 1:1. The negative values of ΔG show the ability of the studied ligand to form stable complex with Cu(II) ion and the complexation proceed spontaneously.

Acknowledgements. The authors are grateful to the Departmental Special Assistance Scheme under the University Grants Commission, New Delhi (SAPDRS-III, No. 540/12/DRS/2013) for financial support.

ИЗВОД

ТЕРМОДИНАМИКА ФОРМИРАЊА КОМПЛЕКСА Cu(II) СА САЛИЦИЛАЛДЕХИД-ТИОСЕМИКАРБАЗОНОМ У БИНАРНИМ РАСТВОРИМА МЕТАНОЛ–1,4-ДИОКСАН

RASHMIDIPTA BISWAS, DHIRAJ BRAHMAN и BISWAJIT SINHA

Department of Chemistry, University of North Bengal, Darjeeling-734013, India

Реакција комплексирања Cu(II) и салицилалдехид тиосемикарбазона (STSC) испитивана је у бинарним растворима метанол–1,4 диоксан применом метода спектрофотометрије у ултраљубичастој и видљивој области и кондуктометрије на различитим температурама. Константе формирања (K_f) за 1:1 комплекс, Cu(II)–STSC, су израчунате коришћењем података о апсорбацији и моларној проводљивости у функцији различитих односа концентрација ($c_M:c_L$ или $c_L:c_M$) у бинарним растворима. Добијена је нелинерана корелација између промене $\log K_f$ комплекса и састава раствора. Из температурске зависности константи формирања одређени су термодинамички параметри (ΔH , ΔS и ΔG) формирања Cu(II)–STSC комплекса. Добијени резултати показују да природа и састав коришћених раствора утичу на реакција комплексирања.

(Примљено 30. јула, ревидирано 7. новембра, прихваћено 19. новембра 2013)

REFERENCES

1. P. A. Vigato, S. Tamburini, *Coord. Chem. Rev.* **248** (2004) 1717
2. C. T. Barboiu, M. Luca, C. Pop, E. Brewster, E. M. Dinculescu, *Eur. J. Med. Chem.* **31** (1996) 597
3. A. S. M. Al-Shiri, H. M. Abdel-Fattah, *J. Therm. Anal. Calorim.* **71** (2003) 643
4. S. B. Padhye, G. B. Kaffman, *Coord. Chem. Rev.* **63** (1985) 127
5. F. Basuli, S. M. Peng, S. Bhattacharya, *Inorg. Chem.* **36** (1997) 5645
6. A. F. Petrović, V. M. Leovac, B. Ribár, G. Argay, A. Kálmán, *Transition Met. Chem.* **11** (1986) 207
7. S. Purohit, A. P. Koley, L. S. Prasad, P. T. Manoharan, S. Ghosh, *Inorg. Chem.* **28** (1989) 3735
8. A. P. Koley, S. Purohit, L. S. Prasad, P. T. Manoharan, S. Ghosh, *Inorg. Chem.* **31** (1992) 1764
9. R. K. Mahajan, I. Kaur, T. S. Lobana, *Talanta* **59** (2003) 101
10. R. K. Mahajan, I. Kaur, T. S. Lobana, *Indian J. Chem., A* **45** (2006) 639
11. R. K. Mahajan, T. P. S. Walia, Sumanjit, T. S. Lobana, *Talanta* **67** (2005) 755
12. L. S. Sarma, J. R. Kumar, C. J. Kumar, A. V. Reddy, *Anal. Lett.* **36** (2003) 605
13. K. J. Reddy, J. R. Kumar, C. Ramachandraiah, T. Thriveni, A. V. Reddy, *Food Chem.* **101** (2007) 585
14. J. R. Turnlund, W. R. Keyes, H. L. Anderson, L. L. Acord, *Am. J. Clin. Nutr.* **49** (1989) 870
15. M. C. Linder, *Biochemistry of Copper*, Plenum Press, New York, 1991
16. E. A. Enyedy, E. Zsigo, N. V. Nagy, C. R. Kowol, A. Roller, B. K. Keppler, T. Kiss, *Eur. J. Inorg. Chem.* **25** (2012) 4036
17. A. Shokrollahi, M. Ghaedi, H. Ghaedi, *J. Chin. Chem. Soc.* **54** (2007) 933
18. A. Shokrollahi, M. Ghaedi, M. Montazerzohori, A. H. Kainfar, H. Ghaedi, N. Khanjari, S. Noshadi, S. Joybar, *E-J. Chem.* **8** (2011) 495
19. Y. K. Syrkin, M. E. Dyatkina, *Structure of Molecules and the Chemical Bond*, Dover, 1964, p. 127
20. G. E. Papanastasiou, I. I. Zlogas, *J. Chem. Eng. Data* **37** (1992) 167
21. J. Costamagna, L. E. Lillo, B. Matsuhira, M. D. Nosedá, M. Villagran, *Carbohydr. Res.* **338** (2003) 1535
22. S. Sahoo, S. E. Muthu, M. Baral, B. K. Kanungo, *Spectrochim. Acta, A* **63** (2006) 574
23. D. M. Boghaei, M. Gharagozlou, *Spectrochim. Acta, A* **61** (2005) 3061
24. K. Takao, Y. Ikeda, *Inorg. Chem.* **46** (2007) 1550
25. Y. Fang, Z. Sun, *Huaxue Xuebao* **47** (1989) 487 (in Chinese)
26. C. K. Bhaskare, P. P. Hankare, R. S. Rampure, V. B. Mane, *J. Ind. Chem. Soc.* **66** (1989) 215
27. D. Brahman, B. Sinha, *J. Chem. Eng. Data* **56** (2011) 3073
28. J. Lu, H. Guo, X. Zeng, Y. Zhang, P. Zhao, J. Jiang, L. Zang, *J. Inorg. Biochem.* **112** (2012) 39
29. B. Sinha, P. K. Roy, B. K. Sarkar, D. Brahman, M. N. Roy, *J. Chem. Thermodyn.* **42** (2010) 380
30. M. Joshaghani, M. B. Gholivand, F. Ahmadi, *Spectrochim. Acta, A* **70** (2008) 1073
31. H. A. Benesi, J. H. Hildebrand, *J. Am. Chem. Soc.* **71** (1949) 2703
32. B. K. Sarkar, M. N. Roy, B. Sinha, *Indian J. Chem., A* **48** (2009) 63
33. A. J. Sharma, A. I. Popov, *J. Chem. Thermodyn.* **11** (1979) 1145
34. K. M. Tawarah, S. A. Mizyed, *J. Solution Chem.* **18** (1989) 387

35. P. Debye, H. Huckel, *Phys. Z.* **24** (1928) 305
36. V. S. Ijari, A. K. Srivastava, *Eur. J. Inorg. Chem.* (2001) 943
37. V. Gutmann, *The Donor–Acceptor Approach to Molecular Interactions*, Plenum Press, New York, 1978, p. 26
38. A. I. Popov, J. M. Lehn, in *Coordination Chemistry of Macrocyclic Compounds*, G. A. Melson, Ed., Plenum Press, New York, 1979, Ch. 9, p. 557
39. B. O. Strasser, A. I. Popov, *J. Am. Chem. Soc.*, **107** (1985) 7921
40. M. R. Ganjali, A. Rohollahi, A. Monghimi, M. Shamsipur, *Pol. J. Chem.* **70** (1996) 1172
41. Z. Pourghobadi, F. Seyyed-Majidi, M. Daghighi-Asli, F. Parsa, A. Monghimi, M. R. Ganjali, H. Aghabozorg, M. Shamsipur, *Pol. J. Chem.* **74** (2000) 837
42. R. M. Izatt, J. S. Bradshaw, S. A. Nielsen, J. D. Lamb, J. J. Christensen, D. Sen, *Chem. Rev.* **85** (1985) 271
43. R. M. Izatt, K. Pawlak, J. S. Bradshaw, R. L. Bruening, *Chem. Rev.* **91** (1991) 1721
44. G. H. Rounaghi, R. S. Khoshnood, M. H. A. Zavvar, *J. Incl. Phenom. Macrocycl. Chem.* **54** (2006) 247
45. J. Szymańska-Cybulska, E. Kamieńska-Piotrowich, *J. Solution Chem.* **35** (2006) 1631
46. G. Khayatian, S. Shariati, M. Shamsipur, *J. Incl. Phenom. Macrocycl. Chem.* **45** (2003) 117
47. M. Shamsipur, M. Saeidi, *J. Solution. Chem.* **29** (2000) 1187.



J. Serb. Chem. Soc. 79 (5) 579–586 (2014)
JSCS–4609

SHORT COMMUNICATION

Chromatographic analysis of immobilized cefotaxime

DANIELA STIRBET¹, SIMONA-CARMEN LITESCU² and GABRIEL-LUCIAN RADU^{1*}

¹Department of Analytical Chemistry and Environmental Engineering, Faculty of Applied Chemistry and Material Sciences, "Politehnica" University of Bucharest, 1–7 Gheorghe Polizu, District 1, Bucharest-011061, Romania and ²Centre of Bioanalysis, National Institute of Biological Sciences, Bucharest, 296 Splaiul Independentei, District 6, Bucharest-060031, Romania

(Received 21 August 2013, revised and accepted 22 January 2014)

Abstract: The aim of the present work was to widen the application of an in-house developed fast, flexible and sensitive high performance liquid chromatography (HPLC) method to the assessment of cefotaxime sodium from aqueous samples. The method was applied to establish the release profile of cefotaxime sodium immobilised in MCM-41 nanoparticles using pH-controlled release in an aqueous medium. The analytical method proved to be sensitive, repeatable ($RSD < 1.5\%$) and reproducible ($RSD < 1\%$) in the studied concentration range ($0.01\text{--}10\ \mu\text{g}\cdot\text{mL}^{-1}$). The limit of detection and limit of quantification were 0.036 and $0.12\ \mu\text{g}\cdot\text{mL}^{-1}$, respectively, suitable for the analysis of the release of a single active ingredient, and the analysis time was short (10 min).

Keywords: cefotaxime sodium; cephalosporins; controlled release; HPLC.

INTRODUCTION

Cefotaxime sodium (Fig. 1) is a third generation cephalosporin antibiotic that has wide clinical applications for treatment of infections of the respiratory tract, gynaecologic, skin, bone and joint, urinary tract, septicaemia, and documented or suspected meningitis.¹

For the analysis of cefotaxime sodium, several methods have been employed: electrochemical (cyclic voltammetry, square wave voltammetry),^{2–4} spectrofluorimetric and chemiluminescent,^{5,6} and high performance liquid chromatographic methods.^{7,8} Some performance characteristics of methods applied in the determination cefotaxime or its metabolites are presented in Table I.

* Corresponding author. E-mail: gl_radu@chim.upb.ro
doi: 10.2298/JSC130821008S



The aim of this study was the development and application of a sensitive chromatographic method with dual detection (diode array and mass spectrometry, HPLC-DAD-MS) for the determination of cefotaxime immobilized on the mesoporous material MCM-41, which is an ordered mesoporous silicate that displays cylindrical mesopores having a unit cell size of 4.6–4.8 nm. In recent years, it is the most used support for the controlled release of drugs.^{9–14} Cefotaxime sodium was used as the model drug, a dual detection mode being chosen to ensure a better selectivity of the method. According to the British Pharmacopoeia (2009), cefotaxime sodium is an easily degradable antibiotic. Any detectable impurities might affect the efficacy of the bioactive compound (*e.g.*, cefotaxime dimers if present at a sufficient level). Therefore, the employment of MS analysis was justified in order to provide exact information on the nature and form in which the analyte occurred.

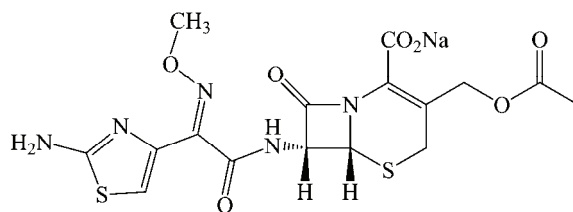


Fig. 1. Chemical structure of cefotaxime sodium.

TABLE I. Comparison between the performance characteristics of previous methods applied in cefotaxime determination

Analyte	Sample matrix	Method	<i>LOD</i> / $\mu\text{g mL}^{-1}$	Reference
Cefotaxime, desacetylcefotaxime,	Ocular aqueous	HPLC	0.08	7
	humour			
Cefotaxime, desacetylcefotaxime,	Plasma	HPLC-UV	0.31	7
Cefotaxime	Plasma	HPLC-UV	1.0	8

EXPERIMENTAL

Chemicals and reagents

The cefotaxime sodium standard (MW 477.5) used in this study was purchased from Sigma-Aldrich (Steinheim, Germany). HPLC grade methanol was from Merck (Darmstadt, Germany). All stock solutions and samples were prepared with ultrapure water.

Instrumentation and procedure

The HPLC analysis was realised on a Shimadzu HPLC system (SCL-10A VP, Kyoto, Japan), consisting of a degasser (DGU-20A5), two pumps (LC-10AD VP) for the delivery of the mobile phase, a thermostatic system (CTO-10AS), and a system controller (SCL – 10A VP). Detection was achieved using a diode array detector (SPD – M20A). A C18 analytical column (150 mm×4.6 mm, 5 μm i.d., Fortis) was used in the analysis. The oven temperature was set at 25 °C. A CyberScan PCD6500 pH/ion/conductivity/DO meter from Eutech Instruments was used for pH measurements of the mobile phase.

A Shimadzu mass spectrometer, model 2010, was employed, using an electro-spray ionization interface, in positive mode. The tuning of the detector was accomplished prior each set of determinations, using an appropriate tuning mixture. The detector settings were ESI (+) CDL temperature 250 °C, nebulizing gas flow 1.5 L min⁻¹, heat block 200 °C.

Chromatographic procedure. The chromatographic analysis was performed in isocratic mode, using as mobile phase a mixture of methanol and water (30:70, V/V), adjusted at pH 4.0 with acetic acid. The flow rate was 0.8 mL min⁻¹. The chromatographic conditions were as follows: the injection volume was 20 µL, column temperature 25 °C, detection was performed at 235 nm and the time of analysis was 10 minutes.

The calibration curve for HPLC-DAD analysis was obtained in a range between 0.01 to 10 µg·mL⁻¹, using the average area from triplicate analysis.

Preparation of the standard solution

A stock standard solution of cefotaxime sodium (2000 µg·mL⁻¹) was prepared in ultrapure water. The solution was kept in the refrigerator to prevent degradation. Working standard solutions were freshly prepared before analysis in water at concentrations ranging from 0.01 to 10 µg·mL⁻¹. Before use, the solutions were filtered through a 0.20 µm filter.

Drug immobilisation

Cefotaxime sodium was immobilised in MCM-41 by mixing 0.32 g of active substance with 0.07 g of MCM-41 in 10 mL of ultrapure water. The mixture was left to settle for 24 h, filtered and dried in a vacuum desiccator for 24 h. The amount of cefotaxime immobilised was 9.19 % (0.098 g, calculated from the difference in initial concentration of cefotaxime solution and final concentration of the supernatant (determined by HPLC)).

Conditions of release

The release profile for cefotaxime immobilized in MCM-41 was adjusted considering the BP releasing tests appropriate for β-lactam antibiotics: 20 mg of the composite (cefotaxime sodium and MCM-41) was mixed with 20 mL of phosphate buffer (to simulate body fluid) at pH 4.80 and kept at a constant mixing rate of 200 rpm. The total release time was 6 h. Samples of 1 mL were collected, centrifuged for 10 min at 9000 rpm, two times, and afterwards the supernatants were filtered through a 0.20 µm PTCE membrane and injected into the HPLC system for analysis.

RESULTS AND DISCUSSIONS

In the present work, the development and partial validation (in terms of linearity, limit of detection, limit of quantification, repeatability and reproducibility) of the HPLC-DAD-MS method was performed and the releasing process of immobilized cefotaxime sodium in mesoporous supports was studied. Different mobile phase compositions were tested and it was found that a mobile phase of methanol:water 30:70 (V/V) (pH 4.00, buffered with acetic acid) resulted in an acceptable resolution (retention times), peak shape (Gaussian) and time of analysis at a column temperature of 25 °C for the studied antibiotic. Various stationary phases were tested, a Fortis C18 analytical column was successfully used being more efficient than a classical silica-based packing. The detection wavelength was 235 nm.

The peak specific for cefotaxime sodium was characterized by a retention time of 4.6 min. A typical chromatogram for the standard compound, obtained under the described optimal experimental conditions, is shown in Fig. 2. The chromatographic peak corresponding to the studied drug eluted at a retention time of 4.6 min and presented a well-shaped Gaussian form, separated from the solvent front. A total analysis time of around 10 min was employed to ensure adequate column equilibration between two subsequent analyses. No significant interfering chromatographic peaks were observed in the HPLC chromatograms during the analysis of cefotaxime sodium samples released from the support nanoparticles. No interferences from the sample solvent or from impurities were observed at the employed detection wavelength.

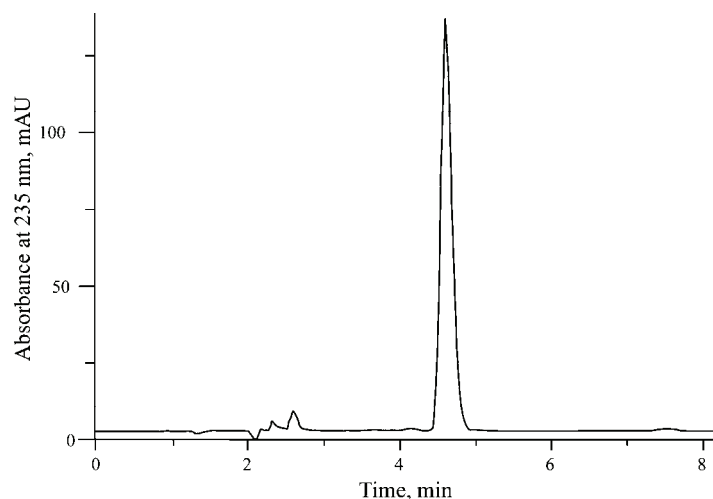


Fig. 2. HPLC-DAD chromatogram for cefotaxime sodium standard ($1 \mu\text{g}\cdot\text{mL}^{-1}$).

Partial validation of the method

The linear response ranged from 0.01 to $10 \mu\text{g}\cdot\text{mL}^{-1}$. The *LOD* and *LOQ* values were calculated from the slope and the standard deviation of a blank signal. For repeatability and reproducibility, every level of concentration was injected three times into the chromatographic system and three injections from three different solutions with the same concentration of standard working solution ($0.5 \mu\text{g}\cdot\text{mL}^{-1}$) were analysed. All results are presented in Table II.

The presence of the studied compound was confirmed by HPLC-DAD-MS analysis. The previously developed and validated method was adjusted to the MS conditions. The column and the mobile phase were the same as those used for the HPLC-DAD analysis. The only adjustment was in the flow rate (0.2 mL min^{-1}), with an analysis time of 10 minutes and injection volume of $10 \mu\text{L}$.

The MS spectrum of cefotaxime sodium is given in Fig. 3.

TABLE II. Several performance characteristics of the HPLC-DAD method applied to cefotaxime sodium determination

Parameter	Reference solution, cefotaxime sodium
Linearity range, $\mu\text{g}\cdot\text{mL}^{-1}$	0.05–10
Retention time, min	4.6
Slope	1443423.72
Intercept	32855.62
Correlation coefficient	0.9988
$LOD / \mu\text{g}\cdot\text{mL}^{-1}$	0.036
$LOQ / \mu\text{g}\cdot\text{mL}^{-1}$	0.12
Repeatability, $RSD / \%$	1.28
Reproducibility, $RSD / \%$	0.70

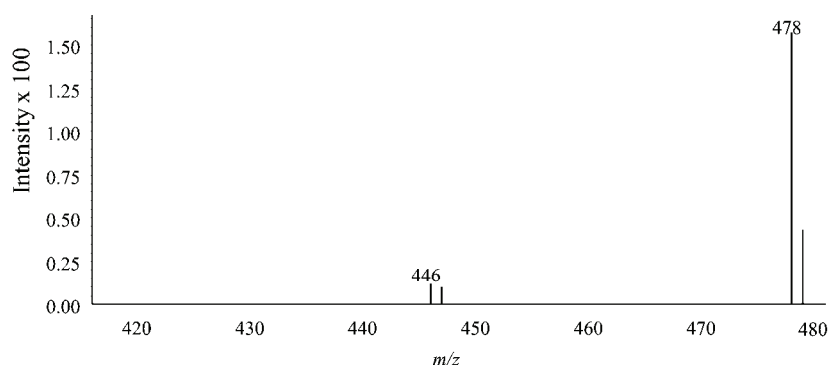


Fig. 3. MS (ESI+) spectrum of cefotaxime sodium.

Application of the HPLC method to the release of cefotaxime sodium

One of the applications of HPLC method is the determination of antibiotics in pharmaceuticals. For this purpose, the release of cefotaxime sodium immobilised in MCM-41 nanoparticles was studied.

The release profile of the biologically active compound from the MCM-41 composite and the corresponding chromatograms are given in Figs. 4 and 5, respectively.

The released cephalosporin was identified using the retention time and the MS spectrum, since the obtained coefficient of variation was appropriate. The observed retention time (4.6 min) enabled the rapid determination of the analyte. The method provides better limits of detection (LOD) and quantification (LOQ) than those of other reported methods (Table I); even compared to those of a method able to discriminate between cefotaxime enantiomers since Wang *et al.* reported the separation and determination of cefotaxime enantiomers in injections by capillary zone electrophoresis with an LOD of $0.5 \mu\text{g mL}^{-1}$.¹⁵

Thus, the method was successfully applied to *in vitro* release of cefotaxime sodium into an aqueous medium of controlled pH.

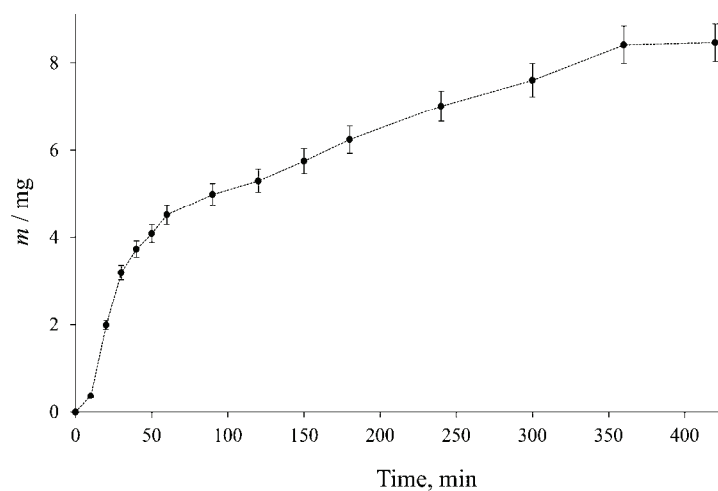


Fig. 4. The release profile of cefotaxime sodium (as adsorbed mass) immobilised in mesoporous silica MCM-41.

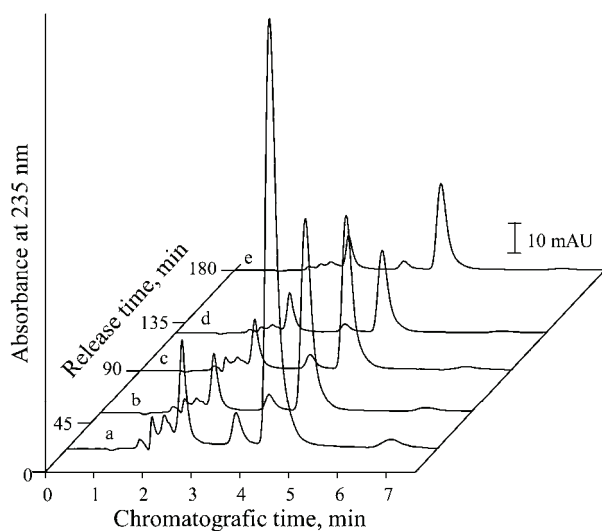


Fig. 5. HPLC-DAD chromatogram for cefotaxime sodium sample at different release times (a – 20 min, b – 50 min, c – 90 min, d – 120 min, e – 180 min).

CONCLUSIONS

An HPLC-DAD method was developed and partially validated, in terms of linearity, limit of detection, limit of quantification, repeatability and reproducibility to determine cefotaxime sodium and then applied to the controlled release of the drug immobilised in mesoporous MCM-41 nanoparticles.

The main improvement of the proposed method with respect to published methods is the increase in sensitivity (with two magnitude folds) of the *LOD* and *LOQ* and also the relatively low cost of the chemicals used.

The proposed chromatographic method is a simple (uses common solvents, and there is no necessity for a particular preparation of the samples, standards or mobile phase) and rapid procedure (the total analysis time is only 10 min and the retention time is short) for the determination of cefotaxime sodium in aqueous samples. Moreover, its application in establishing the release profiles was proved.

Acknowledgements. The work has been funded by the Sectoral Operational Programme Human Resources Development 2007–2013 of the Romanian Ministry of Labour, Family and Social Protection through the financial agreement POSDRU/107/1.5/S/76909. The financial support of the European Commission through European Regional Development Fund and of the Romanian State Budget, Project POSCCE-O2.1.2-2009-2, ID 691, "New mesoporous aluminosilicate materials for controlled release of biologically-active substances" is gratefully acknowledged.

ИЗВОД

ХРОМАТОГРАФСКА АНАЛИЗА ИМОБИЛИСАНОГ ЦЕФОТАКСИМА

DANIELA STIRBET¹, SIMONA-CARMEN LITESCU² и GABRIEL-LUCIAN RADU¹

¹Department of Analytical Chemistry and Environmental Engineering, Faculty of Applied Chemistry and Material Sciences, "Politehnica" University of Bucharest, 1–7 Gheorghe Polizu, District 1, Bucharest-011061, Romania и ²Centre of Bioanalysis, National Institute of Biological Sciences, Bucharest, 296 Splaiul Independentei, District 6, Bucharest-060031, Romania

Циљ овог рада је проширење примене једне, лабораторијски већ развијене, брзе, флексибилне и осетљиве методе високоефикасне течне хроматографије (HPLC), за одређивање натријум-цефотаксима у воденим узорцима. Метода је примењена ради одређивања профила ослобађања натријум-цефотаксима, имобилисаног на МСМ-41 наночестицама, применом рН контролисаног ослобађања у воденој средини. Доказано је да је метода осетљива, са добром поновљивошћу ($RSD < 1,5 \%$) и репродуктивношћу ($RSD < 1 \%$) у испитиваном концентрационом опсегу ($0,01\text{--}10 \mu\text{g}\cdot\text{mL}^{-1}$), са границама детекције и квантификације $0,036$, односно $0,12 \mu\text{g}\cdot\text{mL}^{-1}$, и погодна за анализу ослобађања појединачних активних компоненти са кратким временом анализе (10 min).

(Примљено 21. августа 2013, ревидирано и прихваћено 22. јануара 2014)

REFERENCES

1. F. J. Muhtadi, M. M. A. Hassan, K. Florey, *Analytical Profiles of Drug Substances*, vol. 11, Academic Press, New York, 1982, p. 139
2. P. Nigam, S. Mohan, S. Kundu, R. Prakash, *Talanta* **77** (2009) 1426
3. M. M. Aleksić, V. Kapetanović, *J. Electroanal. Chem.* **593** (2006) 258
4. M. M. Aleksić, V. Kapetanovic, B. Jocić, M. Zecevic, *Talanta* **77** (2008) 131
5. D. Chen, H. Wang, Z. Zhang, L. Ci, X. Zhang, *Spectrochim. Acta, A* **78** (2011) 553
6. M. A. Omar, O. H. Abdelmageed, T. Z. Attia, *Talanta* **77** (2009) 1394
7. H.-J. Kraemer, R. Gehrke, A. Breithaupt, H. Breithaupt, *J. Chromatogr., B* **700** (1997) 147
8. M. T. Rosseel, K. H. Vandewoude, *J. Chromatogr., B* **811** (2004) 159

9. A. Bernardos, E. Aznar, C. Coll, R. Martínez-Mañez, J. M. Barat, M. D. Marcos, F. Sancenón, A. Benito, J. Soto, *J. Controlled Release* **131** (2008) 181
10. M. G. Rimoli, M. R. Rabaioli, D. Melisi, A. Curcio, S. Mondello, R. Mirabelli, E. Abignente, *J. Biomed. Mater. Res., A* **87** (2008) 156
11. G. Wang, A. N. Otuonye, E. A. Blair, K. Denton, Z. A. Tao, A. Tewodros, *J. Solid State Chem.* **182** (2009) 1649
12. I. Ivanovic, L. Zivanovic, M. Zecevic, *J. Chromatogr., A* **1119** (2006) 209
13. M. S. Arayne, N. Sultana, M. Nawaz, *J. Anal. Chem.* **63** (2008) 881
14. A. J. Smith, J. L. Balaam, A. Ward, *Mar. Pollut. Bull.* **54** (2007) 1940
15. R. Wang, Z. P. Jia, J. J. Fan, J. Ma, X. Hua, Q. Zhang, J. Wang, *Pharmazie* **64** (2009) 156.



J. Serb. Chem. Soc. 79 (5) 587–596 (2014)
JSCS–4610

Effect of polar additives on melt electrospinning of non-polar polypropylene

ZHIYUAN CHEN¹, JIANYUN HE¹, FENGWEN ZHAO¹, YUEXING LIU¹,
YONG LIU^{1*} and HUILIN YUAN²

¹College of Mechanical and Electrical Engineering, Beijing University of Chemical Technology, Beijing 100029, China and ²College of Materials Science and Engineering, Beijing University of Chemical Technology, Beijing 100029, China

(Received 2 July, revised 17 November, accepted 3 December 2013)

Abstract: Melt or solution electrospinning are effective and direct techniques for producing nanoscale fibers. Polypropylene (PP) cannot be easily dissolved at ambient temperature. Thus, it is commonly electrospun in the melt state. However, compared with solution electrospun fibers, melt electrospun PP fibers are more uneven and with larger diameters. In this study, to remedy this problem, polar additives, namely stearic acid and sodium stearate, were added into pure PP. The effects of the additives were investigated. The results showed that in contrast to those of pure PP, the fiber diameter of PP with 8 wt. % stearic acid was decreased by 69.3 % (from 5.4 to 1.6 μm). The smallest fiber diameter was 600 nm and the smallest average fiber diameter was 1.8 μm when the sodium stearate contents were 10 and 8 wt. %, respectively. The addition of polar compounds altered not only the diameters of PP microfibers, but also the distribution of diameters, the processing current, and even the thermal properties of the fibers. The microcosmic mechanisms for these changes were interpreted.

Keywords: diameter; microfiber; non-polar polymer; sodium stearate; stearic acid; crystallization.

INTRODUCTION

Electrospinning from polymer solutions or melts are effective and direct techniques for producing nanofibers.^{1–4} Solution electrospinning conducted at ambient temperature is a convenient way to obtain superfine fibers,^{5,6} but not every polymer can be dissolved in an appropriate organic solvent at room temperature. Moreover, the volatility of organic solvents may lead to environmental pollution. A trace amount of organic solvent trapped in a spun polymer will negatively impact the mechanical properties of the resulting fibers.⁷ Without

* Corresponding author. E-mail: yongsd@iccas.ac.cn
doi: 10.2298/JSC130702150Z

polymer solvation, melt electrospinning compared with solution treatment is more environment friendly and highly efficient.^{8–10} However, the development of melt electrospinning is slow because of the high viscosity of the melt, resulting in impaired flow and thick fibers (only a few can attain a thickness of several hundreds of nanometers).¹¹

To decrease the viscosity and obtain small-diameter fibers, two ways have been attempted. The first was to change the conditions^{12–16} of the melt electrospinning, such as the voltage, melt temperature, receiving distance, *etc.* The second was to change the polymer content, for instance the addition of a plasticizer,¹² or decreasing the molecular weight of the polymer,⁵ *etc.* Malakhov *et al.*¹⁷ used sodium stearate and oleate as additives to reduce the viscosity of polyamide 6 melt in electrospinning. They found that the addition of 10 wt. % additive decreased the average diameter of the fibers 40-fold because of the 60-fold decrease in the viscosity of the melt. Polyamide 6, sodium stearate and oleate are polar materials, so strong interactions exist among these molecules. Thus, using a polar additive is effective. However, non-polar polymers, such as polypropylene (PP), polyethylene, polybutadiene, polystyrene, *etc.*, are very common in the fiber industry. Thus, whether a polar additive could also affect a non-polar polymer in melt electrospinning should be determined. □

A self-made melt electrospinning system^{18–20} was used to spin PP fibers, which can be used in many fields, such as in filtration or clothing. Polar stearic acid or sodium stearate was added into the PP.^{21–23} The detailed effects of polar additives on PP fiber diameter and other properties were studied.

EXPERIMENTAL

Materials

PP (iPP) was obtained from Shanghai Expert in the Developing of New Material Co., China. The melt flow index of the PP was 1500 g/10 min. Stearic acid and sodium stearate were purchased from Xilong Chemical Co., China. Stearic acid, with relative molecular mass of 284.48, is a short chain polymer. Sodium stearate, with relative molecular mass of 306.46, is an organic salt. All reagents were used as received without any further treatment.

Electrospinning equipment

A homemade electrospinning device, consisting of a heating system, a high-voltage supply device, and a collector, was used.^{18–20} The collector was a square aluminum plate with edge length of 20 cm. The high-voltage supply device, purchased from Tianjin High Voltage Power Supply Plant, China, provided a maximum voltage output of 100 kV and a maximum current output of 2 mA. The electrical heating ring covering the cylinder was custom built with a power of 300 W. A piston controlled the flow rate of the polymer melt.

Preparation of the electrospinning materials

Nine PP samples containing 0, 6, 8, 10 and 12 wt. % stearic acid, as well as 6, 8, 10 and 12 wt. % sodium stearate, were prepared. To ensure that the stearic acid or sodium stearate was mixed uniformly with the pure PP, every sample was extruded using a miniature extruder (DYNISCO, LME-230, USA). The screw and die head temperatures were 145 and 140 °C,

respectively. The screw speed was 30 rpm, and each sample had a mass of 0.5 g. Then, each sample was broken down into fine powders in a mill. The PP samples containing stearic acid or sodium stearate were considered as composites, while the pure PP sample was denoted as PP.

Electrospinning

The temperatures of the top and low electrical heating rings were set to 180 and 220°C, respectively. The distance between the spinneret head and the collecting plate was 10 cm. The samples were added into the cylinder individually. When the device reached the set temperature, it was maintained for 10 min. Subsequently, the piston weight was adjusted to control the quantity of the melt flow. When PP or its composite melts had uniformly covered the whole spray head, the high-voltage supply device was switched on and the voltage adjusted to approximately 37 kV.

Characterization

The diameters of the electrospun fibers were measured by scanning electron microscopy (SEM, Hitachi S4700). The fiber samples were coated with a 10 nm layer of platinum before observation. The scanning voltage was 20 kV. The average fiber diameters and their standard deviation (*SD*) were calculated from 100 fibers of one sample using software Image J 1.44P (National Institutes of Health, USA). The thermal transition of the PP was examined using differential scanning calorimetry (DSC, Perkin Elmer Pyris1) to discuss the crystallization of PP. Fiber samples (3 mg) were loaded into the DSC pan. The scanned temperature range was from 25 to 300 °C, at a heating rate of 10 °C min⁻¹. The FT-IR measurements were realized over the wavenumber range 4000–400 cm⁻¹, using 32 scans at a resolution of 1 cm⁻¹, employing a Nicolet Avatar 320 FT-IR spectrometer.

RESULTS AND DISCUSSION

Effect of polar additives on the electrospinning current

The polar additive is easily polarized under a strong electrical field. Thus, the addition of a polar material in PP will result in a fundamental change in the electrospinning process. During the experiment, the current of the high-voltage generator was recorded when PP or its composites with different stearic acid contents were spun. Under the same spinning conditions, the current first increased with increasing stearic acid content, which illustrates that the polarized electron cloud of stearic acid increased the charge of the fibers containing additives (Fig. 1). However, the current decreased when the stearic acid content was increased from 10 to 12 wt. %. The explanation of this phenomenon is shown schematically in Fig. 2. Although the amount of tiny stearic acid particles in the surface layer of thick fibers is equal to or slightly higher than those in the surface layer of thin fibers, the charge density per surface area of the thick fibers is lower. Moreover, when the stearic acid content reached 12 wt. %, more stearic acid molecules probably aggregated to form larger domain phases while fewer molecules were dispersed in the PP melt phase. The stearic acid could not be uniformly distributed in the PP phase, which led to a discontinuous distribution that decreased the number of charges in a fiber unit. Hence, the current was lower when the stearic acid was 12 wt. % compared with that at 10 wt. %.

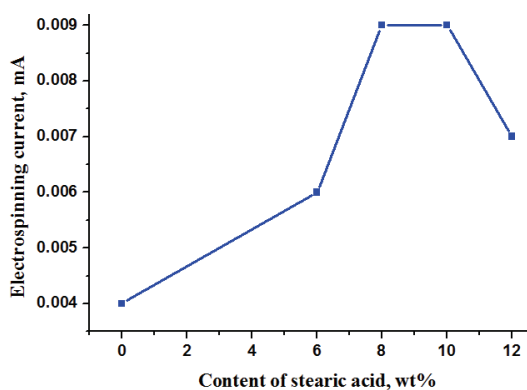


Fig. 1. Changes in the electrospinning current of PP containing different contents of stearic acid.

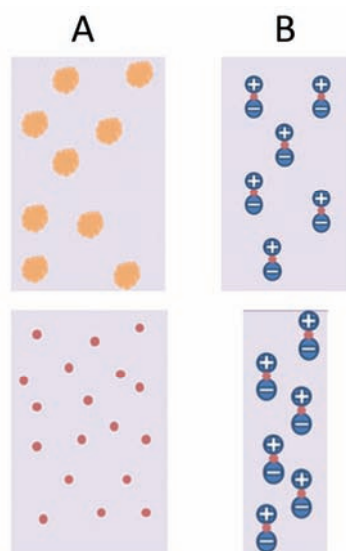


Fig. 2. Mimic diagrams of different PP fibers containing additives. The dark rectangles represent fibers. A shows the PP fibers with sodium stearate (irregular particles) (upper) and with stearic acid (points) (lower). B shows the PP fibers with stearic acid (dipole) electrospun at low (upper) and high (lower) voltages.

Effect of polar additive on the fiber diameters

The polar additive apparently affects the fiber diameters of PP. The SEM images of PP with different contents of polar additive are illustrated in Fig. 3 and the statistical data are listed in Table I. The average fiber diameter of the PP composite initially decreased with increasing stearic acid or sodium stearate content (Fig. 4 and Table I). When stearic acid content was 8 wt. %, the minimum diameter was 1.65 μm , but the *SD* was not the smallest. The minimum *SD* appeared at 10 wt. % stearic acid. However, the average diameter increased when the content exceeded 10 wt. %.

The possible reason for the variations in the diameters is the presence of the carboxyl group in the stearic acid molecule. Under a high electric field, the electron cloud of the carboxyl oxygen double bond and the carboxyl oxygen single

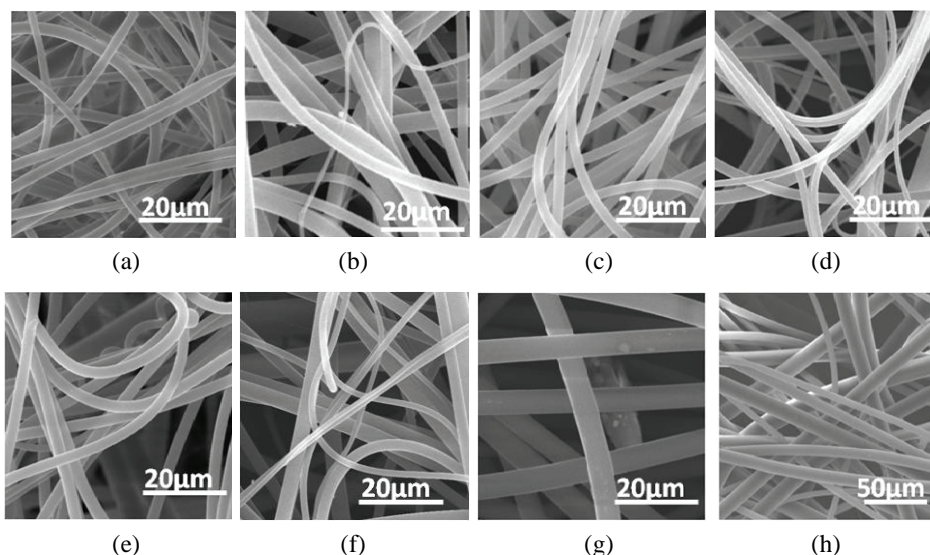


Fig. 3. SEM images of PP fibers containing different contents of additive, electrospun at 220 °C, 10 cm spinning distance, and 30 kV. a) 6 wt. % stearic acid; b) 6 wt. % sodium stearate; c) 8 wt. % stearic acid; d) 8 wt. % sodium stearate; e) 10 wt. % stearic acid; f) 10 wt. % sodium stearate; g) 12 wt. % stearic acid; h) without additives.

TABLE I. Statistical data of diameters of PP fibers containing different additive contents (*AVG*: average diameter, *SDEV*: standard values of deviation, *MIN*: minimum value)

Parameter	6 wt. % stearic acid	6 wt. % sodium stearate	8 wt. % stearic acid	8 wt. % sodium stearate	10 wt. % stearic acid	10 wt. % sodium stearate	12 wt. % stearic acid	Without additives
<i>AVG</i> / μm	2.1	2.4	1.6	1.8	2.1	2.2	4.9	5.4
<i>SDEV</i>	0.2	0.7	0.1	0.8	0.1	2.2	0.2	1.7
<i>MIN</i> / μm	1.7	0.9	1.3	0.8	2.0	0.6	4.5	3.0

bond is easily changed and polarized. Then, the polymer chains connected, entangled or wrapped with stearic acid will bear a strong electric field force. Moreover, stearic acid can plastify PP. With the increase in stearic acid content, the PP composite melt suffered more force from the electric field. Under a high tensile force, the diameter of the PP microfibers that formed at the end of the Taylor cone was small. However, when the stearic acid content was increased to 12 wt. %, the fiber diameter became thick again, reaching 4.8 μm . This condition may have been caused by the increased formation of tiny phases of stearic acid molecules, with low molecule dispersal in the PP melt phase, when stearic acid content reached 12 wt. %. Therefore, the continuous stearic acid phase moved very easily and the PP melt phase became more viscous, resulting in a second increase in the fiber diameter.

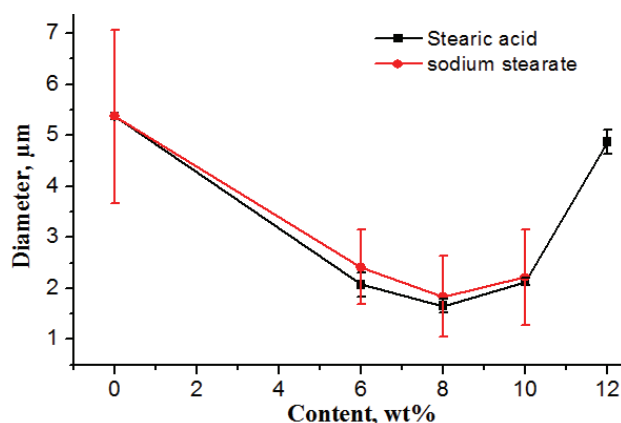


Fig. 4. Changes in the average diameter of PP fibers containing additives at different contents of stearic acid and sodium stearate.

The minimum fiber diameter of PP with sodium stearate was significantly smaller than that achieved with stearic acid (Fig. 4 and Table I), probably because sodium stearate is a salt. Salts can be easily ionized in an electric field. The positive and negative ions move to opposite ends and then produce an electric force along the direction of the electric field. For the stearic acid under a strong electric field, only a shift in the electron cloud occurs, and the polarization is much smaller than that obtained with sodium stearate. The force from the electron movement is significantly greater than the force from the electron cloud shift. Thus, the fiber diameters of the PP composites containing sodium stearate were smaller than those containing stearic acid. However, the diameter distributions of the PP with sodium stearate were extremely inhomogeneous compared with those containing stearate acid. This condition may have been because sodium stearate is a hydrophilic salt, which has no plastification effect on the organic PP melt. Stearic acid as an organic material can be evenly distributed in the PP melt and had an apparent plastification effect on the melt. This phenomenon resulted in the presence of both thick and thin fibers from the PP with sodium stearate, which led to uneven diameter distributions.

Effect of polar additive on the diameter distribution of PP fibers

The effect of polar additive on the fiber diameter distribution varied with the additive content. The diameter distribution of PP fibers containing different amounts of stearic acid is shown in Fig. 5. The PP (0 wt. % stearic acid) showed a broad and multiple peak distribution of the fiber diameters. The distribution peak generally shifted to the large diameter side with increasing stearic acid content, but the distribution remained at the small fiber diameter side when the stearic acid content was at 6 wt. %. The average diameter of the PP fibers with

8 wt. % stearic acid was 1.6 μm , which was smaller than that (2.1 μm) of the PP fibers with 10 wt. % stearic acid, but had a larger *SD* (Table I and Fig. 4). The data from Table I agree well with those of Fig. 5. The fiber diameters of PP with 8 wt. % stearic acid had a distribution range from 1.0 and 1.75 μm . A bimodal fiber diameter distribution was visible on the curve. However, the fiber diameters of PP with 10 wt. % stearic acid had a distribution range from 2.0 to 2.25 μm with one major peak. Thus, the diameter distribution of PP with 8 wt. % stearic acid was broader than that with 10 wt. % stearic acid, but both composites had narrower diameter distributions than that of PP.

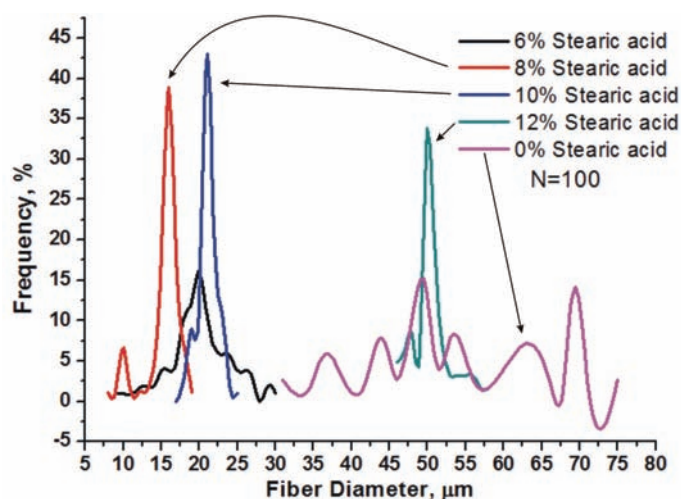


Fig. 5. Diameter distribution of PP fibers containing different contents of stearic acid. $N = 100$ indicates 100 fibers from each photomicrograph measured.

Effect of the polar additives on fiber crystallization

The degree of crystallinity is very important for the performance of fibers. DSC was used to check the thermal properties of the fibers. The thermal analysis curves of PP powder, PP fibers, and microfibers of PP with 10 wt. % stearic acid are shown in Fig. 6. PP had the maximum melting peak, as shown by the thermogram. The peak shifted to a low temperature and its magnitude was decreased after the PP had been electrospun. The smallest peak value and the lowest temperature were exhibited by the PP fibers with 10 wt. % stearic acid. A cold crystallization peak was found on the curves of the PP fiber and the PP fibers containing additives, indicating that crystallization in the two types of fibers was complete. The size of the melting peak reflects the degree of crystallinity. The decrease in the melting peak of electrospun microfibers, as well as the appearance of cold crystallization, showed the decrease in PP crystallinity. PP is a slow crystallizing polymer, and its crystallization needs sufficient time. As the

electrospinning process is very fast, the PP melt jet did not have sufficient time to crystallize before falling on the collection plate and cooling quickly. On the other hand, the fluidity of the PP melt increased for two reasons, one is the plastication effect of stearic acid and another is the movement of the electron cloud of stearic acid that increased the force on the PP melt in the electric field. The faster is the flow, the shorter is the time to crystallize. Hence, the degree of crystallinity of PP with stearic acid was the smallest and its crystallization was the most imperfect, as evidenced by the minimal height of the melting peak.

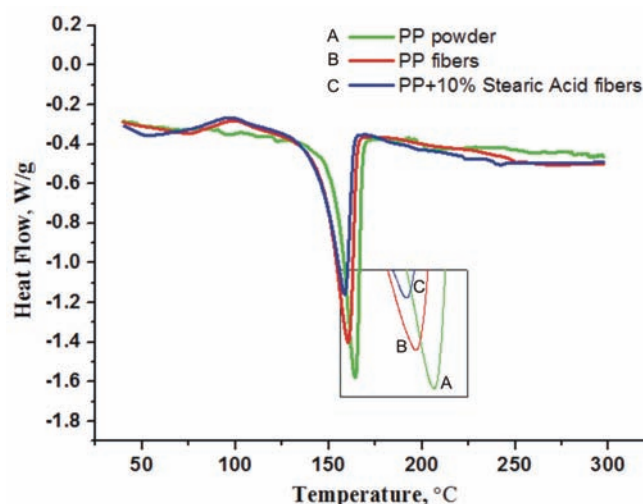


Fig. 6. DSC thermograms of PP powder, PP fibers, and PP fibers containing 10 wt. % stearic acid. The inset is the enlarged tip area of the main curves.

Effect of polar additive on the structure of the fibers

To gain some insight into the change in chemical structure of PP accompanying electrospinning, IR spectroscopy was conducted on the PP before and after spinning. The results are shown in Fig. 7 for the PP powder, PP fibers containing 10 wt. % stearic acid and PP fibers. The representative bands can be assigned as follows: the intense bands extending from 1350 to 1470 cm^{-1} are super-positions of alkanes, $\nu_{\text{C-H}}$. The bands extending between 2500 and 3000 cm^{-1} mainly resulted from different stretch vibrations of C-H bands ($-\text{CH}_3$ and $-\text{CH}_2$). The peak at 1709 cm^{-1} can be assigned to $\nu_{\text{C=O}}$ of a carboxylic acids. As seen in Fig. 7 (curves A and C), no appreciable difference could be observed in the IR spectra between the virgin powder and the PP fibers, except for the change of 2361 cm^{-1} that arises from CO_2 absorbed by the fibers. Comparing the IR spectra of Fig. 7B and C, one new peak appeared at 1709 cm^{-1} , corresponding to $\nu_{\text{C=O}}$. This phenomenon can be attributed to the stearic acid. No other chemical changes were apparent. Hence, the polar additive did not change the structure of the fibers.

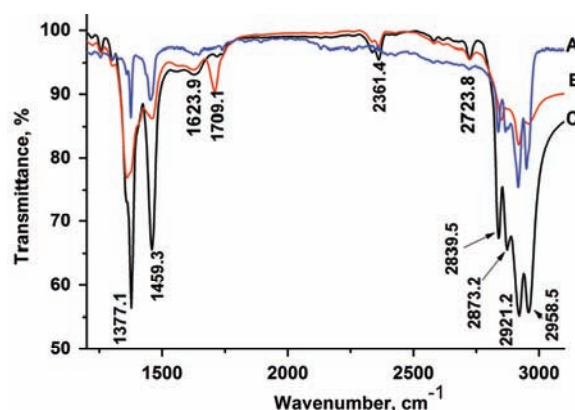


Fig. 7. FT-IR spectra of: A) PP powder; B) fibers of PP containing 10 wt. % stearic acid; C) PP fibers.

CONCLUSIONS

In summary, stearic acid and sodium stearate are promising additives for decreasing the fiber diameter and the diameter distribution in the electrospinning of PP because of their polarity and plastification effect. The smallest fiber diameter was 600 nm and the smallest average fiber diameter was 1.8 μm when the sodium stearate content was 10 and 8 wt. %, respectively. The narrowest diameter distribution appears when the stearic acid content was 10 wt. %. Both additives can reduce the fiber diameter and diameter distribution when compared to the fibers from neat PP.

The crystallinity of resulting PP fibers containing additives was smaller than those of PP and electrospun PP fibers, indicating that the addition of polar compounds in PP can alter not only the diameter of resulting fibers, but also the thermal property and microstructure.

Acknowledgement. The authors would like to thank Professor Xiaozhen Yang and Delu Zhao of Institute of Chemistry, Chinese Academy of Science (ICCAS); Professor Ping Hu, Xiaogong Wang of Tsinghua University, China, for their valuable discussions. The paper was financially supported by the National Natural Science Foundations of China (Grant No. 21374008).

ИЗВОД

УТИЦАЈ ПОЛАРНИХ АДТИВА НА ПРОЦЕС ИЗРАДЕ НЕПОЛАРНИХ ПОЛИПРОПИЛЕНСКИХ ВЛАКАНА ЕЛЕКТРОСПИНИНГОМ ИЗ РАСТОПА

ZHIYUAN CHEN¹, JIANYUN HE¹, FENGWEN ZHAO¹, YUEXING LIU¹, YONG LIU¹ и HUILIN YUAN²

¹College of Mechanical and Electrical Engineering, Beijing University of Chemical Technology, Beijing 100029, China и ²College of Materials Science and Engineering, Beijing University of Chemical Technology, Beijing 100029, China

Полимерна влакна нанометарских димензија могу се добити електроспинингом из раствора или растопа, који је веома ефикасан и директан поступак. Како је поли(про-

пилен) (PP) тешко растваран на собној температури, његова влакна се израђују електро-спинингом из растопа. Међутим, у поређењу са влакнима добијеним електро-спинингом из раствора, PP влакна из растопа су неуједначених димензија и већих пречника. Да би се побољшао поступак прераде из растопа, неполарном PP се додају поларни адитиви, као што су стеаринска киселина и натријум-стеарат. Утицај додатка поларних адитива на процес израде PP влакана електро-спинингом из растопа је приказан у овом раду. Резултати су показали да у поређењу са полазним PP влакнима, пречници влакана PP са 8 мас. % стеаринске киселине су смањени за 69,3 % (од 5,4 до 1,6 μm). Најмањи пречник влакана од 600 nm је добијен у присуству 10 мас. % натријум-стеарата у полимерној матрици, док је најмањи средњи пречник влакана износио 1,8 μm при садржају од 8 мас. %. Додатак поларних једињења утиче не само на пречник PP микровлакна, већ и на расподелу величина влакана, јачину струје при преради, као и на термичка својства добијених влакана. У раду је предложен механизам деловања поларних адитива на поступак израде PP микровлакна.

(Примљено 2. јула, ревидирано, 17. новембра, прихваћено 3. децембра 2013)

REFERENCES

1. L. Lu, D. Wu, M. Zhang, W. Zhou, *Ind. Eng. Chem. Res.* **51** (2012) 3682
2. Y. E. Miao, G. N. Zhu, H. Hou, Y. Y. Xia, T. Liu, *J. Power Sources* **226** (2013) 82
3. R. F. Service, *Science* **328** (2010) 304
4. F. Zhang, B. Zuo, Z. Fan, Z. Xie, Q. Lu, X. Zhang, D. L. Kaplan, *Biomacromolecules* **13** (2012) 798
5. N. Bhardwaj, S. C. Kundu, *Biotechnol. Adv.* **28** (2010) 325
6. M. Xue, F. Li, Y. Wang, X. Cai, F. Pan, J. Chen, *Nanoscale* **5** (2013) 1803
7. S. Agarwal, A. Greiner, *Polym. Adv. Technol.* **22** (2011) 372
8. D. W. Hutmacher, P. D. Dalton, *Chem. Asian J.* **6** (2011) 44
9. D. Cho, H. J. Zhou, Y. Cho, D. Audus, Y. L. Joo, *Polymer* **51** (2010) 6005
10. E. Basturk, M. V. Kahraman, *Polym. Compos.* **33** (2012) 829
11. N. Bhardwaj, S. C. Kundu, *Biotechnol. Adv.* **28** (2010) 325
12. N. Ogata, S. Yamaguchi, N. Shimada, G. Lu, T. Iwata, K. Nakane, T. Ogihara, *J. Appl. Polym. Sci.* **104** (2007) 1368
13. S. Tian, N. Ogata, N. Shimada, K. Nakane, T. Ogihara, M. Yu, *J. Appl. Polym. Sci.* **113** (2009) 1282
14. P. D. Dalton, D. Grafahrend, K. Klinkhammer, D. Klee, M. Moeller, *Polymer* **48** (2007) 6823
15. N. Detta, T. D. Brown, F. K. Edin, K. Albrecht, F. Chiellini, E. Chiellini, P. D. Dalton, D. W. Hutmacher, *Polym. Int.* **59** (2010) 1558
16. E. Zhmayev, D. Cho, Y. L. Joo, *Polymer* **51** (2010) 4140
17. S. N. Malakhov, A. Y. Khomenko, S. I. Belousov, A. M. Prazdnichnyi, S. N. Chvalun, A. D. Shepelev, A. K. Budyka, *Fibre Chem.* **41** (2009) 355
18. Y. Liu, R. J. Deng, M. F. Hao, H. Yan, W. M. Yang, *Polym. Eng. Sci.* **50** (2010) 2074
19. Y. Liu, F. Zhao, C. Zhang, J. Zhang, W. M. Yang, *J. Serb. Chem. Soc.* **77** (2012) 1071
20. F. Zhao, Y. Liu, H. Yuan, W. M. Yang, *J. Appl. Polym. Sci.* **125** (2012) 2652
21. D. Binias, W. Binias, J. Broda, *J. Appl. Polym. Sci.* **125** (2012) 1020
22. S. Sengupta, P. Maity, D. Ray, A. Mukhopadhyay, *J. Appl. Polym. Sci.* **130** (2013) 1996
23. N. Kiattipanich, N. Kreua-ongarjnukool, T. Pongpayoon, C. Phalakornkule, *J. Polym. Eng.* **27** (2011) 411.



J. Serb. Chem. Soc. 79 (5) 597–612 (2014)
JSCS–4611

The use of biological markers in the determination of the origin and type of organic matter in the sediments of the Tisza River

SNEŽANA ŠTRBAC¹, GORDANA GAJICA^{2#}, ALEKSANDRA ŠAJNOVIĆ^{2#},
NEBOJŠA VASIĆ³, KSENIJA STOJANOVIĆ^{4**} and BRANIMIR JOVANČIĆEVIĆ^{4#}

¹Faculty of Environmental Protection, University EDUCONS, Vojvode Putnika 87, 21207 Sremska Kamenica, Serbia, ²University of Belgrade, ICTM, Center of Chemistry, Njegoševa 12, 11000 Belgrade, Serbia, ³University of Belgrade, Faculty of Mining and Geology, Džušina 7, 1100 Belgrade, Serbia and ⁴University of Belgrade, Faculty of Chemistry, Studentski trg 12–16, 11000 Belgrade, Serbia

(Received 14 June, revised 28 August, accepted 29 August 2013)

Abstract: The objective of this study was to determine the origin and type of organic matter (OM) in recent sediments of the Tisza River, along a distance of 153 km through the territory of Serbia. For this purpose, group organic–geochemical parameters and biomarker compositions were used. All samples contained approximately same amount of OM, which was deposited under uniform, slightly reducing conditions. Based on the distribution of *n*-alkanes, the origin and type of OM could not be precisely estimated. However, the *n*-alkane patterns suggest the presence of immature singenetic organic matter of terrestrial origin. The distributions of terpanes and steranes and the values of the corresponding maturity parameters indicate that the Tisza River sediments, apart from immature singenetic organic matter, contain oil pollutants of anthropogenic origin. The identical compositions of these biomarkers in all samples confirmed that the recent sediments of the Tisza River, from Kanjiža Town to the confluence into the Danube River, contain the same type of oil pollutants. Based on the compositions of terpanes and steranes and the values of the biomarker parameters in Tisza sediments, it is supposed that the oil pollution generally could be related to heavy fuel oil from tankers, due to intense river transport and, to lower extent, to crude oils from the Elemir and Rusanda oil fields.

Keywords: sediments; Tisza River; organic matter; biomarkers; oil pollutants.

INTRODUCTION

Biological markers (biomarkers) in bitumen (soluble organic matter extracted from sediments, coals, oil shales and source rocks) and oil are complex organic

* Corresponding author. E-mail: ksenija@chem.bg.ac.rs; xenasyu@yahoo.com

Serbian Chemical Society member.

doi: 10.2298/JSC130614087S

compounds with a strong resemblance in structure to their parent organic molecules in living organisms. In organic geochemistry, they are extensively used to estimate the origin of sedimentary organic matter (OM) and its geological evolution.¹ In other words, based on the presence, abundance and distribution of respective biomarkers in oils, the origin, depositional environment and maturity of the organic matter, as well as the relative length of migration pathways and the degree of biodegradation could be assessed.² For this purpose, numerous biomarkers, *n*-alkanes, isoprenoid aliphatic alkanes, polycyclic alkanes of the sterane and terpane types and alkylaromatics have been used. Recently, the application of biological markers in environmental chemistry has proved its self to be a promising tool for the determination and identification of petroleum pollutants in soils, recent sediments, ground and surface waters.^{3,4} The content of singenic organic matter in recent sediments varies over a wide range from 0 to 80 %² and therefore can not be used as an indicator of the origin of organic matter. For this reason, biomarker fingerprints typical for crude oils, as highly mature organic matter, can be useful in evaluating whether the organic matter extracted from the environment, is singenic or it represents anthropogenic organic matter of petroleum origin. This primarily refers to *n*-alkanes. In crude oils, *n*-alkanes have uniform distribution of odd and even homologues (the Carbon Preference Index, *CPI*, is about 1), usually in the range of C₁₀–C₃₅. An *n*-alkane distribution with a strong predominance of lower homologues C₁₂–C₂₂ indicates algal organic matter input and/or high maturity.¹ On the other hand, elevated concentrations of odd long-chain homologues (C₂₅–C₃₃) show that terrestrial OM also contributed to the precursor biomass.^{5,6} It should be noticed that oil derivatives, such as gasoline and diesel, have different *n*-alkane distributions, which range from *n*-C₆ to *n*-C₁₂, and *n*-C₁₂ to *n*-C₂₅, respectively. Moreover, these derivatives do not contain polycyclic biomarkers of the sterane and terpane types.^{7,8}

Similarly to *n*-alkanes, the distributions of polycyclic alkanes (C₂₁–C₂₂ and C₂₇–C₃₀ diasteranes and steranes, C₁₉–C₂₇ tricyclic diterpenes and C₂₇–C₃₅ pentacyclic triterpenes) in oils are distinctive and noticeably different from those observed in bitumen of recent sediments, due to their higher maturity.^{1,9} However, different crude oils show unequal distributions of biomarkers. Each oil is characterized by a distinctive distribution of biomarkers as a kind of “fingerprint”, which depends on the origin, depositional environment, age, maturity, relative length of migration and mineral composition of the source and reservoir rocks.^{10,11} This feature of oil can be very useful in environmental chemistry for the determination of the source of pollution. Consequently, analyses of this type obtain a forensic character.

In this paper, the surface sediments of the Tisza River, in the part of river flow from Kanjiža Town to its confluence into the Danube, were investigated. Considering the navigable character of the Tisa River, and thus its exposure to

anthropogenic impact, an investigation of the origin and type of organic matter in its sediments was the defined objective of this study. For this purpose, group organic–geochemical data and biomarker compositions were used.

EXPERIMENTAL

A total of 10 sediment samples were collected from 9 sites along the Tisza River on the territory of Serbia (Fig. 1; Table I). These sites are located near Kanjiža Town (entrance area of the River from Hungary to Serbia) up to its confluence into the Danube. The length of this river section is 153 km and it covers almost the entire length of the Tisza River through the territory of Serbia. The sediments consist of sand, silt and clay. Silt is predominant, with the exception of two samples (M22 and M9), in which sand is the most prominent (Table I).

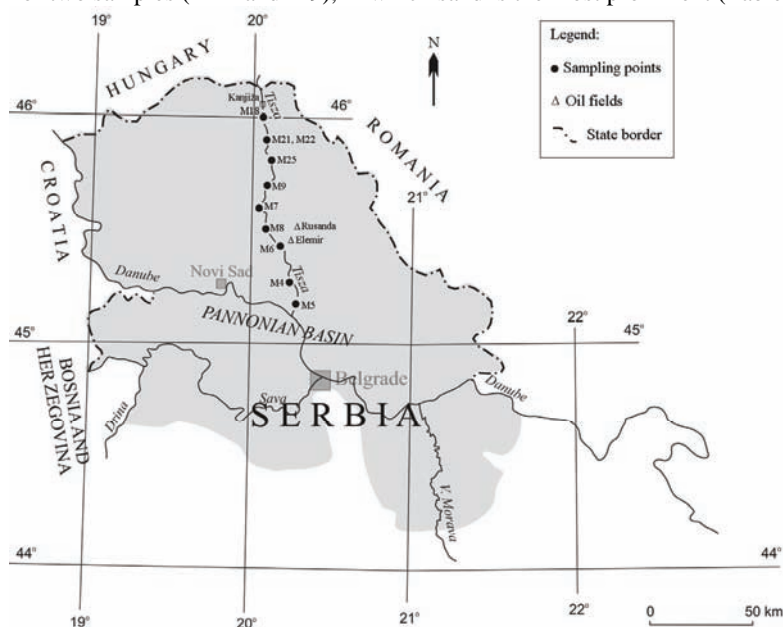


Fig. 1. Map showing the sampling points.

TABLE I. List of the investigated samples

Sample	Distance from confluence into the Danube River, km	Depth interval cm	Lithology		
			Sand, %	Silt, %	Clay, %
M18	153	20	25	52	23
M21	136	0–10	29	50	21
M22	136	0–10	47	41	12
M25	123	0–10	20	55	25
M9	88	20	54	33	13
M7	60	20	28	53	19
M8	50	20	28	52	20
M6	12	0–5	3	65	32
M4	8	0–10	16	57	27
M5	6	20	36	41	23

Samples from the sediment top layer (0–20 cm) were collected using a plastic corer and transported to laboratory in polyethylene bags. The sediment samples were wet-sieved through a 63 μm sieve and then air dried at room temperature. The dried samples were gently pounded in a porcelain mortar. Subsequently, the samples were split into smaller aliquots by coning and quartering.

Elemental analysis was performed to determine the contents of total organic carbon (C_{org}), sulphur and nitrogen. The total organic carbon content was determined after removal of carbonates with 1:3 diluted hydrochloric acid. The measurements were realized using a Vario EL III, CHNS/O elemental analyzer, Elementar Analysensysteme GmbH.

Soluble organic matter (bitumen) was extracted (36 h) from pulverized samples using a Soxhlet apparatus with an azeotropic mixture of CH_2Cl_2 and CH_3OH and quantified.

The bitumen extracts and crude oils were separated into saturated, aromatic and NSO fractions using column chromatography over silica gel. The saturated hydrocarbon fraction was eluted with *n*-hexane, aromatic hydrocarbons with mixture of *n*-hexane and dichloromethane (4:1 volume ratio) and the NSO fractions (polar fraction, which contains nitrogen, sulphur, and oxygen compounds) with mixture of dichloromethane and methanol (1:1 volume ratio).

The saturated hydrocarbons were analyzed by gas chromatography–mass spectrometry (GC–MS). A gas chromatograph Agilent 7890A GC (H5-MS capillary column, 30 $\text{m} \times 0.25$ mm, He carrier gas 1.5 $\text{cm}^3 \text{min}^{-1}$, FID) coupled to an Agilent 5975C mass selective detector (70 eV) was used. The column was heated from 80 to 310 $^\circ\text{C}$, at a rate of 2 $^\circ\text{C} \text{min}^{-1}$, and the final temperature of 310 $^\circ\text{C}$ was maintained for an additional 25 min. Detailed analyses of the target compounds were conducted using the following ion chromatograms: $m/z = 71$ (*n*-alkanes and isoprenoids), $m/z = 191$ (terpanes) and $m/z = 217$ (steranes). The individual peaks were identified by comparison with literature data¹² and based on the total mass spectra (library: NIST5a). The biomarker parameters were calculated from the GC–MS chromatogram peak areas (software GCMS Data Analysis).

RESULTS AND DISCUSSION

Group organic–geochemical parameters

The amount of the total organic carbon (C_{org}) and soluble organic matter (bitumen) in the surface sediments of the Tisa River, from the most upstream analyzed point near Kanjiža Town down to its confluence into the Danube River are given in Table II.

The results indicate that in the relatively long part of the river flow (153 km), the contents of the total organic carbon (C_{org} 0.85–1.66 %) and soluble organic matter (bitumen 0.07–0.14 %) in the surface sediments remained approximately uniform. Based on the predefined quantities, it could not be assessed whether it was singenetic organic matter, or polluting matter of anthropogenic origin. The soluble organic matter was mainly represented by polar, NSO compounds (87–93 %). The relative contents of saturated and aromatic hydrocarbons were low, which is in accordance with the low maturity of the surface sedimentary organic matter (Table II). The contents of nitrogen and sulphur were also relatively uniform. The content of sulphur did not exceed 0.1 %, indicating that pollution with sulphur compounds could be discounted.

TABLE II. Group organic–geochemical parameters; C_{org} – total organic carbon content; db – dry basis; HC – hydrocarbons; NSO – polar compounds containing nitrogen, sulphur and oxygen

Sample	Content of						
	C _{org} , % db	N, % db	S, % db	Bitumen, %	Saturated HC, %	Aromatic HC, %	NSO, %
M18	1.23	0.10	<0.1	0.08	5.9	5.1	89.0
M21	0.85	0.07	<0.1	0.07	5.3	2.7	92.0
M22	0.96	0.07	<0.1	0.14	6.6	7.6	85.8
M25	1.19	0.10	0.1	0.09	4.0	2.9	93.1
M9	1.3	0.11	<0.1	0.11	6.9	1.7	91.4
M7	1.18	0.09	<0.1	0.11	6.1	3.4	90.5
M8	1.13	0.08	<0.1	0.07	6.5	6.2	87.3
M6	1.29	0.10	<0.1	0.11	6.9	3.4	89.7
M4	1.66	0.13	<0.1	0.08	3.3	3.7	93.0
M5	1.36	0.09	<0.1	0.09	3.6	4.6	91.8

Molecular composition of the organic matter

n-Alkanes and isoprenoids. All samples showed very similar distributions of *n*-alkanes and isoprenoids. The *n*-alkanes were identified in the range C₁₆ to C₃₅, with a maximum at *n*-C₂₇ or *n*-C₂₉ (Fig. 2).

The mass chromatograms (*m/z* 71) of the saturated fraction showed two distinct parts. The lower *n*-alkanes, C₁₆–C₂₂, showed a uniform distribution of odd and even homologues, resulting in *CPI* (C₁₆–C₂₂) values lower than 1.40 (Table III). The *n*-alkane patterns in range C₂₃–C₃₅ were characterized by a marked odd over even predominance, with a maximum at *n*-C₂₇ or *n*-C₂₉, which resulted in high *CPI* values for full distribution of *n*-alkanes (C₁₆–C₃₅) and high *CPI* values in the range C₂₃–C₃₅ (Table III).

Based on these results, an explicit conclusion about the origin of the organic matter in the analyzed sediments could not be drawn. However, the *n*-alkane maximum at *n*-C₂₇ or *n*-C₂₉, along with a sharp predominance of odd homologues in the range of C₂₃–C₃₅ *n*-alkanes imply that the surface sediments of the Tisza River contain singenetic organic matter of terrestrial origin.¹³ The uniform distribution of lower *n*-alkanes, C₁₆–C₂₂, in all samples could be considered as an indicator of the anthropogenic oil type pollutants.^{8,14} However, such a distribution of lower *n*-alkanes could be attributed to algal singenetic organic matter as well.^{1,5}

The pristane (Pr) to phytane (Ph) ratio is widely used as an indicator for the redox settings of the depositional environment.^{1,15} The relatively uniform values of this parameter that were lower than 1 (with exception of sample M25; Table III) indicate that organic matter of all sediments was deposited under uniform, slightly reducing conditions. The concentrations of Pr and Ph were slightly lower than the concentrations of *n*-alkanes C₁₇ and C₁₈ (parameters Pr/*n*-C₁₇ and Ph/*n*-C₁₈; Table III). However, this result is not useful, because it could be related to both singenetic organic matter and oil pollutants.^{14,16}

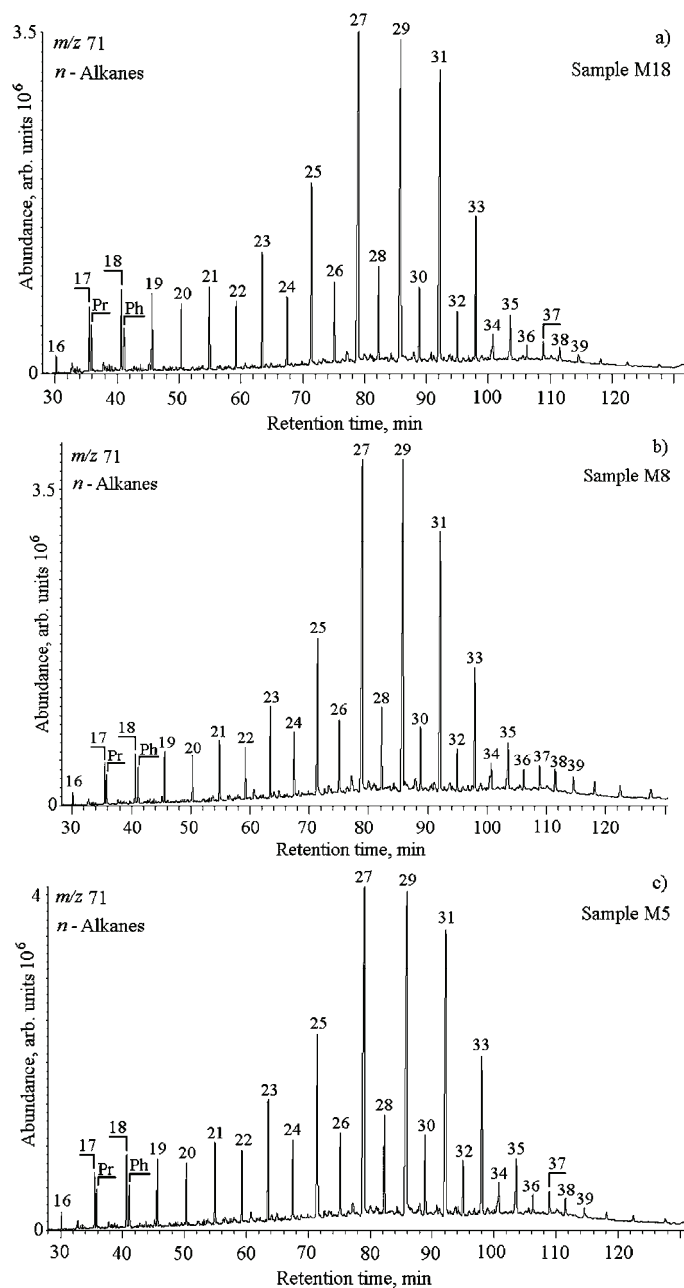


Fig. 2. GC-MS chromatograms of *n*-alkanes and isoprenoids, m/z 71 of the saturated fraction isolated from the most upstream sample (a), a sample from the middle part of the analyzed river flow (b) and from the location close to the confluence into the Danube River (c). Peak assignments: *n*-alkanes are labelled according to their carbon number; Pr – pristane; Ph – phytane.

TABLE III. Parameters calculated from the distributions and abundances of *n*-alkanes and isoprenoids

Sample	<i>n</i> -Alkane range	<i>n</i> -Alkane maximum	<i>CPI</i> (C ₁₆ –C ₃₅) ^a	<i>CPI</i> (C ₁₆ –C ₂₂) ^b	<i>CPI</i> (C ₂₃ –C ₃₅) ^c	Pr/Ph ^d	Pr <i>n</i> -C ₁₇	Ph <i>n</i> -C ₁₈
M18	C ₁₆ –C ₃₅	C ₂₇ ; C ₂₉	3.40	1.25	5.64	0.95	0.90	0.71
M21	C ₁₆ –C ₃₅	C ₂₇ ; C ₂₉	4.00	1.26	5.10	0.83	0.70	0.64
M22	C ₁₆ –C ₃₅	C ₂₇ ; C ₂₉	3.98	1.32	5.14	0.88	0.63	0.69
M25	C ₁₆ –C ₃₅	C ₂₇ ; C ₂₉	4.77	1.36	6.18	1.12	0.81	0.78
M9	C ₁₆ –C ₃₅	C ₂₇ ; C ₂₉	5.07	1.27	6.01	0.75	0.78	0.70
M7	C ₁₆ –C ₃₅	C ₂₇ ; C ₂₉	5.17	1.32	6.24	0.90	0.97	0.83
M8	C ₁₆ –C ₃₅	C ₂₇ ; C ₂₉	4.39	1.26	5.24	0.76	1.00	0.94
M6	C ₁₆ –C ₃₅	C ₂₇ ; C ₂₉	5.50	1.32	6.66	0.89	0.96	0.89
M4	C ₁₆ –C ₃₅	C ₂₇ ; C ₂₉	4.68	1.13	5.28	0.54	0.65	0.50
M5	C ₁₆ –C ₃₅	C ₂₇ ; C ₂₉	4.39	1.23	5.38	0.82	0.93	0.77

^aCarbon Preference Index (*CPI*) determined for the full distribution of *n*-alkanes C₁₆–C₃₅ (mass chromatogram *m/z* 71), $CPI(C_{16}-C_{35}) = 1/2 [\Sigma_{\text{odd}}(n-C_{17}-n-C_{35}) / \Sigma_{\text{even}}(n-C_{16}-n-C_{34}) + \Sigma_{\text{odd}}(n-C_{17}-n-C_{35}) / \Sigma_{\text{even}}(n-C_{18}-n-C_{36})]$; ^b*CPI* determined for the distribution of *n*-alkanes C₁₆–C₂₂ (mass chromatogram *m/z* 71), $CPI(C_{16}-C_{22}) = 1/2 [\Sigma_{\text{odd}}(n-C_{17}-n-C_{21}) / \Sigma_{\text{even}}(n-C_{16}-n-C_{20}) + \Sigma_{\text{odd}}(n-C_{17}-n-C_{21}) / \Sigma_{\text{even}}(n-C_{18}-n-C_{22})]$; ^c*CPI* determined for distribution of *n*-alkanes C₂₃–C₃₅ (mass chromatogram *m/z* 71), $CPI(C_{23}-C_{35}) = 1/2 [\Sigma_{\text{odd}}(n-C_{23}-n-C_{35}) / \Sigma_{\text{even}}(n-C_{22}-n-C_{34}) + \Sigma_{\text{odd}}(n-C_{23}-n-C_{35}) / \Sigma_{\text{even}}(n-C_{24}-n-C_{36})]$; ^dPr/Ph = pristane/phytane

Tricyclic and pentacyclic terpanes. The distribution of tricyclic diterpanes and pentacyclic triterpanes (hopanes) in the saturated fractions of the sediments (ion chromatograms *m/z* = 191) for the most upstream sample, a sample from the middle part of the analyzed river flow and a sample from the part that is close to the confluence into the Danube river are shown in Fig. 3. The values of specific organic–geochemical parameters, calculated from the distributions of these biomarkers are given in Tables IV and V.

All the samples had almost identical distributions of tricyclic and pentacyclic terpanes (Fig. 3). The values of the terpane source parameters indicate the same origin of the organic matter in the sediments (Table IV). The terpane distributions in all samples were typical for oils. They were characterized by a predominance of the thermodynamically more stable isomers with 17 α (H)21 β (H) and 22(S) configurations, as well as by the presence of typical geo-isomers, 18 α (H)-neohopanes (Fig. 3). These compounds have never been reported in biosphere and recent singenetic organic matter. The presence of singenetic immature organic matter in the sediments was confirmed by the identification of isomers with the biogenic 17 β (H)21 β (H) configuration in all samples (Fig. 3). The values of terpane maturity ratio (Table V) are in the range typical for crude oils.¹

Based on distributions of terpanes in the saturated fractions of the sediments and the values of the corresponding maturity parameters, it could be concluded that, in addition to singenetic organic substance, the analyzed samples contained organic matter of anthropogenic origin, which could be related to crude oil. Furthermore, the identical distributions of these biological markers in all samples

represent strong evidence that the sediments of the Tisza River, in its flow from Kanjiža town to the confluence into the Danube River, contain the same type of petroleum pollutants.

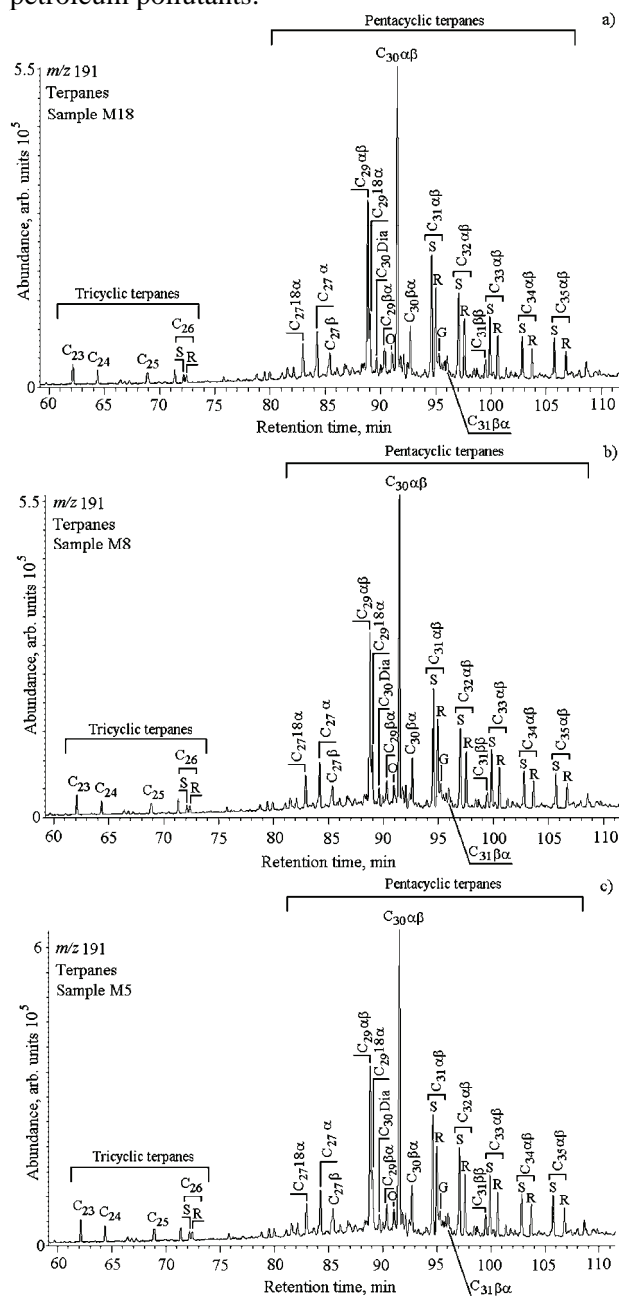


Fig. 3. GC-MS chromatograms of C_{23} – C_{26} tricyclic terpanes and C_{27} , C_{29} – C_{35} pentacyclic terpanes, m/z 191 of the saturated fraction isolated from the most upstream sample (a), a sample from the middle part of the analyzed river flow (b) and from the location close to the confluence into the Danube river (c). Peak assignments: $\beta\beta$, $\beta\alpha$ and $\alpha\beta$ designate the configurations at C_{17} and C_{21} in the pentacyclic terpanes; (S) and (R) designate configuration at C_{22} in the tricyclic and pentacyclic terpanes; Dia – diahopane; O – oleanane; G – gammacerane.

TABLE IV. Source parameters calculated from distributions and abundances of tricyclic and pentacyclic terpanes; *OI* – oleanane index = oleanane×100/(oleanane+C₃₀17α(H)21β(H)-hopane); *GI* – gammacerane index = gammacerane×100/(gammacerane+C₃₀17α(H)21β(H)-hopane)

Sample	<i>OI</i>	<i>GI</i>	C ₂₆ tricyclic terpane / C ₂₅ tricyclic terpane	C ₂₉ β/C ₃₀ αβ ^a
M18	12.73	10.36	0.88	0.59
M21	13.91	9.68	0.97	0.60
M22	12.15	10.48	0.89	0.59
M25	12.56	9.07	0.95	0.60
M9	12.07	10.20	0.95	0.61
M7	11.63	10.99	0.88	0.60
M8	12.34	10.82	0.95	0.60
M6	13.45	10.29	0.99	0.60
M4	13.15	11.24	0.94	0.61
M5	13.66	10.41	0.85	0.60
Rusanda crude oil	12.59	9.68	0.85	0.51
Elemir crude oil	12.39	10.34	0.74	0.47

^aC₂₉17α(H)21β(H)-30-norhopane/C₃₀17α(H)21β(H)-hopane; oleanane, gammacerane, tricyclic terpanes and pentacyclic terpanes (hopanes) were quantified from the mass chromatogram *m/z* 191

TABLE V. Maturity parameters calculated from the distributions and abundances of pentacyclic terpanes

Sample	C ₃₁ αβ(S)/C ₃₁ αβ(S+R) ^a	C ₃₀ β/C ₃₀ αβ ^b	C ₂₉ Ts/C ₂₉ αβ ^c	Ts/(Ts+Tm) ^d
M18	0.57	0.16	0.35	0.44
M21	0.56	0.17	0.34	0.40
M22	0.57	0.15	0.35	0.43
M25	0.56	0.16	0.34	0.44
M9	0.56	0.16	0.33	0.40
M7	0.57	0.16	0.34	0.41
M8	0.57	0.16	0.35	0.45
M6	0.56	0.16	0.35	0.41
M4	0.56	0.16	0.34	0.42
M5	0.56	0.16	0.39	0.46
Rusanda crude oil	0.60	0.11	0.27	0.44
Elemir crude oil	0.56	0.11	0.33	0.42

^aC₃₁17α(H)21β(H)22(S)-hopane/C₃₁17α(H)21β(H)22(S+R)-hopanes; ^bC₃₀17β(H)21α(H)-hopane/C₃₀17α(H)-21β(H)-hopane; ^cC₂₉18α(H)-30-norneohopane/C₂₉17α(H)21β(H)-30-norhopane; ^dC₂₇18α(H)-22,29,30-trisnorneohopane/(C₂₇18α(H)-22,29,30-trisnorneohopane+C₂₇17α(H)-22,29,30-trisnorhopane)

Steranes and diasteranes. The sterane biomarkers in all samples had almost identical distributions (Fig. 4). The uniform distributions of the C₂₇–C₂₉ 14α(H)17α(H)20(R) regular steranes¹⁷ (Table VI) in all samples confirmed that the organic matter in the sediments was of the same genetic type.

The sterane distributions in all samples were typical for oils, which corroborates the presence of oil-type pollutants in the sediments of the Tisza River. Apart from the regular steranes with a biogenic 14α(H)17α(H)20(R)-configur-

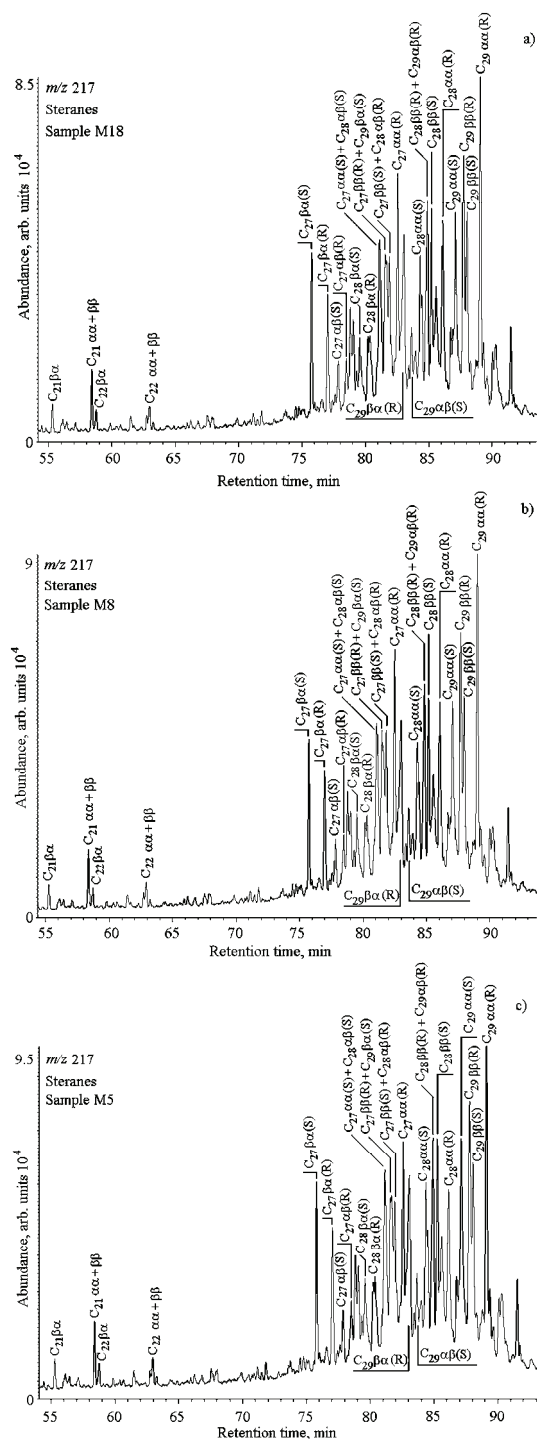


Fig. 4. GC-MS chromatograms of C_{21} – C_{22} and C_{27} – C_{29} steranes and diasteranes, m/z 217 of the saturated fraction isolated from the most upstream sample (a), a sample from the middle part of the analyzed river flow (b) and from the location close to the confluence into the Danube river (c). Peak assignments: $\alpha\alpha$ and $\beta\beta$ designate the $14\alpha(H)17\alpha(H)$ and $14\beta(H)17\beta(H)$ configurations in the steranes; $\alpha\beta$ and $\beta\alpha$ designate the $13\alpha(H)17\beta(H)$ and $13\beta(H)17\alpha(H)$ configurations in the diasteranes; (S) and (R) designate configuration at C_{20} in both the steranes and diasteranes.

TABLE VI. Source and maturity parameters calculated from the distributions and abundances of steranes and diasteranes

Sample	% C ₂₇ ^a	% C ₂₈ ^b	% C ₂₉ ^c	C ₂₉ αα(S)/ C ₂₉ αα(S+R) ^d	C ₂₉ ββ(R)/ C ₂₉ (ββ(R)+αα(R)) ^e	C ₂₇ βα(S)/ C ₂₇ (βα(S)+αα(R)) ^f
M18	33.2	29.4	37.4	0.49	0.49	0.30
M21	27.4	32.8	39.8	0.48	0.46	0.31
M22	31.8	30.9	37.3	0.49	0.50	0.29
M25	29.3	32.4	38.3	0.48	0.47	0.31
M9	32.2	31.0	36.8	0.52	0.49	0.28
M7	33.1	30.7	36.2	0.51	0.51	0.29
M8	28.6	31.6	39.8	0.48	0.48	0.34
M6	29.3	31.4	39.3	0.48	0.49	0.34
M4	27.5	33.0	39.5	0.51	0.48	0.32
M5	27.6	35.4	37.0	0.55	0.52	0.37
Rusanda crude oil	28.1	35.6	36.3	0.62	0.64	0.32
Elemir crude oil	27.0	36.8	36.2	0.57	0.59	0.22

^a100×C₂₇14α(H)17α(H)20(R)-sterane/Σ(C₂₇–C₂₉)14α(H)17α(H)20(R)-steranes; ^b100×C₂₈14α(H)17α(H)20(R)-sterane/Σ(C₂₇–C₂₉)14α(H)17α(H)20(R)-steranes; ^c% C₂₉ = 100×C₂₉14α(H)17α(H)20(R)-sterane/Σ(C₂₇–C₂₉)14α(H)17α(H)20(R)-steranes; ^dC₂₉14α(H)17α(H)20(S)-sterane/C₂₉14α(H)17α(H)20(S+R)-steranes; ^eC₂₉14β(H)17β(H)20(R)-sterane/(C₂₉14β(H)17β(H)20(R)-sterane + C₂₉14α(H)17α(H)20(R)-sterane); ^fC₂₇13β(H)17α(H)20(S)-diasterane/(C₂₇13β(H)17α(H)20(S)-diasterane + C₂₇14α(H)17α(H)20(R)-sterane); the steranes and diasteranes were quantified from the mass chromatogram *m/z* 217

ation, the short chain, C₂₁–C₂₂, and C₂₇–C₂₉ isomers with the thermodynamically more stable 14α(H)17α(H)20(S)-, 14β(H)17β(H)20(R)-, and 14β(H)17β(H)-20(S)-configurations, as well as the typical geo-isomers, 13β(H)17α(H)- and 13α(H)17β(H)-diasteranes, were present (Fig. 4). The values of the sterane maturity ratios are in a range typical for crude oils (Table VI).¹ The slightly lower values of these parameters than in crude oils could be attributed to the influence of singenetic immature terrestrial organic matter (expressed through an elevated concentration of C₂₉14α(H)17α(H)20(R)-sterane), the presence of which was confirmed by the distribution of the long-chain *n*-alkane homologues and identification of pentacyclic hopanes with the biogenic 17β(H)21β(H) configuration.

Therefore, distributions of sterane biomarkers clearly prove that in addition to the singenetic immature terrestrial organic matter, the analyzed samples also contain oil pollutants of anthropogenic origin. Moreover, the identical compositions of the steranes in all samples confirmed that the sediments of the Tisza River from Kanjiža Town to the confluence into the Danube River, along a distance of 153 km, contained the same type of oil pollutant.

Assessment of the oil pollutant source

Based on previous discussion, it was established that sediments of the Tisza River, in addition to some singenetic immature terrestrial organic matter, con-

tains an oil type pollutant. Considering navigable character of the Tisza River, the observed continuous oil pollution most probably resulted from persistent and extensive transport *via* river barges, which commonly use heavy fuel oil.

As mentioned above, the crude oils represent mature organic matter and are characterized by specific distributions of steranes and terpanes with a predominance of the thermodynamically more stable isomers, which are not found in biosphere and recent singenetic sedimentary organic matter. Consequently, most values of the maturity biomarker of the crude oils parameters, which represent the ratios of more and less stable isomers, vary in a relatively narrow range.¹ On the other hand, each crude oil sample has a characteristic distribution of biomarkers as a kind of “fingerprint”, which in addition to maturity, depends on the origin, depositional environment, age, relative length of migration and the mineral composition of the source and reservoir rocks. Therefore, crude oils can significantly differ in values of source parameters, such as distribution of C₂₇–C₂₉ 14 α (H)17 α (H)20(R) regular steranes¹⁷, gammacerane and oleanane indices,^{18–20} ratio of C₂₆ to C₂₅ tricyclic terpanes¹ and C₂₉17 α (H)21 β (H) to C₃₀17 α (H)21 β (H) hopane.¹ Comparison of the distributions of terpanes and steranes and the values of the corresponding biomarker parameters in the extracts of sediments of the Tisza River and previously investigated crude oils from oil deposits in the Serbian part of Pannonian Basin showed great similarity between extracts of investigated sediments and crude oils from Rusanda (well 5; depth interval 2665–2675 m) and Elemir (well 19; depth interval 1640–1644 m) oil fields (Figs. 3–8; Tables IV and V), which are located close to the investigated area

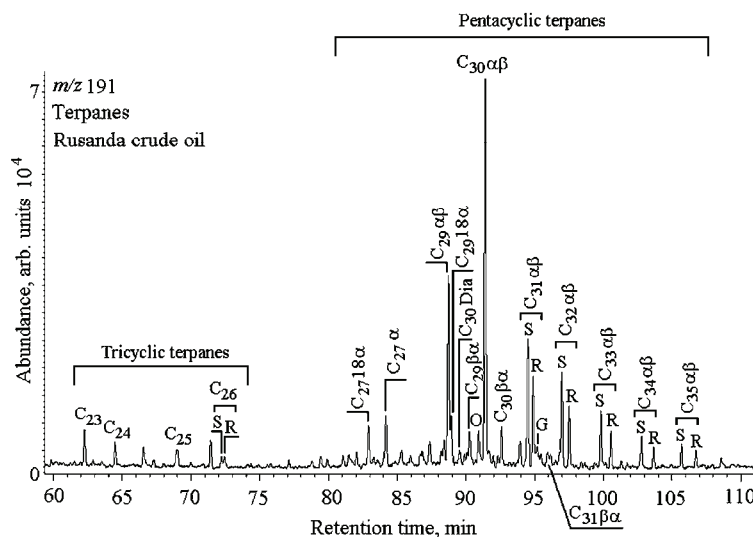


Fig. 5. GC–MS chromatograms of terpanes m/z 191 of the saturated fraction isolated from Rusanda crude oils. For peak assignments, see the legend to Fig. 3.

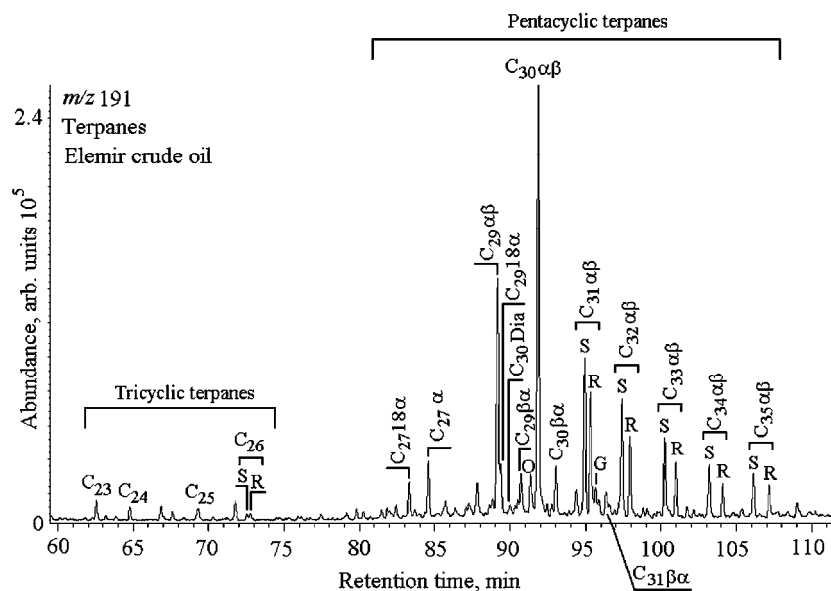


Fig. 6. GC-MS chromatograms of terpanes m/z 191 of the saturated fraction isolated from Elemir crude oils. For peak assignments, see the legend to Fig. 3.

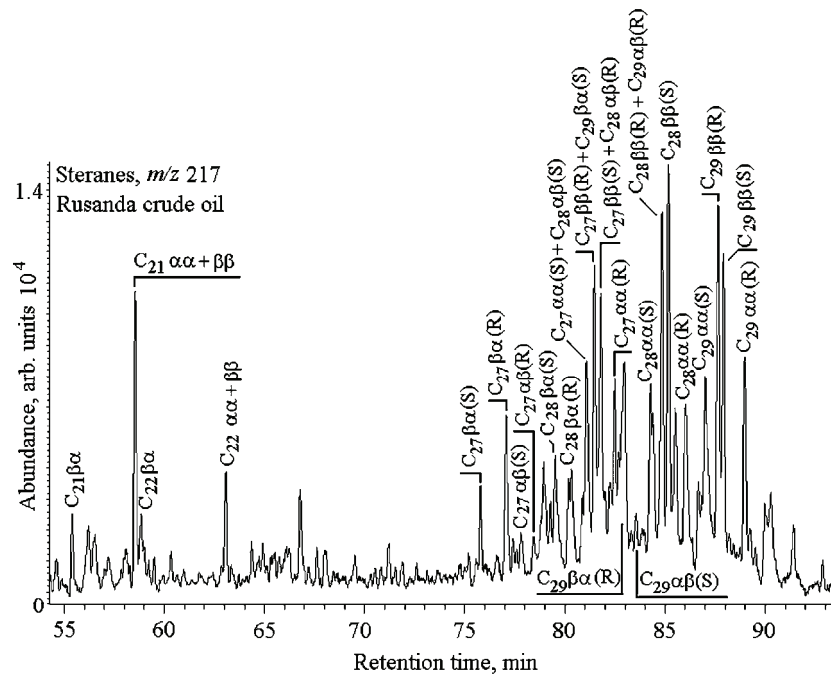


Fig. 7. GC-MS chromatograms of steranes m/z 217 of the saturated fraction isolated from Rusanda crude oils. For peak assignments, see the legend to Fig. 4.

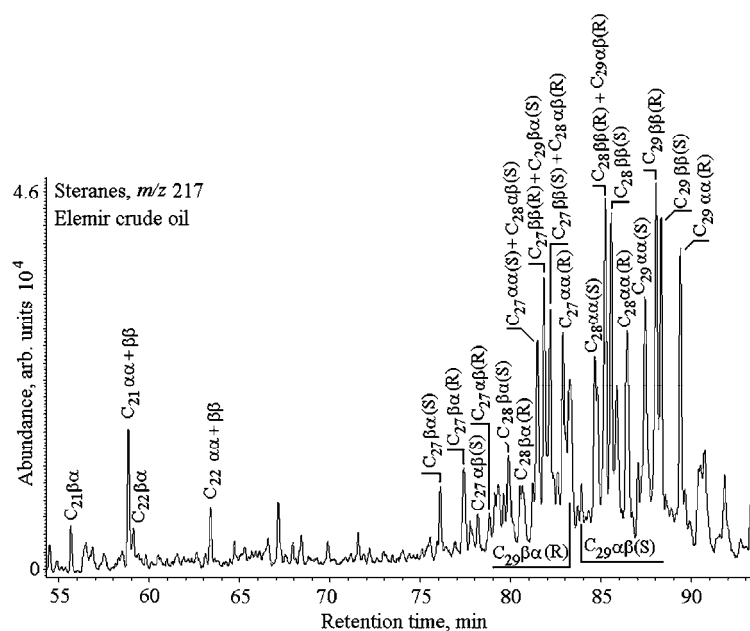


Fig. 8. GC-MS chromatograms of steranes, m/z 217 of the saturated fraction isolated from Elemir crude oils. For peak assignments, see the legend to Fig. 4.

(Fig. 1). Therefore, the oil contamination observed in the Tisza sediments, apart from heavy fuel oil from barges, to a lower extent can probably be related to the Rusanda and Elemir crude oils. According to the geological setting of the terrain, there is no possibility of natural migration of oils from the oil fields to the Tisza River surface sediments. Therefore it could be assumed that observed oil pollution resulted from oil shipment at the station located on the river bank and further transport by barges.

CONCLUSIONS

The origin and type of organic matter of the Tisza sediments along its 153 km distance through the territory of Serbia were evaluated using group organic-geochemical data and the biomarker compositions.

The contents of the total organic carbon and soluble organic matter were similar in all samples. The organic matter was deposited under slightly reducing conditions. All the samples had almost identical distributions of *n*-alkanes, steranes, and tricyclic and pentacyclic terpanes, indicating the same origin of the organic matter.

Based on distribution of *n*-alkanes, the origin and type of organic matter could not be precisely estimated. However, the *n*-alkane maximum at *n*-C₂₇ or *n*-C₂₉ and the marked odd over even predominance in the range of *n*-C₂₃-*n*-C₃₅ suggested the presence of immature singenetic organic matter of terrestrial origin.

Typical oil distributions of terpanes and steranes along with values of the corresponding maturity parameters clearly indicated that the sediments of the Tisza River, in addition to immature singenetic organic matter, contained oil pollutants of anthropogenic origin. The identical distributions of these biomarkers in all samples represent strong evidence that the recent sediments of the Tisza River, in its flow from Kanjiža Town to its confluence into the Danube River contained the same type of oil pollutants.

Based on the compositions of terpanes and steranes and the values of the biomarker parameters in the Tisza sediments, it is supposed that oil pollution generally could be related to heavy fuel oil from barges, due to intense river transport. Comparison of the distributions of terpanes and steranes and the values of corresponding biomarker parameters in the extracts of sediments of the Tisza River and previously investigated crude oils from oil deposits in the Serbian part of Pannonian Basin showed that the oil contaminants observed in Tisza sediments, apart from heavy fuel oil from tankers, to a lower extent, could be attributed to Rusanda and Elemir crude oils.

Acknowledgements. The study was funded by the Ministry of Education, Science and Technological Development of the Republic of Serbia (Project Nos. 176006 and 176019). Nikola Vuković, M.Sc., in Geology is acknowledged for linguistic corrections. We are also grateful to the anonymous reviewers.

ИЗВОД

ПРИМЕНА БИОЛОШКИХ МАРКЕРА У ОДРЕЂИВАЊУ ПОРЕКЛА И ТИПА ОРГАНСКЕ СУПСТАНЦЕ У СЕДИМЕТИМА РЕКЕ ТИСЕ

СНЕЖАНА ШТРЕБАЦ¹, ГОРДАНА ГАЛИЦА², АЛЕКСАНДРА ШАЈНОВИЋ², НЕБОЈША ВАСИЋ³,
КСЕНИЈА СТОЈАНОВИЋ⁴ и БРАНИМИР ЈОВАНЧИЋЕВИЋ⁴

¹Факултет за заштитне животне средине, Универзитет ЕДУКОНС, Војводе Пушника 87, 21207 Сремска Каменица, ²Центар за хемију, ИХТМ, Студенски шир 12–16, 11000 Београд, ³Рударско–геолошки факултет, Универзитет у Београду, Бушина 7, 1100 Београд и ⁴Хемијски факултет, Универзитет у Београду, Студенски шир 12–16, 11000 Београд

Циљ рада је био да се утврди порекло и тип органске супстанце у рецентним седиментима реке Тисе, у делу тока који се налази на територији Србије, укупне дужине 153 километра. У ту сврху коришћени су групни органско–геохемијски параметри и састав биомаркера. Сви узорци садрже приближно исту количину органске супстанце таложене у благо редукционој средини. На основу расподеле *n*-алкана није било могуће прецизно утврдити порекло и тип органске супстанце. Међутим, *n*-алканске расподеле указале су на присуство незреле нативне органске супстанце сувоземног порекла. Расподеле терпана и стерана и вредности одговарајућих матурационих параметара указују да седименти реке Тисе, поред незреле нативне органске супстанце садрже нафтну загађујућу супстанцу антропогеног порекла. Идентичне расподеле ових биомаркера у свим узорцима потврђују да рецентни седименти реке Тисе, у делу тока од места Кањижа до ушћа у реку Дунав, садрже исти тип нафтног загађивача. На основу расподела терпана и стерана и вредности биомаркерских параметара претпостављено је да нафтно загађење

генерално потиче од мазута из танкера, услед интензивног речног транспорта и, у мањој мери, од сирових нафти из нафтних поља Елемир и Русанда.

(Примљено 14 јуна, ревидирано 28. августа, прихваћено 29. августа 2013)

REFERENCES

1. K. E. Peters, C. C. Walters, J. M. Moldowan, *The Biomarker Guide, Vol. 2: Biomarkers and Isotopes in the Petroleum Exploration and Earth History*, Cambridge University Press, Cambridge, 2005, pp. 483–486, 499–500, 483–486, 493, 499, 558, 569, 612
2. B. P. Tissot, D. H. Welte, *Petroleum Formation and Occurrence*, 2nd Ed., Springer-Verlag, Heidelberg, Germany, 1984, pp. 57, 424
3. B. Jovančičević, M. Vrvić, J. Schwarzbauer, H. Wehner, G. Scheeder, D. Vitorović, *Water Air Soil Pollut.* **183** (2007) 225
4. V. Beškoski, G. Gojgić-Cvijović, B. Jovančičević, M. Vrvić, *Gas Chromatograph in Environmental Sciences and Evaluation of Bioremediation*, in *Gas Chromatography – Biochemicals, Narcotics and Essential Oils*, B. Salih, Ö. Çelikbıçak, Eds., InTech, Rijeka, Croatia, 2012, Ch. 1, p. 3
5. R. A. Bourbonniere, P. A. Meyers, *Limnol. Oceanogr.* **41** (1996) 352
6. A. Bechtel, R. F. Sachsenhofer, I. Kolcon, R. Gratzner, A. Otto, W. Püttmann, *Int. J. Coal Geol.* **51** (2002) 31
7. I. R. Kaplan, Y. Galperin, S. Lu, R. Lee, *Org. Geochem.* **27** (1997) 289
8. Z. Wang, M. Fingas, D. S. Page, *J. Chromatogr., A* **843** (1999) 369
9. K. Stojanović, A. Šajnović, T. Sabo, A. Golovko, B. Jovančičević, *Energ. Fuels* **24** (2010) 4357
10. O. Sonibare, H. Alimi, D. Jarvie, O. A. Ehinola, *J. Petrol. Sci. Eng.* **61** (2008) 99
11. H. I. Petersen, B. Holland, H. P. Nytoft, A. Cho, S. Piasecki, J. de la Cruz, J. H. Cornec, *J. Petrol. Geol.* **35** (2012) 127
12. R. P. Philp, *Fossil Fuel Biomarkers. Applications and Spectra*. Elsevier, Amsterdam, 1985, pp. 153, 159–161, 164–169, 229, 246, 250, 253
13. A. Zdravkov, A. Bechtel, R. F. Sachsenhofer, J. Kortenski, R. Gratzner, *Org. Geochem.* **42** (2011) 237
14. B. Jovančičević, P. Polić, *Fresenius Envir. Bull.* **10** (2001) 527
15. B. M. Didyk, B. R. T. Simoneit, S. C. Brassell, G. Eglinton, *Nature* **272** (1978) 216
16. M. Obermajer, M. G. Fowler, L. R. Snowdon, *Am. Assoc. Petrol. Geol. Bull.* **83** (1999) 1426
17. J. M. Moldowan, W. K. Seifert, E. J. Gallegos, *Am. Assoc. Petrol. Geol. Bull.* **69** (1985) 1255
18. J. S. Sinninghe Damsté, F. Kenig, M. P. Koopmans, J. Köster, S. Schouten, J. M. Hayes, J. W. de Leeuw, *Geochim. Cosmochim. Acta* **59** (1995) 1895
19. O. T. Udo, C. M. Ekweozor, *Energ. Fuels* **4** (1990) 248
20. H. P. Nytoft, G. Kildahl-Andersen, O. J. Samuel, *Org. Geochem.* **41** (2010) 1104.



J. Serb. Chem. Soc. 78 (5) 613–626 (2013)
JSCS–4612

Optimization of electrocoagulation process to treat biologically pretreated bagasse effluent

KARICHAPPAN THIRUGNANASAMBANDHAM, VENKATACHALAM SIVAKUMAR*
and JEGANATHAN PRAKASH MARAN

*Department of Food Technology, Kongu Engineering College, Perundurai,
Erode-638052, TN, India*

(Received 8 April, revised 24 June, accepted 27 June 2013)

Abstract: The main objective of the present study was to investigate the efficiency of the electrocoagulation process as a post-treatment to treat biologically pretreated bagasse effluent using iron electrodes. The removal of the chemical oxygen demand (COD) and the total suspended solids (TSS) were studied under different operating conditions, such as amount of dilution, initial pH, applied current and electrolyte dose using the response surface methodology (RSM) coupled with a four-factor three-level Box–Behnken experimental design (BBD). The experimental results were analyzed by the Pareto analysis of variance (ANOVA) and second order polynomial mathematical models were developed with high correlation of efficiency (R^2) for COD, TSS removal and electrical energy consumption (EEC). The individual and combined effects of the variables on the responses were studied using three dimensional response surface plots. Under the optimum operating conditions, *i.e.*, amount of dilution at 30 %, initial pH of 6.5, applied current of 8 mA cm⁻² and electrolyte dose of 740 mg L⁻¹, high removal efficiencies of COD (98 %) and TSS (93 %) were obtained with an EEC of 2.40 Wh, which were confirmed by validation experiments.

Keywords: electrocoagulation; iron electrode; post treatment; model development; optimization.

INTRODUCTION

The pulp and paper industry is one of the most water-dependent industries that consumes 500 m³ of fresh water to produce a ton of paper.¹ The effluent characteristics of the pulp and paper industry vary according to the pulp process and the characteristics of raw material used in each industry. However, in general, most of the pulp and paper industries used bagasse as a raw material, due to its easy availability and eco-friendly nature. The effluents generated from bag-

*Corresponding author. E-mail: drvsivakumar@yahoo.com
doi: 10.2298/JSC130408074T

asse-based pulp and a paper industry contain high amounts of organic material and suspended solids, which are considered as major pollutants to an ecosystem. The discharge of untreated bagasse effluent to the ecosystem degrades the environmental and causes harmful effects to living organisms.² To overcome this problem, numerous treatment technologies have been reported for the treatment of bagasse effluent, such as bioremediation, upflow anaerobic sludge blanket (UASB) reactor treatment and fungal treatment. However, these treatment processes have drawbacks, such as long treatment time, start-up problems, maintaining environmental conditions and low removal efficiency of organic pollutants. These characteristics of a biological treatment process makes it unfit for large-scale application. Even though, biological treatment of bagasse effluent produces valuable by-products (biogas), the discharge of this effluent to ecological system is still questionable due to the presence of considerable amounts of organic matter. With environmental regulations becoming more stringent, regulatory compliance has also become a matter of increasing concern for the pulp and paper industries. Therefore, there is a critical need to install an effective post-treatment method to treat biologically pretreated bagasse effluent.³

In recent years, there has been increased interest in the application of electrocoagulation in the treatment of industrial wastewater. Some of the advantages of electrocoagulation are the simple equipment required, low operating cost, high removal efficiency of toxic matters at short treatment times, easily available electrode materials and easy automation of the process. In addition, it does not require any addition of chemicals, the dosing of coagulant reagents depends on the applied current.⁴ Electrocoagulation is a process that generates metallic hydroxides *in situ via* electro-dissolution of a soluble sacrificial anode immersed in the wastewater. The electrochemically generated metallic ions hydrolyze near the anode to form a series of metal hydroxides that are able to destabilize the dispersed particles present in the wastewater to be treated. The destabilized particles are believed to be responsible for the aggregation and precipitation of suspended particles. Moreover, most of the electrocoagulation process use iron as the electrode material due to its higher electrical potential compared to other materials, such as aluminum and stainless steel.⁵

To the best of our knowledge, the electrocoagulation process has hitherto been applied as a pre-treatment process for various industry effluents. No investigations have been reported for the efficiency of an electrocoagulation process as a post-treatment to treat industrial effluents. Hence, in this study, it was planned to investigate and optimize the operating variables, such as amount of dilution, initial pH, applied current and electrolyte dose on the removal efficiency of *COD* and *TSS* removal in the treatment of biologically pretreated bagasse effluent using electrocoagulation (post-treatment) process *via* the response surface methodology (RSM).⁶ Response surface methodology (RSM), a collection of mathe-

mathematical (statistical) techniques, is useful for developing, optimizing and understanding the performance of complex systems applying the minimum number of experiments. This technique conforms closely to practical results compared to theoretical models as it arises from an experimental methodology.⁷

EXPERIMENTAL

Materials

The wastewater investigated in this study was collected from a bagasse-based pulp and paper factory near Erode, Tamilnadu, India. Sample collection, preservation and characterization (pH, *COD* and *TSS*) were realized in accordance with the American Public Health Association (APHA) Standard Methods for the Examination of Wastewater.¹ Characterization was performed immediately after arrival of the samples in the laboratory. The obtained values were pH 7.04, *COD* = 1574 mg⁻¹ and *TSS* = 986 mg L⁻¹. All the chemicals employed in the study were analytically pure. The electrolyte used in the study was sodium chloride, which was purchased from local suppliers, Erode, India.

Experimental procedure

The electrochemical reactor (acrylic) having a working volume of 3 L was used to treat the wastewater with iron sheets (33 cm×6 cm×0.2 cm) as the electrode. The effective surface area of each electrode was 108 cm². The distance between the anode and cathode was fixed at 4 cm. The assembly was connected to DC power source (Dolphin; 0–6 A and 0–30 V) to fix the desired current density. Distilled water was used to dilute the effluent and the effluent was then adjusted to the required pH using sodium hydroxide or hydrochloric acid. A schematic diagram of electrocoagulation reactor is shown in Fig. 1. In each run, 1.6 L of wastewater was placed into the reactor and all the runs were performed for a constant treatment time of 15 min under stirring at 250 rpm. The treated effluents were collected, filtered and used for the determination of the *COD* and *TSS*. All experiments were performed in triplicate and the average values were recorded. The removal efficiency (*R* in %) was calculated using the following equation:

$$R = \frac{Y_0 - Y}{Y} \times 100 \quad (1)$$

where Y_0 and Y represent the initial and final value of *COD* or *TSS*.

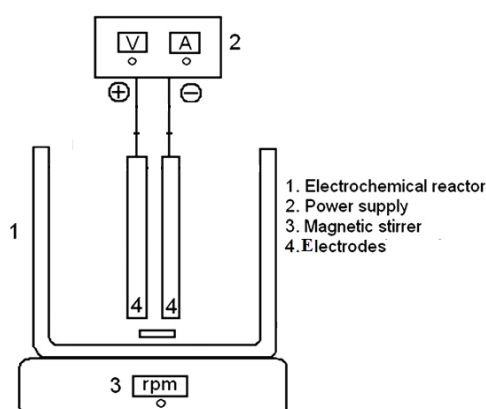


Fig. 1. Schematic diagram of the electrocoagulation unit.

Experimental design

In the present study, the response surface methodology (RSM) was used to optimize and determine the relationship between removal efficiencies of *COD*, *TSS* and *EEC* with respect to the crucial operating parameters, *i.e.*, the amount of dilution, 5–15 %, initial pH 5–9, applied current, 5–15 mA cm⁻² and electrolyte dose, 350–750 mg L⁻¹. Box–Behnken response surface experimental design (BBD) with 29 experiments with five centre points and their results were analyzed by multiple regression analysis to evaluate the adequacy of various models (linear, interactive (2FI), quadratic and cubic) using the Stat ease Design Expert 8.0.7.1 statistical software package (Stat-Ease Inc., Minneapolis, MN, USA). The regression coefficients of the linear, quadratic and the interaction involved in the model and their effects were analyzed by the *F*-test and *P*-value. The statistical significance of the model was analyzed by pareto analysis of the variance (ANOVA). The relationship between the response and the four independent variables were correlated by a second order polynomial equation, the generalized form of which was given in elsewhere,⁷ and it was used for the construction of three dimensional response surface plots to study the effect of the independent variables on the dependent variables. Finally, the numerical optimization methodology was performed to determine the effective electrocoagulation operating conditions, which was validated by conducting additional experiments.

RESULTS AND DISCUSSION

Experimental design analysis

The total number of 29 statistically designed batch experiments were performed for different combinations of the process variables in order to optimize and study the combined effect of independent variables (amount of dilution, initial pH, applied current and electrolyte concentration) on the removal efficiencies of *COD*, *TSS* and *EEC*, which are shown in Table I. The experimental data was fitted to the various mathematical models (linear, interactive (2FI), quadratic and cubic) in order to obtain regression equations. To realize this, model summary statistics (Table II) were performed to decide about the adequacy of a models among the various models, *i.e.*, the model that exhibits the highest *R*², adjusted *R*², predicted *R*² and *F* values and also lowest *p*-values for when compared with those of the other models.^{6–8} Thus, the quadratic model was selected for further analysis to represent the electrocoagulation process. The obtained second-order polynomial equations in terms of coded factors are given below:

$$Y_1 = 95.42 + 6.11X_1 - 4.94X_2 + 11.38X_3 + 10.46X_4 - 5.64X_1X_2 - 1.41X_1X_3 + 1.77X_1X_4 - 3.46X_2X_3 - 3.70X_2X_4 - 4.37X_3X_4 - 3.52X_1^2 - 21.46X_2^2 - 9.56X_3^2 - 11.90X_4^2 \quad (2)$$

$$Y_2 = 91.58 + 5.04X_1 - 4.09X_2 + 12.64X_3 + 10.17X_4 - 5.87X_1X_2 - 1.43X_1X_3 + 1.72X_1X_4 - 3.73X_2X_3 - 3.55X_2X_4 - 6.82X_3X_4 - 3.67X_1^2 - 22.06X_2^2 - 9.49X_3^2 - 12.44X_4^2 \quad (3)$$

$$\begin{aligned}
 Y_3 = & 3.51 + 0.19X_1 + 0.21X_2 + 3.16X_3 - 0.53X_4 + 0.14X_1X_2 + \\
 & + 0.371.43X_1X_3 - 0.06X_1X_4 + +0.44X_2X_3 + 0.00X_2X_4 - \\
 & - 0.57X_3X_4 + 0.034X_1^2 + 0.67X_2^2 + 0.20X_3^2 + 0.54X_4^2
 \end{aligned} \quad (4)$$

where, Y_1 , Y_2 and Y_3 are the percentage removal of *COD*, *TSS* and *EEC*, respectively, and X_1 , X_2 , X_3 and X_4 are the coded values of the amount of dilution, initial pH, applied current and electrolyte concentration, respectively.

TABLE I. Box–Behnken experimental design and observed responses

Run No.	Dilution of effluent (X_1)	Initial pH (X_2)	Applied current (X_3)	Electrolyte concentration (X_4)	<i>COD</i> removal, %	<i>TSS</i> removal, %	<i>EEC</i> W h
1	20 (0)	5(-1)	15(+1)	600(0)	84.23	79.48	7.29
2	10(-1)	5(-1)	10(0)	600(0)	65.24	63.48	3.78
3	20(0)	7(0)	10(0)	600(0)	95.42	91.58	3.51
4	10(-1)	7(0)	5(-1)	600(0)	66.48	59.48	1.08
5	20 (0)	5(-1)	10(0)	350(-1)	55.32	48.18	5.13
6	20(0)	9(+1)	10(0)	850(+1)	63.43	58.94	4.05
7	20(0)	7(0)	10(0)	600(0)	95.42	91.58	3.78
8	20(0)	5(-1)	5(-1)	600(0)	53.16	47.98	1.08
9	20(0)	7(0)	15(+1)	350(-1)	78.64	82.45	8.91
10	30 (+1)	9(+1)	10(0)	600(0)	64.83	58.48	4.86
11	20(0)	9(+1)	10(0)	350(-1)	53.48	45.84	4.86
12	10(-1)	7(0)	15(+1)	600(0)	88.14	84.27	5.67
13	20(0)	5(-1)	10(0)	850(+1)	80.13	75.48	4.32
14	30(+1)	7(0)	10(0)	850(+1)	98.46	94.86	4.05
15	20(0)	7(0)	5(-1)	350(-1)	44.58	38.98	1.22
16	20(0)	7(0)	10(0)	600(0)	95.42	91.58	3.78
17	20(0)	7(0)	5(-1)	850(+1)	78.48	72.48	0.67
18	20(0)	7(0)	10(0)	600(0)	95.42	91.58	2.97
19	30(+1)	5(-1)	10(0)	600(0)	85.36	75.86	3.78
20	10(-1)	9(+1)	10(0)	600(0)	67.25	69.58	4.32
21	30(+1)	7(0)	15(+1)	600(0)	97.45	94.57	6.88
22	10(-1)	7(0)	10(0)	850(+1)	79.24	74.96	3.78
23	10(-1)	7(0)	10(0)	350(-1)	62.54	57.48	4.32
24	20(0)	9(+1)	15(+1)	600(0)	66.18	62.58	8.91
25	20(0)	9(+1)	5(-1)	600(0)	48.96	45.98	0.94
26	20(0)	7(0)	10(0)	600(0)	95.42	91.58	3.51
27	20(0)	7(0)	15(+1)	850(+1)	95.04	88.67	6.07
28	30(+1)	7(0)	5(-1)	600(0)	81.43	75.48	0.81
29	30(+1)	7(0)	10(0)	350(-1)	74.68	70.48	4.86

Generally, it is important to confirm that the fitted model gives an adequate estimation to predict the responses, unless the model shows poor or misleading results. Considering this phenomenon, diagnostic plots, *i.e.*, predicted *versus* actual values (Fig. 2a–c) were plotted to evaluate the model suitability and to deter-

TABLE II. Model summary statistics for *COD* and *TSS* removal

Source	<i>SD</i>	R^2	Adjusted R^2	Predicted R^2	<i>PRESS</i>	Remarks
Model summary statistics for <i>COD</i> removal						
Linear	12.9022	0.4746	0.3871	0.2968	5347	–
2FI	14.2750	0.5177	0.2497	–0.0555	8026	–
Quadratic	2.7010	0.9866	0.9731	0.9226	588	Suggested
Cubic	1.9070	0.9971	0.9866	0.5868	3142	Aliased
Model summary statistics for <i>TSS</i> removal						
Linear	13.5630	0.4534	0.3623	0.2624	5957	–
2FI	14.8420	0.5091	0.2363	0.2363	8793	–
Quadratic	3.7712	0.9753	0.9507	0.8580	1146	Suggested
Cubic	1.6519	0.9980	0.9905	0.7081	2357	Aliased
Model summary statistics for <i>EEC</i>						
Linear	0.6713	0.9199	0.9066	0.8827	15.84	–
2FI	0.6704	0.9401	0.9068	0.8384	21.83	–
Quadratic	0.5216	0.9718	0.9436	0.8511	20.10	Suggested
Cubic	0.3697	0.9939	0.9717	0.5869	55.80	Aliased

mine the relationship between the predicted and experimental values.^{9,10} The data points on these plots lie reasonably close to a straight line, which indicates that an adequate agreement between real data and the data obtained from the models.¹¹ The statistical significance of the regression equation was evaluated by Pareto analysis of variance (ANOVA) and the results are presented in Table III. The *F* and *p*-values of the individual and combined effects of the operating variables were found to be in the range of acceptable levels, which indicated that the model was highly statistically significant.¹² These results indicated that the developed mathematics is good enough to represent the electrocoagulation treatment process significantly.

Influence of the process variables

Four factors at five levels BBD were used in this study to investigate the influence of process variables on responses such as *COD* and *TSS* removal. To understand the interaction between the independent variables and estimate the removal efficiency of *COD*, *TSS* and *EEC* over the independent variables, three dimensional response surface plots were constructed from the developed models (Equations (2)–(4)), which are shown in Figs. 3–5.

Effect of amount of dilution

Dilution of the effluent is key parameter that strongly influenced the performance of the electrocoagulation process. The concentration of the effluent discharged after biological treatment of the bagasse effluent is not constant over time. Hence, an adopted post treatment method should be capable of treating bagasse effluent of varying concentrations. Considering this, the amount of dilution

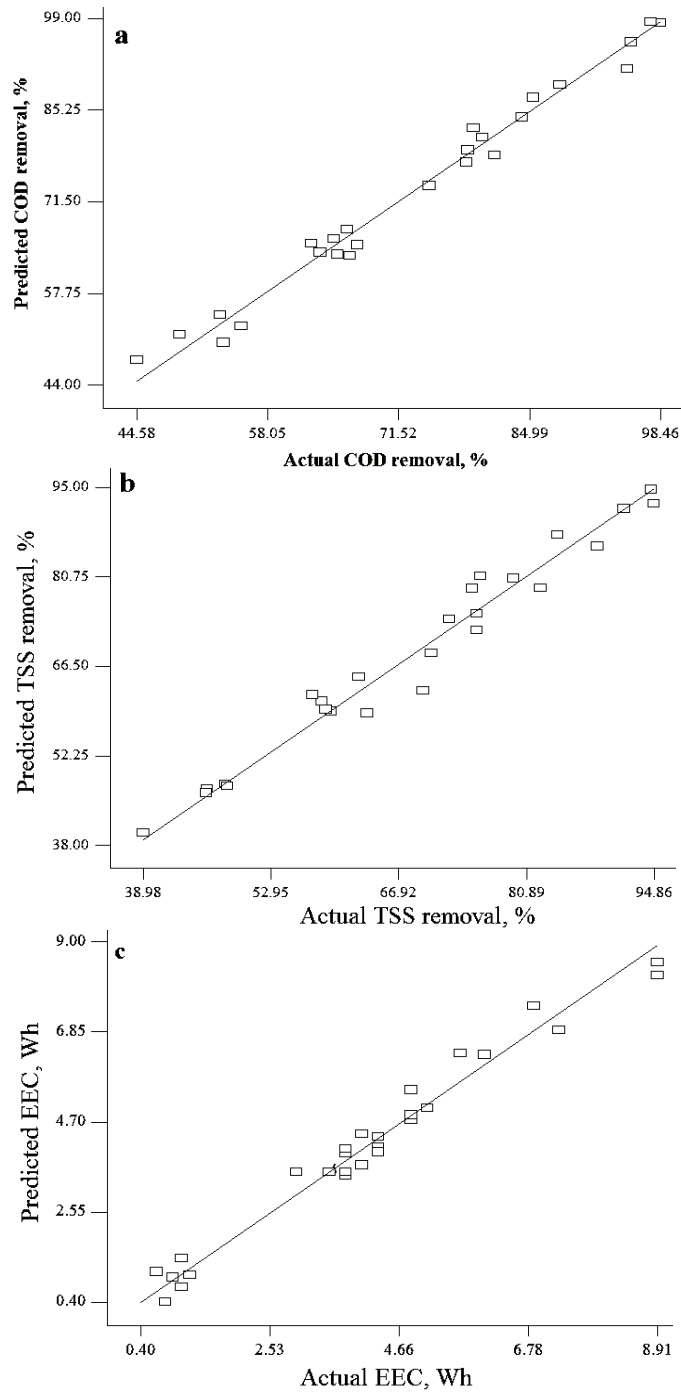


Fig. 2. Actual vs. predicted plot for the removal efficiency of *COD* (a), *TSS* (b) and *EEC* (c).

TABLE III. ANOVA table for responses

Response	COD removal		TSS removal		EEC	
	<i>F</i> -value	<i>p</i> -value	<i>F</i> -value	<i>p</i> -value	<i>F</i> -value	<i>p</i> -value
Model	73.45	< 0.0001	39.56	< 0.0001	34.4579	< 0.0001
X_1	61.41	< 0.0001	21.43	0.0004	1.60624	0.2257
X_2	40.18	< 0.0001	14.10	0.0021	2.00733	0.1784
X_3	213.11	< 0.0001	134.74	< 0.0001	440.661	< 0.0001
X_4	180.02	< 0.0001	87.18	< 0.0001	12.3895	0.0034
X_1X_2	17.41	0.0009	9.69	0.0076	0.26795	0.6128
X_1X_3	1.09	0.3142	0.57	0.4623	2.01272	0.1779
X_1X_4	1.72	0.2111	0.84	0.3758	0.06699	0.7995
X_2X_3	6.57	0.0225	3.90	0.0683	2.84633	0.1137
X_2X_4	7.57	0.0156	3.54	0.0807	0	1.0000
X_3X_4	10.49	0.0059	13.08	0.0028	4.81871	0.0455
X_1^2	11.01	0.0051	6.14	0.0266	0.02716	0.8715
X_2^2	409.49	< 0.0001	221.92	< 0.0001	10.8627	0.0053
X_3^2	81.27	< 0.0001	41.08	< 0.0001	0.96561	0.3425
X_4^2	126.00	< 0.0001	70.59	< 0.0001	6.95212	0.0195

was selected as a primary parameter in the electrocoagulation process. From the results (Figs. 3a and 4a), it was observed that the efficiencies for the removal of COD and TSS increased with increasing amount of dilution. This could be explained by the fact that higher amounts of dilution lead to decreasing concentrations of COD and TSS in wastewater; thus, the removal efficiencies were increased with respect to increasing dilution of the wastewater.

Effect of initial pH

In an electrocoagulation treatment process, the pH plays an important role in determining the removal efficiencies. From the obtained results (Figs. 3a and 4a), it was found that the efficiencies of COD and TSS removal increased with increasing pH up to 6.5. Thereafter, there was a drastic decrease in the efficiencies of COD and TSS removal. This is because the formation of $\text{Fe}(\text{OH})_3$ flocks is significant in the pH range 5–7, which removes the COD and TSS via sweep coagulation. Above pH 6.5, monomeric anions, namely $\text{Fe}(\text{OH})^{4-}$ species, are formed that are ineffective¹³ for removal of COD and TSS from bagasse effluent. These results indicated that the initial pH value of the effluent is a primary parameter that affects the electrocoagulation process significantly.

Effect of applied current

Applied current is one of the important factors influencing the electrocoagulation process. From the obtained results (Fig. 3b and 4b), it was found that the efficiency of COD and TSS removal increased with increasing current density up to 10 mA cm^{-2} , thereafter the current density had almost negligible effects on the removal efficiencies. This could be explained by the fact that the formation of

$\text{Fe}(\text{OH})_3$ flocks increased with increasing applied current and hence an improvement in the efficiency of *COD* and *TSS* removal was observed. However, above an applied current of 10 mA cm^{-2} , almost all the *COD* and *TSS* were removed via sweep coagulation and thus, the removal efficiencies were constant.¹⁴

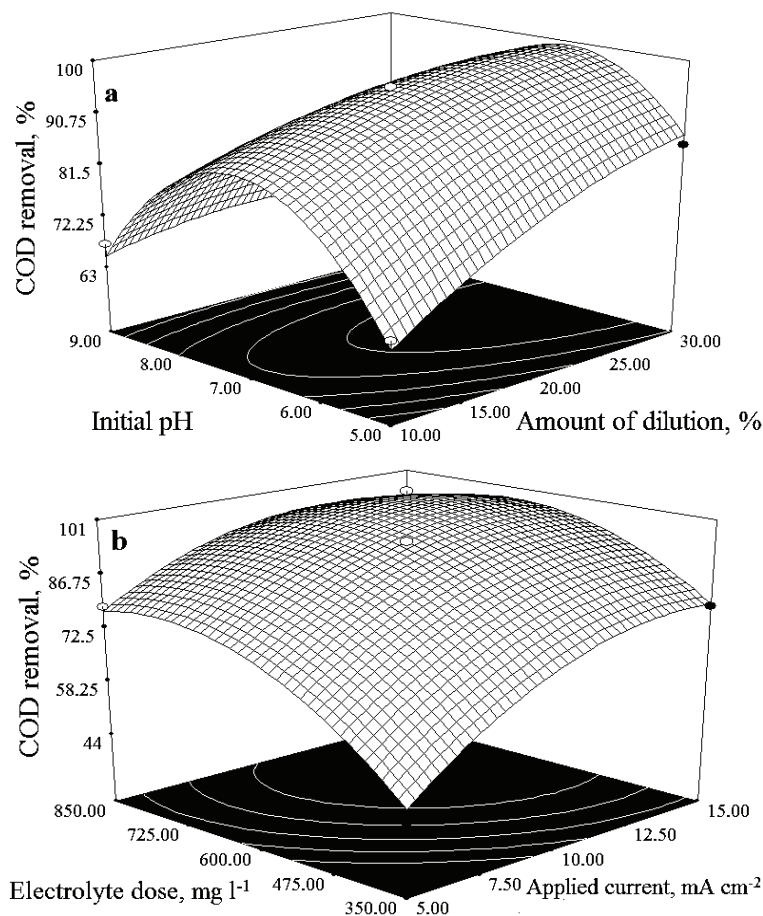
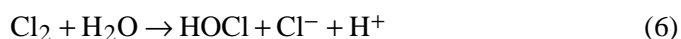


Fig. 3. Effect of operating variables on *COD* removal.

Effect of electrolyte (NaCl) dose

The electrolyte concentration is one of the prime parameter that significantly affects the performance of an electrocoagulation process. From the obtained results (Figs. 3b and 4b), it was found that efficiencies of *COD* and *TSS* removal increased with increasing electrolyte concentration up to 600 mg L^{-1} . This is due to the formation of hypochlorite (an oxidizing agent), which strongly affects the removal of the *COD* and *TSS*. The detailed mechanism is given below:¹⁵



Further increases in the electrolyte concentration show negligible effects on the removal efficiency of *COD* and *TSS*.

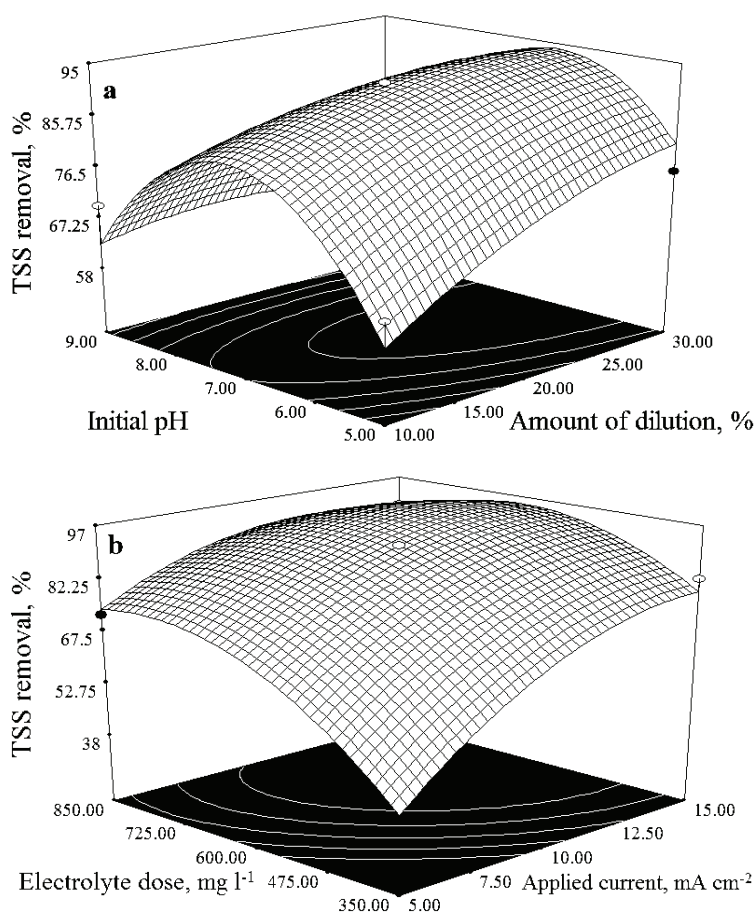


Fig. 4. Effect of operating variables on *TSS* removal.

Effect of process variables on the electrical energy consumption

Electrical energy consumption (*EEC*) is a crucial parameter in electrocoagulation process that significantly affects the economy of the process. From the obtained results (Fig. 5a and b), it was found that, the *EEC* of the electrocoagulation process is significantly affected by the initial pH (X_2), applied current (X_3)

and electrolyte concentration (X_4), whereas amount of dilution (X_1) shows a negligible effect. The EEC value of present study was calculated as follows:¹⁶

$$EEC \text{ (Wh)} = VA t \text{ (h)} \quad (8)$$

The EEC value increased with increasing applied current (X_3) and decreased with increasing electrolyte concentration (X_4). Meanwhile, the EEC decreased with increasing pH up to 7, beyond that there was a drastic increase in the EEC. Finally, the EEC values of present electrocoagulation process varied in the range from 0.4 to 7.5 Wh. These results indicated that all the selected independent variables showed a considerable effect on the EEC value, except for X_1 .

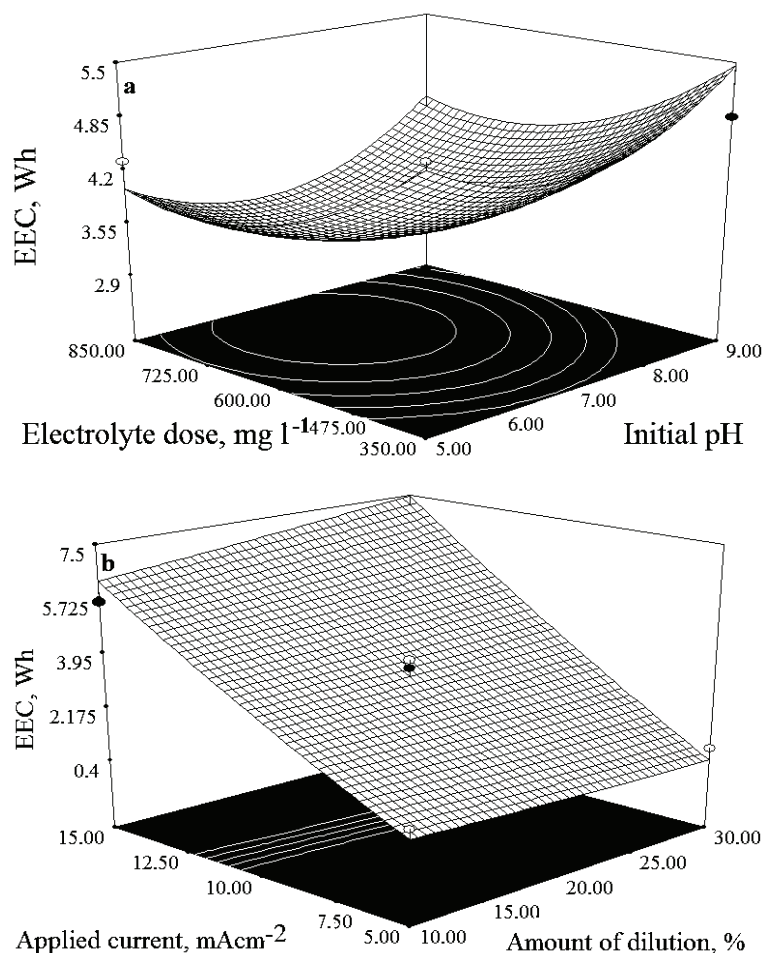


Fig.5. Effect of operating variables on EEC.

Effect of process variables on the iron concentration

In an electrocoagulation process, the quantity of produced iron is a key step. To examine the production of iron in the electrocoagulation process, the following calculations were used:¹⁷

$$n = \frac{It}{zF} \quad (9)$$

where n – number of moles; I – current, A; t – time (treatment time), s; z – charge on the cation, ($z = 2$) and F – the Faraday constant, $96.5 \times 10^4 \text{ C mol}^{-1}$.

The iron concentration in solution was theoretically calculated as follows:

$$c_{\text{Fe}} = \frac{nM_{\text{Fe}}}{V} \quad (10)$$

where c_{Fe} – iron concentration in solution, g L^{-1} ; M_{Fe} – molar mass of iron; n – number of moles; and V – volume of the cell, L. In this present study, the production of iron mainly depended on one independent parameter, namely the applied current (X_3), only. The produced iron concentration in the present study was varied between 0.89 to 2.65 g L^{-1} .

Optimization and validation

The objective of the optimization was to determine the operating conditions that gave the maximum efficiency of *COD* and *TSS* removal with a minimum *EEC* in the selected parameter ranges. In this study, the desirability function approach was applied to optimize the electrocoagulation process *via* a numerical optimization technique (The Derringer desired function methodology), which evaluates a point that maximizes the desirability function. The optimum operating conditions were predicted to be: amount of dilution 30 %, initial pH of 6.5, applied current of 8 mA cm^{-2} and an electrolyte dose of 740 mg L^{-1} , resulted in high efficiencies of *COD* (98 %) and *TSS* (93 %) removal with an *EEC* of 2.40 Wh, and a desirability value of 0.986. The suitability of the optimized conditions for predicting the optimum response values was tested experimentally using the same set of optimal conditions, which gave removal efficiencies of 98.06 and 92.54 % for *COD* and *TSS*, respectively, with an *EEC* of 2.34 Wh. These results clearly validated the optimized conditions.¹⁸

CONCLUSIONS

In this study, BBD was employed to study and optimize the process variables, *i.e.*, amount of dilution, initial pH, applied current and electrolyte concentration on the removal of *COD* and *TSS* from biologically pretreated bagasse effluent using an electrocoagulation process with iron electrodes. The results showed that all the operating variables had a significant effect on the responses and quadratic models were developed for predicting the responses. Three dimen-

sional response surface plots were used to study the combined effect of the process variables on the responses. The optimum set of operating variables was obtained using the Derringer desired function methodology. The optimal set was found to be: amount of dilution, 30 %; initial pH, 6.5; applied current, 8 mA cm⁻² and an electrolyte dose of 740 mg L⁻¹, which gave high efficiencies for COD (98 %) and TSS (93 %) removal with an EEC of 2.40 Wh. The results demonstrated the technical feasibility of electrocoagulation as a possible and reliable technique for the post-treatment of biologically pretreated bagasse effluent.

Acknowledgments. The authors are thankful to the University Grant Commission (UGC), the Government of India, for financial support (F. No: 39-853/2010) and to fabricate and use the experimental setup.

ИЗВОД

ОПТИМИЗАЦИЈА ПРОЦЕСА ЕЛЕКТРОКОАГУЛАЦИЈЕ ЗА ТРЕТИРАЊЕ БИОЛОШКИ ПРЕДТРЕТИРАНОГ ЕФЛУЕНТА ОД ОТПАДА ПЕРЕРАДЕ ШЕЋЕРНЕ ТРСКЕ

K. THIRUGNANASAMBANDHAM, V. SIVAKUMAR и J. PRAKASH MARAN

Department of Food Technology, Kongu Engineering College, Perundurai, Erode-638052, TN, India

Главни циљ ове студије био је да се испита ефикасност процеса електрокоагулације помоћу електрода од гвожђа као накнадног третмана биолошки предтретираног ефлуента од отпада прераде шећерне трске. Уклањање хемијске потрошње кисеоника (COD) и укупних суспендованих честица (TSS) испитивани су под различитим радним условима, као што су степен разблажења, почетни pH, јачина струје и доза електролита, коришћењем анализе површине одговора (RSM) уз четворофакторијални Бокс–Бенкенов (*Box–Behnken*) експериментални дизајн са три нивоа. Експериментални резултати су анализирани Парето анализом варијансе (ANOVA) и развијени математички модели полинома другог реда са високом корелацијом за ефикасност (R^2) за COD, уклањање TSS и потрошњу електричне енергије (EES). Појединачни и заједнички утицаји променљивих проучавани су коришћењем тродимензионалних графика површине одговора. Под оптималним радним условима, као што је разблажење од 30 %, почетни pH од 6,5, јачина струје од 8 mA cm⁻² и доза електролита од 740 mg L⁻¹ добија се виша ефикасност уклањања COD (98 %) и TSS (93 %) са EES од 2,40 Wh, што је потврђено експериментима.

(Примљено 8. априла, ревидирано 24. јуна, прихваћено 27. јуна 2013)

REFERENCES

1. R. Sridhar, V. Sivakumar, V. Prince Immanuel, J. P. Maran, *J. Hazard. Mater.* **186** (2011) 1495
2. M. Sharari, A. Jahan Latibari, A. Guillet, M. Aourousseau, B. Mouhamadou, Gh. Rafeiee, A. Mirshokraei, D. Parsapaghoh, *Biodegradation* **22** (2011) 421
3. S. Chinnaraj, V. Venkoba Rao, *Biomass Bioenerg.* **30** (2006) 273
4. N. Bektas, H. Akbulut, H. Inan, A. Dimoglo, *J. Hazard. Mater.* **106** (2004) 101
5. F. Akbal, S. Camc, *Desalination* **269** (2011) 214
6. R. Sridhar, V. Sivakumar, V. P. Immanuel, J. P. Maran, *Environ. Prog. Sustain. Energ.* **31** (2012) 558

7. K. Thirugnanasambandham, V. Sivakumar, J. P. Maran, *J. Serb. Chem. Soc.* (2013) doi: 10.2298/JSC130201053T
8. J. P. Maran, V. Sivakumar, R. Sridhar, V. P. Immanuel, *Ind. Crop. Prod.* **42** (2013) 159
9. J. P. Maran, V. Sivakumar, R. Sridhar, K. Thirugnanasambandham, *Carbohydr. Polym.* **92** (2013) 1335
10. K. Thirugnanasambandham, V. Sivakumar, J. P. Maran, *Carbohydr. Polym.* **97** (2013) 451
11. J. P. Maran, S. Manikandan, K. Thirugnanasambandham, C. V. Nivetha, R. Dinesh, *Carbohydr. Polym.* **92** (2013) 604
12. J. P. Maran, V. Sivakumar, R. Sridhar, V. P. Immanuel, *Ind. Crop. Prod.* **42** (2013) 159
13. S. Irdemez, N. Demircioglu, Y. Yildiz, *J. Hazard. Mater.* **B137** (2006) 1231
14. R. Sridhar, V. Sivakumar, V. P. Immanuel, J. P. Maran, *Environ. Prog. Sustain. Energ.* **31** (2012) 558
15. R. Sridhar, V. Sivakumar, J. P. Maran, K. Thirugnanasambandham, *Int. J. Environ. Sci. Technol.* (2013), doi: 10.1007/s13762-013-0301-5
16. M. S. Bhatti, D. Kapoor, R. K. Kalia, A. S. Reddy, A. K. Thukral, *Desalination* **274** (2011) 74
17. D. Kliugaite, K. Yasadi, G. Euverink, M. F. M. Bijmans, V. Racys, *Sep. Purif. Tech.* **108** (2013) 37
18. J. P. Maran, V. Sivakumar, K. Thirugnanasambandham, a R. Sridhar, *Prep. Biochem. Biotech.* (2013), doi: 10.1080/10826068.2013.791629.